Experimental Validation of a Model for the Motion of an Uncontrolled Bicycle

J. D. G. Kooijman

MSc Thesis

Delft University of Technology, 2006
The Netherlands

Examination committee:

Prof.dr.ir. D.J. Rixen
Dr.ir. A.L. Schwab
Dr.ir. W.L.T. Thijs
Dr.ir. P. Gosselet

Preface

This report was written as part of the final project for my mechanical engineering masters degree at the Delft University of Technology. The work was supervised by Arend L. Schwab, assistant professor at the Laboratory for Engineering Mechanics.

Readers who are particularly interested in the measurement method of the parameters of a bicycle are directed to chapter 4. Those interested in the measurement of the dynamic response of a freely coasting bicycle and the analysis of such measurements are directed to chapter 5.

Naturally I would like to thank Arend Schwab for his guidance and enthusiasm. I would also like to thank Jos van Driel for his help, connecting and installing the electronic sensors and the Labview programming. I also wish to thank Jan Sterk for his help with milling, turning and welding parts and in particular for his sound engineering advice. Finally I would like to thank my parents for their endless (financial) support and patience.

J.D.G. Kooijman
April 2006

Contents

Summary

Recently a model of the motion of an uncontrolled bicycle was benchmarked. In this model, many physical aspects of the real bicycle are considered negligible, such as the flexibility of the frame and wheels, play in the bearings, and precise tire characteristics. Apart from flexibility and play, in this model the most uncertain aspect, that had to be verified was the replacement of the tires by ideal rolling, knife-edge wheels. The admissibility of these assumptions was checked by comparing experimental results with numerical simulation results.

The experimental system consisted of an instrumented bicycle without rider. Sensors were installed on the bicycle for measuring the lean rate and the yaw rate, the steering angle and the rear wheel rotation. Sidewheels were added to the bicycle to prevent it from completely falling over under unstable conditions.

All twenty five parameters of the instrumented bicycle required for the linearised model were measured. The lengths were measured with a tape measure, angles with an integrated protractor and spirit-level and the mass of the different parts with scales accurate to ± 0.01kg. For the measurement of the mass moment of inertia of the front frame, rear frame, front wheel and rear wheel a torsion pendulum was constructed.

Measurements were recorded for the case in which the bicycle coasted freely on a level surface. From the measured data, eigenvalues for the bicycle were extracted by means of curve fitting. These eigenvalues were then compared with the results from the linearised equations of motion of the model.

The experimental results show a very good agreement with the results as obtained by the linearised analysis of the dynamic model of an uncontrolled bicycle. This shows that the tire slip and frame and fork compliance are not important for the lateral dynamics of the bicycle in the speed range up to 6 m/s.

Chapter 1

Introduction

1.1 Thesis Motivation

Everybody knows that a bicycle is highly unstable at low speeds whereas it is easy to stabilize at moderate to high speeds. This speed dependant stability is already present in one of the simplest bicycle models, consisting of four rigid bodies connected by three revolute joints, figure 1.1. In this model the rider is rigidly attached to the frame and his hands are free from the handlebar. For the knife edge wheels we assume pure rolling contact, and no side slip. The resulting non-holonomic mechanical model has three velocity degrees of freedom: forward speed v, lean rate $\dot{\phi}$ and steering rate $\dot{\delta}$. Starting from an upright steady motion this uncontrolled model can show, after perturbing laterally, asymptotically stable motion in a certain speed range, despite the fact that the model is energy conservative. The governing dynamic equations for this model have recently been benchmarked [1] and after more than a century of bicycle dynamics literature we are now certain that these equations are correct. However in this simple model, many physical aspects of a real bicycle are considered negligible, such as for example the flexibility of the frame and wheels, play in the bearings, and the precise tire characteristics. Apart from flexibility and play,

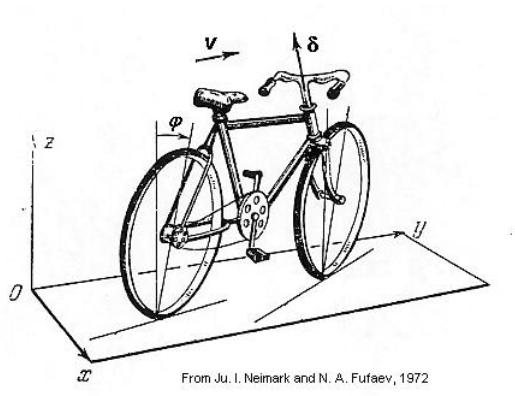

Figure 1.1: The bicycling model

the greatest uncertainty in this model is the replacement of the tires by ideal rolling knife-edge wheels.

It is therefore still vital that the admissibility of these assumptions is checked with regard to the motion of an actual bicycle. This can be done by carrying out experiments with a real bicycle and comparing them with those of the numerical simulations and is the subject of this thesis.

1.1.1 A Short Introduction To The Bicycle Model

The mechanical model of the bicycle is described in [1] and consists of four rigid bodies, viz. the rear frame, the front frame being the front fork and handlebar assembly and the two knife-edge wheels. The bodies are interconnected by revolute hinges at the steering head between the rear frame and the front frame and at the two wheel hubs. In the reference configuration, all bodies are assumed to be symmetric relative to the bicycle midplane. The contact between the wheels and the flat level surface is modelled as stiff and non-slipping by holonomic constraints in the normal direction and by non-holonomic constraints in the longitudinal and lateral direction. It is assumed that there is no friction, apart from the idealized friction between the non-slipping wheels and the surface, and no propulsion. These assumptions make the model energy-conserving. In the reference position, the global Cartesian coordinate system is located at the rear wheel contact point O, where the x-axis points in the longitudinal direction of the bicycle and the z-axis is directed downwards. Figure 1.2 shows the directions of the axes.

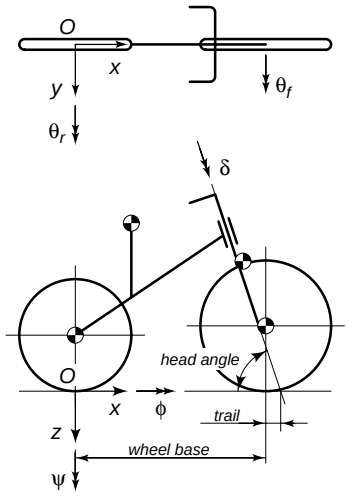

Figure 1.2: Diagram showing the parameters of a bike

The mechanical model of the bicycle has three velocity degrees of freedom: the roll rate $\dot{\phi}$ of the rear frame, the steering rate $\dot{\delta}$, and the angular rate $\dot{\theta}_r$ of the rear wheel with respect to the rear frame. The instrumented bicycle is assumed symmetric about the vertical longitudinal plane and the wheels are assumed rotationally symmetric about their axles. The mass moments of inertia are given with respect to axis through the centre of mass and parallel to the global

xyz-axes in the reference position. The governing equations of motion represent a linear perturbation of a constant-speed straightahead upright solution: $\phi = 0$, $\delta = 0$, and the constant forward speed is $v = -\dot{\theta}_r R_{rw}$. The lateral symmetry of the system, combined with the linearity in the equations precludes any coupling between the forward motion and the lean and steer. For example, a lean to the right must cause the same speed-up as a lean to the left. But linearity requires the effects to be the opposite of each other. Thus there can be no linear coupling. Therefore the first linearised equation of motion is

$$\ddot{\theta}_r = 0. \tag{1.1}$$

Consequently the nominal forward speed $v = -\dot{\theta}_r R_{rw}$ is constant. The linearised equations of motion for the bicycle expressed in the two remaining degrees of freedom, the lean angle ϕ and the steer angle δ, are two coupled second-order constant coefficient ordinary differential equations with the forward speed as a parameter. The first equation is called *the lean equation* and the second is called *the steer equation*. Written in matrix form we have [1]:

$$\mathbf{M}\ddot{\mathbf{q}} + [v\mathbf{C_1}]\dot{\mathbf{q}} + [\mathbf{K_0} + v^2\mathbf{K_2}]\mathbf{q} = \mathbf{f}, \tag{1.2}$$

where the time-varying variables are

$$\mathbf{q} = \begin{bmatrix} \phi \\ \delta \end{bmatrix} \quad \text{and the forcing} \quad \mathbf{f} = \begin{bmatrix} T_\phi \\ T_\delta \end{bmatrix}.$$

The constant coefficients of $\ddot{\mathbf{q}}$, $\dot{\mathbf{q}}$ and $\mathbf{q}$ are presented algorithmically in terms of the bicycle design parameters in [1]. Briefly, they are a symmetric mass matrix, $\mathbf{M}$, a damping matrix $v\mathbf{C_1}$ which is linear in the forward speed, and a stiffness matrix which is the sum of a constant (symmetric) part, $\mathbf{K_0}$, and a part, $v^2\mathbf{K_2}$, which is quadratic in the forward speed.

The transient response of the system, in the absence of any forcing, is given by a linear combination of the eigenmodes. These eigenmodes together with their eigenvalues are found by assuming an exponential solution of the form $\mathbf{q} = \mathbf{q}_0 \exp(\lambda t)$ for the homogeneous equations from 1.2. This leads to a characteristic polynomial which is quadratic in λ. The coefficients in this polynomial are complex expressions of the 25 design parameters, gravity, and speed v.

An example of a set of solutions λ of the characteristic polynomial for a range of forward speeds is shown in figure 1.3. Eigenvalues with positive real part correspond to unstable motions whereas eigenvalues with a negative real part correspond to asymptotically stable motions for the corresponding mode. Imaginary eigenvalues correspond to oscillatory motions.

In principle there are up to four eigenmodes, where oscillatory eigenmodes come in pairs. Two are significant and are traditionally called the *capsize mode* and *weave mode*. The capsize mode corresponds to a real eigenvalue with eigenvector dominated by lean: when unstable, the bicycle just falls over like a capsizing ship. The weave mode is an oscillatory motion in which the bicycle sways about the headed direction. The third remaining eigenmode is the *caster mode* which corresponds to a large negative real eigenvalue with eigenvector dominated by steering.

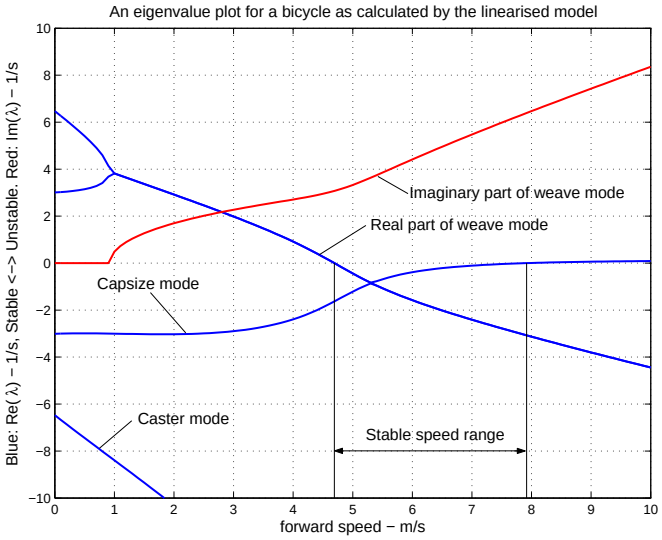

Figure 1.3: The eigenvalues for a modelled bicycle as calculated by the linearised model

1.2 Experimental Validation

After carrying out literature research on previously executed experiments with single track vehicles we went about verifying the linearised dynamic model. An instrumented, riderless, bicycle was prepared and it's parameters were measured. Next its' motion was measured during free coasting and eigenvalues were extracted and compared with those of the model.

1.2.1 Literature

The literature on experimental verification of modelling aspects in single-track vehicles can be divided in two sections: bicycles and motorcycles. We know from experience that tires play a dominant role in the dynamic behaviour of a motorcycle at high speed. Since the model under study here operates at low speed and assumes ideal rolling contact, it seems that many motorcycle studies lie outside the current scope. Döhring [2, 3] was the first to measure the lateral motion of a single track vehicle. Although he measured on three motorcycles he compared his results with the same model as presented here and this can therefore be classified as bicycle dynamics. Rice and Roland [4] measured the lateral stability and control of two distinct bicycles, both in hands-free as well as controlled operation. Roland and Lynch [5] performed an extensive study in lateral bicycle dynamics. They measured tire characteristics and then performed a number of tests on an instrumented uncontrolled bicycle and compared the results with their model (Roland and Massing [6]). Wächter [7] and Suhr [8] performed some experimental validation for their bicycle dynamics model. Jackson and Dragovan [9] measured the state of a bicycle ridden hands-free and compared the time history with results from their model.

Many measurement have been made on the lateral dynamics of motorcycles.

We discuss here only some distinct contributions. Eaton [10] measured the transient response of a light motorcycle to a lateral disturbance and compared this with his model. Rice [11] performed a number of tests on motorcycles in order to obtain performance characteristics for handling and safety. Weir and Zellner [12] tested transient behaviour of motorcycles in some standard manoeuvrers and compared some results with their model. Ruijs and Pacejka [13] built a rider robot to validate their computer model eliminating disturbances originating from the human rider. Rider robots have also been built by the group of Kageyama [14] and the Blue Team [15], a group of Berkeley students engaged in the DARPA challenge. Cossalter, Doria and Lot [16] over the past decade performed an extensive range of measurement on several aspects of the dynamic behaviour of motorcycles.

1.2.2 Model Verification Procedure

The bicycle, as shown in figure 1.4, was fitted with a laptop that was connected via a data acquisition unit to sensors that measured the lean-rate, yaw-rate, steering angle and the rear wheel rotation. Sidewheels were also added to ensure that the instrumentation did not breakdown when the bicycle fell over.

The instrumented bicycle was launched on a flat level surface for a variety of

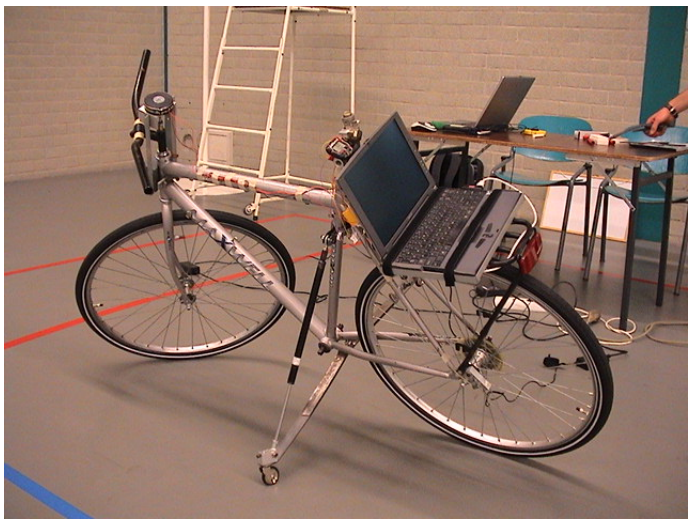

Figure 1.4: The instrumented bicycle

speeds and its dynamic response was measured. The speed of the bicycle during the different tests ranged from stationary up to approximately 6 m/s. At the higher, stable, speeds the bicycle was laterally perturbed to induce a response.

The data analysis was made much easier by choosing to compare eigenvalues of the model with those of the instrumented bicycle. Another method could have been to reconstruct the actual motion of the instrumented bicycle and comparing that to the motion calculated in the model for specified initial conditions. The specification of the initial conditions was not required for the eigenvalue comparison. Instead a harmonic function was optimised to fit on the time response of the signals for each run. From this fit function the eigenvalues

for the instrumented bicycle were extracted for the speed range that the bicycle coasted at during each run. As eigenvalues are coordinate invariant, to calculate them did not require us to know the initial conditions nor did we require to know the exact scaling factors. This greatly simplified the analysis.

A large part of the work carried out however consisted of measuring the twenty five bicycle parameters of the instrumented bicycle. These parameters were required to be able to compare the eigenvalues extracted from the instrumented bicycle measurements with those calculated with the linearised dynamic model. The linearised equations of motion required the mass moments of inertia of the bicycle to be split into four parts; that of the front fork and handlebar construction, the rear frame with measuring equipment and sidewheels, the rear wheel and the front wheel. To measure the mass moments of inertia of these four parts a separate experimental piece of apparatus, a torsional pendulum, was produced.

1.3 Document Structure

The rest of this thesis is organised as follows: Chapter 2 starts by giving an outline of possible and the chosen measuring equipment with which the bicycle was instrumented for the validation of the linearised model. Next in chapter 3 the pre-test preparation is discussed including how the measuring equipment was installed on the bicycle, the data acquisition program and the test procedure. In chapter 4 the measurement of the twenty five parameters of the instrumented bicycle required for the linearised dynamic model are described. Then in chapter 5 the dynamic tests are described, the collected data is analysed, and the model is validated. Finally in chapter 6 the conclusions of this work are summarised and some recommendations for future work are given.

Chapter 2

Measuring Equipment

Before we could choose the required measuring equipment its requirements had to be specified and recorded. Then the possible measuring systems were investigated and assessed with respect to these requirements. Both digital and analogue systems were investigated before a system was chosen. The chosen apparatus is listed in Appendix B.

2.1 System Requirements

The first requirement for the measuring equipment was that it is not allowed to have an effect on the dynamic behavior of the bicycle other than adding weight and extra inertia. The measuring equipment for example could not have cables running from the bicycle to a computer as the tension in the cables between the bicycle and the computer would undoubtedly affect the dynamic behavior of the bicycle (see [6]).

The second requirement is that the equipment was not allowed to add extra degrees of freedom to the bicycle by non-rigidly attaching parts to the bicycle.

The third requirement that the equipment had to fulfil is that it has be placed on the bicycle in such a way that the equipment can be used on most standard bicycles without requiring serious adjustments.

Generally measuring equipment is fragile. However as the bicycle would fall over numerous times during the tests, and even though the bicycle would be fitted with side wheels to reduce the severity of the impacts, the fourth requirement for the measuring equipment is that it has to be able to withstand moderate shocks.

The final requirement for the measuring equipment was that the budget for the validation of the linearised bicycle model project was set at €1500.

2.2 Possible Data Acquisition Options

To carry out the data acquisition we required a computer to record the data collected by the sensors. The foremost physical boundary condition for this computer system was that there were no cables connecting the bicycle to anything else. This meant that the computer either had to be installed on the bicycle or had to have a wireless connection with the sensors. The most important

boundary condition for the computer was the available budget. 1,500 Euros is not much money when it comes to computers.

2.2.1 Wireless Communication

The first idea was to have no computer onboard. The sensors would communicate with a computer via a wireless link. However, after an extensive search no suitable device had been found. The equipment that was located was intended for the process industry and was not only large and cumbersome, but also couldn't be powered by a small battery. Bradatech [1] did have a small Bluetooth wireless data acquisition system, but it only had a 60Hz sample rate, which is to low.

2.2.2 PC104

The first onboard option that was investigated was the PC104 computer system (see appendix A for specification details). This is a light weight computer that has no moving parts in a strong aluminium casing. It is therefore not susceptible to the large shocks such as those caused by a crashing bicycle.

This type of computer was initially looked at because it could then also be used by the department for many other applications where the dynamics of the application or the available space could be a drawback for a normal computer. An example of an application where the dynamics department preferred not to use an ordinary laptop was for a project where the vibrations felt on a racing kart had to be measured.

A standard development kit PC104 computer costs around €1,300 and is equipped with sixteen 16-bit A/D converters and with 24 digital I/O ports but only 2 counters. It is therefore capable of measuring sixteen analogue signals (far more than required!), but only one digital encoder type signal if this signal can act in two directions (for example an incremental encoder that can rotate both clockwise and anticlockwise). If the computer hardware is expanded with an extra counter board the price increases to around €1,500. If the computer is to run on batteries instead of a mains supply an extra DC/DC board is required costing around another 100 euros

If all the sensors supplied analogue signals and all the sensors were already available in the department this computer could be acquired. However this was not the case and thus this option had to be discarded.

2.2.3 DIY Design

A far cheaper option than the PC104 computer, which could be used for many tasks, was to build a computer for just this one application. This is the idea behind the C-control Basic Unit sold by Conrad Electronics. This micro-controller that has eight, 8-bit analogue to digital converter inputs, sixteen digital connections and an 8kb (EEPROM) memory chip for application storage and data registration. An extra memory device, either a solid state memory or hard drive, would have to be connected to C-controller for the data acquisition. Such a microcomputer is very cheap and costs less than €50. A DIY computer has one

[1] http : //72.138.187.243/bradatech_corp//Bluetooth/bluebox.asp

major drawback however and that is that it has to completely be programmed in Basic. With no experience in this field this seemed like a daunting task that we did not want to undertake!

2.2.4 Laptop

Instead of buying a new computer for the project it was also possible to use a laptop that was already in the departments possession. The group had 2 laptops in it's possession that were not being used. The smaller of the two was an Acer Travelmate 340 which weighs just under 2kg. The main advantage that such a computer system had was that with the relatively small budget it was still possible to have a measurement system that could be programmed in Matlab, Simulink, or in LabView. The main disadvantage of a an onboard laptop is that it is more fragile than the two previously mentioned systems. If the bicycle were to fall over the moving parts such as the hard drive and its screen could break, the latter did.

A data acquisition unit (and software) was required in order to be able to store the signals from the sensors on the laptop. This could be carried out by a 14 bit USB data acquistion (USB-DAQ) system from National Instruments (appendix A). This USB-DAQ unit only cost €275.

The Laptop with USB-DAQ was thus chosen because it was the cheapest option that could also be programmed in the normal user friendly Windows surroundings.

The main drawback to the USB-DAQ system however is that it only has one digital counter which means that it can only measure one digital sensor and only in one direction. An example could be a reed relet and magnet style speedometer such as mentioned in appendix A as the speed will always be in the forward direction during the measurements. A two way digital sensor such as the optical encoder (also described in appendix A) cannot be used with this system.

A second problem with the USB-DAQ is that it can only measure analogue signals or digital signals, but not both during the same operation. To be able to measure both the program has to run two separate measuring loops that run alternatively, radically reducing the possible sample rate. As a result it was decided that all the sensors would have to be analogue sensors.

2.3 Possible Sensor Options

There are two methods for validating the dynamic model. The first method is by full state reconstruction where all the states of the dynamic model are measured and compared to the model. The second is by extracting the eigenvalues from the measured data of an arbitrary dynamic response at a given speed.

The variables that we wanted to measure for full state reconstruction are δ the steer angle, $\dot{\delta}$ the steer angle rate, ϕ the lean (roll) angle, $\dot{\phi}$ the lean (roll) angle rate , and v the forward speed (which would range from 0 to 10 m/s). With these state variables and the equations of motion the state derivatives could be calculated. Therefore we also wanted to measure the derivatives of the state variables: $\ddot{\delta}$, the steer angle acceleration and $\ddot{\phi}$, the lean (roll) angle

acceleration. With these variables we could then compare the measured values to the calculated values.

The chosen analogue sensors had to work on a DC power supply because the bicycle could not be connected to a mains supply by a cable and a DC to AC converter would have been a serious weight addition to the bicycle.

2.3.1 Expected State Value Ranges

In figure 1.3 the calculated eigenvalues for the different motions for a standard bicycle are shown for each speed from 0 to 10 m/s.

In the figure it is shown that the the expected maximum value for the imaginary part of the weave eigenmotion (red line) is approximately 8 rad/sec when the bicycle is moving at a speed of 10 m/s. The maximum expected frequency is thus:

$$\text{frequency} = \frac{8}{2\pi} = 1.3 \approx 1.5 \text{ Hz} \tag{2.1}$$

The expected frequencies for the lean and steering rate were thus between 0 and 1.5 Hz. This low value is a problem for measuring the angular acceleration with a standard accelerometer as these usually operate from higher rates onwards.

The equations of motion have been linearised and as such are only applicable for small deviations from the straight ahead position. Therefore the bicycle would only be set off in the straight-ahead position and the maximum steering angle was limited. The maximum deviation expected for the steering angle, $\dot{\delta}$, and lean angle (roll angle), $\dot{\phi}$, from the straight ahead position were expected to be no larger than 15 degrees (0.25 radians), and were restricted from making angles larger than approximately 30 degrees, by stiffly placed bars and side wheels respectively. The maximum expected angular lean and steering rate was therefore not expected to exceed 100°/s.

2.3.2 Angular Sensors

Angle

Due to the dynamic nature of a bicycle, measuring the lean angle, ϕ, of the bicycle by conventional methods is tricky. We can measure ϕ with respect to either the ground or gravity, however because a bicycle leans whilst making a corner measuring the angle by using gravity becomes tricky as the centripetal force also affects the measuring equipment. Döhring [2], measured ϕ with respect to the ground by connecting a trailer to his motorbikes. The trailer remained upright at all times whilst the motorbike rolled whilst making a corner. The lean (roll) angle was measured using a potentiometer. This method was considered however it was decided that the extra trailer would add to many sources of friction and inertia and was thus not applied. Another method that could have been applied was to use outriggers with ultra-sound sensors. This method would have been relatively cheap using a simple Polaroid ultrasound transmitter/reciever unit on both the left and right outrigger. The sensors would then measure the distance from the ground and thus if the experiment is carried out on a flat level surface the angle with respect to gravity can be calculated. It was however decided not to measure the lean angle.

The measurement of the steering angle (δ) between the rear frame and the front handle bar assembly on the other hand is relatively easy. It can be measured both digitally, such as with an optical, or incremental encoder, or with an analogue sensor such as a potentiometer (appendix A). It was thus decided to use a highly linear potentiometer that the department had lying around, to measure the steering angle. This sensor gave an output between 0 and 5V over a 358° range. This meant that over the 30 degree range that δ would be measured the voltage would only vary about 0.42V. however with the 14-bit USB-DAQ, the voltage range would still be split into about 688 levels by the computer and this was deemed sufficient.

Angular Rate

The steering angle δ is easy to measure, However it's rate and acceleration are not. A practical method to measure the steer angle rate is to differentiate the steering angle signal.

The lean angle rate, $\dot{\phi}$, can be measured directly using a gyroscope. Initially we tried to use a Murata Piezoelectric vibrating gyroscope (see appendix A) to measure the lean angle rate. This sensor was also used by Jackson and Dragovan [9]. The resulting signal was so small that it required amplification. The sensor was designed for angular rates up to 300°/s whilst the expected rates below the 100°/s. It was thus decided that another sensor would be used.

The second type of analogue angular rate sensor that we tried was the solid state Coriolis force detecting gyroscope (see appendix A) CRS03 by Silicon Sensing. This sensor gave a far better output, and was cheap costing just €135. It was thus chosen.

The CRS03 sensor gives a full scale output of 5V when rotating at a speed of 100°/s clockwise and 0V when rotating at a speed of 100°/s anticlockwise. When it does not rotate it's output is 2.5V.

Angular Acceleration

We didn't find a suitable angular acceleration sensor on the market. There were a wide range of angular acceleration sensors available but the relatively cheap versions could only measure large accelerations or at high frequencies. The lower the angular acceleration to be measured and the lower the frequency at which these had to be measured, the more expensive the sensors were. The minimum price that we found for an angular acceleration sensor whose range started at around $0.5Hz$ was 450 euro.

2.3.3 Angular Sensor Choice

It was decided that we would not measure the angular accelerations as these sensors were too expensive. As a result we would not carry out full state reconstruction but instead only extract the eigenvalues from arbitrary dynamic responses at given speeds.

We chose to measure the steering angle, δ, using the potentiometer that was in the departments possession, whilst the lean (roll) rate, $\dot{\phi}$, and the yaw rate, $\dot{\psi}$, would be measured using the CRS03 sensors. All the sensors are listed in appendix B.

2.3.4 Speed Sensors

The speed of the bicycle was required by both the data acquisition system and the person that propelled the bicycle along. The bicycle would be tested at a number of different speeds in order to test the complete range of the stability diagram. It was thought imperative that the speed be measured accurately and shown to the person that was propelling the bicycle in order to allow the person to bring the bicycle to the correct speed. In retrospect however we can conclude that the visual feedback from a speedometer was not that important because the person concentrated more on ensuring that the bicycle was upright and stable than on the speed.

The measurement of the speed had to be done in such a way that the bicycle would not rapidly reduce its forward speed. If the speed reduces during the test, then it will not be possible to assign the found eigenvalue for the dynamic response of the bicycle to a specific speed but rather to only a speed range. The larger the speed range the less precise the result would be.

Tachometer

A high quality optical or inductive tachometer (Appendix A) has relatively little friction and gives a large analogue output signal. A type of low quality tacho that was present on the bicycle was its' dynamo (used for powering the lights on the bicycle). The dynamo was initially tested on a drill, as shown in appendix C, to see how linear the output was. It was decided that the output was linear enough. By increasing the diameter of the rotor wheel and adding a diode and capacitor a linearly positive speed dependant voltage could be measured by the USB-DAQ. However after a couple of initial tests it was decided that the resistance caused by the dynamo was to high, the speed of the bicycle reduced to rapidly. The problem that the speed was not available to the person propelling the bicycle also remained.

Optical Encoder

This sensor is similar to the optical sensor used for the measurement of angles (appendixA). It is also a digital sensor. The only difference is that the number of pulses per time are important rather than just the number of pulses. As the angle is equal to the distance ($angle * radius = distance\ covered$), by dividing the distance by the time taken to cover that distance the speed can be calculated. The main advantage of this digital signal sensor compared to the tacho is that it causes practically no resistance and thus it does not reduce the bicycle's speed.

The optical encoder can only be used in conjunction with a digital counter because an analogue system would require an extremely high sample frequency ($> 5kHz$ for a 500 pulse per rotation encoder) to ensure that no pulses are missed. But using the counter on the USB-DAQ greatly reduces possible sample frequency of the other signals because the USB-DAQ cannot measure both analogue and digital signals in one loop.

Reed Relet & Magnet

Another digital speed sensor that was looked at was the reed relet and magnet (appendix A). The main advantages of a reed relet and magnet system over

an optical encoder is that the computer does not have to calculate the speed of the bicycle in real time because the reed relet and magnet system has its own computer that is used for calculating the speed. It is thus possible to see how fast the bicycle is going whilst it is being pushed independently of the sampling frequency of the data acquisition system.

The reed relet and magnet system is a digital sensor and this is its main drawback. If the data acquisition system were to use such a reed-relet and magnet system it would have to measure the number of pulses. This could be done in two manners: digitally with the counter, or analogue by sampling at an extremely high frequency in order to capture the pulses as an analogue signal. The pulses would then have to be counted and converted to a speed when the data was analysed. The problem with the first method is that the sample frequency radically reduces because the USB-DAQ is not capable of measuring both analogue and digital signals in one loop. The second method's drawback is that it is not possible to increase the sample frequency of the parameters independently i.e. increase the sample frequency of one automatically increases the rate of all the others as well.

Induction Method

Eventually we found a somewhat outdated type of bicycle computer made by Avocet the Altimeter 50. These operate on a different principle than most standard bicycle computers. They use a magnetic ring with ten poles that is placed on the hub of the wheel and a coil that is placed near by. When the wheel rotates an EMF is induced in the coil and this is measured by the computer and translated into a speed.

This system seemed to have the advantages of the digital signals mentioned above and the advantage that it was an analogue signal. It was thus chosen. However the signal measured turned out to be a tiny sine wave, with a very high frequency and thus had to be measured at a high (500Hz) rate. The signal at low speeds was so small that it was even difficult to differentiate it from noise. In chapter 5 the measured signal is discussed further.

2.3.5 Power Supply

In order to power the chosen sensors we required a separate power supply to that of the laptop and USB-DAQ, as these were both supplied by the laptop battery. Luckily the potentiometer and the angular rate sensors both required a 5V DC power supply. As the sensors required less than 1 Watt continuous power a small battery pack consisting of four AA batteries in series was sufficient to supply the three sensors for a couple of hours.

The data acquisition system also had to measure the voltage of the battery pack for the three sensors because the output voltage of the three sensors is not only linearly dependant with the angle/angular-rate but also with the input voltage.

Chapter 3

Pre Test Preparation

Now that the measuring equipment had been chosen, the parts had to be installed on the bike. To ensure that the laptop was not destroyed if the bike accidentally fell over sidewheels were added. The bike itself also had to be setup for the tests. In order to be able to record the sensor data a program had to be written for the data acquisition and finally the actual testing procedure had to be organised.

3.1 Bike Configuration

To be able to carry out the validation tests a bike was required. We chose a relatively new bicycle that the department had in it's possession, which didn't seem to have any serious malfunctions. The bicycle, a silver coloured Maxwell Silvercity was identical to the one shown in figure 3.1(a). Due to its colour the bike was given the name "silverbike". The bike is a typical 21 in city-bike, with 28 in wheels, and 6 gears. The bike originally came complete with mudguards, lock, baggage holder, dynamo and lights. For our experiments we removed all the superfluous parts on the bike, including the brakes, chain, derailleur, crankset and pedals. We were left with only the rear frame with bottom bracket and baggage holder, the front fork and bare handelbars, front wheel and the rear wheel with cassette. All the other parts were removed. Next we added the measuring equipment as shown in figure 3.1(b).

3.1.1 Computer and Sensor Positioning

The computer and sensors had to be connected to the test bicycle in such a manner that not only would they easily fit to this test bicycle but also to practically every other bicycle. It was desired to be able to carry out further tests on another bicycle in the future. It was therefore important that the parts were not fastened permanently to the bicycle and that any produced brackets could be used on most bicycles without requiring a redesign.

Laptop Placement

The location that the computer is placed on the bike can be used to increase the stable speed range of the bike. The laptop had to be placed as far forward

(a) The bicycle before most of the components were removed.

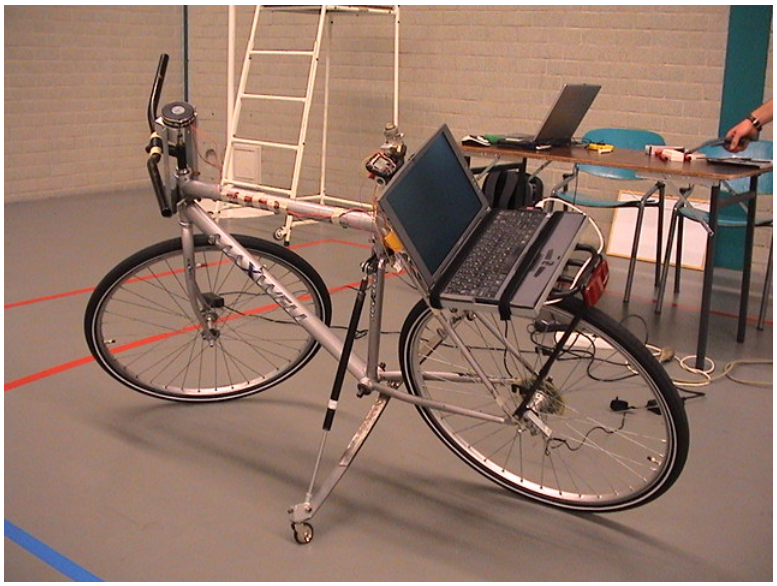

(b) The bicycle fully instrumented.

Figure 3.1: The bicycle in its original and instrumented states.

on the rear frame of the bike as possible for the greatest effect. The laptop could be placed horizontally on the top tube for example. Another option if the screen was not required to be able to operate the laptop, was to place the laptop vertically and under an angle in the diamond frame.Unfortunately this second option is not viable because the laptop, despite its small size, was still to large to fit in the diamond frame of the test bicycle.

Placing the computer on the top tube would have required a rugged bracket to hold the laptop in place. The top tube of a bike is not a standard diameter, and thus such a bracket would not only have to be fixed in such a manner that it will hold the laptop in place even when the bicycle were to fall over, but it also had to be adjustable so that the bracket could be used on many more bicycles.

Placing the laptop on the rear carrier would not help the stability of the bike [5] but fixation was easily achieved. Furthermore most bicycles, certainly those with the same wheel diameter, use the same size rear carrier, and thus these can be interchanged. In figure 3.2 the laptop is placed in a steel frame with padding and is fixed to the rear carrier such that the centre of mass of the laptop and steel frame is over the bike axis of symmetry. The frame is mechanically bolted to the rear carrier and the laptop is kept in place by two velcro straps.

Figure 3.2: Laptop in the bracket on the rear rack

Steering Angle Sensor Placement

There were three factors determining the design of the steer angle sensor location and bracket. Firstly the sensor was only aloud to apply a minimal torque on the steering axis whilst operating as any resistive torque would restrict the motion of the front frame with respect to the rear frame. Secondly because the angles that are to be measured are very small, at the most around 10° from the straight ahead position, any form of play between the sensor and the steering angle it self would cause a large measurement inaccuracy. Finally the sensor and mount had to be able to fit on most bicycles.

Most "standard" Dutch bikes have a head tube with an outer diameter equal to 34 mm. Therefore a bracket that used this parameter was designed. minimal play was achieved by directly connecting the sensor to the steering axis, via a flexible coupling that compensated for a small misalignment of the steering axis with the sensor axis. A transmission can thus be avoided, with as added advantage that the resulting resisting torque was smaller than with a transmission. A drawback to this method is that the output signal of the sensor is smaller than for a method where a transmission is incorporated because the full range of the steer angle sensor was not used.

In figure 3.3 the steering angle sensor and bracket are shown. The two vertically

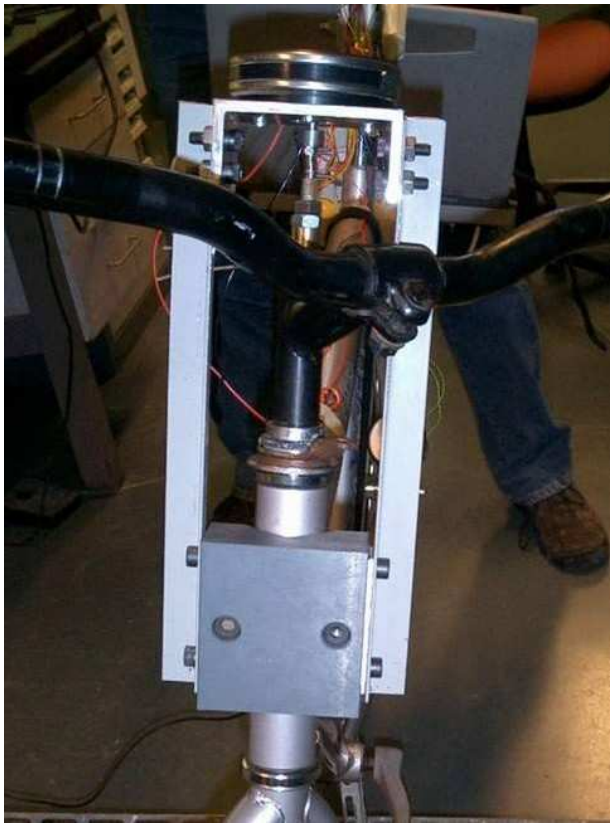

Figure 3.3: The steering angle sensor and bracket on the test bike

mounted steel L shaped rods that are connect to the Aluminium U profile and keep the sensor in position. The rods also restrict the maximum angle that the front frame can make with respect to the rear to about 30°. If the maximum angle were allowed to be much larger there is a chance that the bicycle could flip over.

Angular Rate Sensor Placement

The location was not such an important issue for the placement of the angular rate sensors. As long as they were placed on the rear frame they would measure the angular rate of the rear frame. In figure 3.4 the angular yaw rate sensor and the angular lean rate sensor are shown. The two sensors were placed on a T profile and as such are perpendicular to each other. The T-profile was clamped to the saddle post by the same clamp that is normally used to mount the saddle. A rotational spirit level was placed on top of the yaw rate sensor to ensure that it was placed horizontally (and thus that the lean rate sensor was placed vertically).

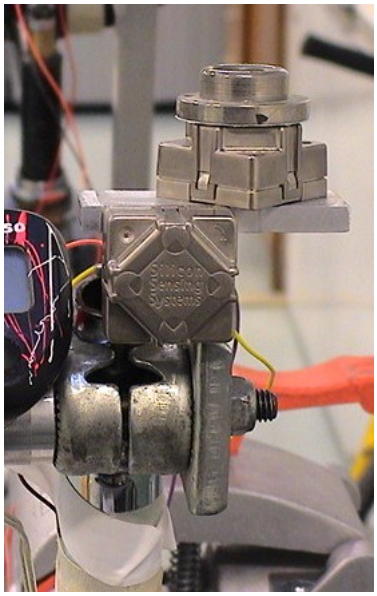

Figure 3.4: The lean and yaw rate sensors

Speed Sensor Placement

The forward speed of the bicycle in the linearised model is defined as the rear wheel rotation speed times the effective tire radius:

$$V = -R_{eff}\dot{\theta}_r$$

The Avocet Altimeter 50 however was designed to be placed on the front wheel. The magnetic ring that connects (via a click mechanism) to the front wheel hub therefore did not fit on the rear wheel hub because this hub had a larger

diameter than that of the front wheel. If we measured the speed of the front wheel, then the speed of the rear wheel would have to be calculated from the state. It was thus decided that it was better to measure the speed of the rear wheel directly by fastening the magnetic ring in another manner.

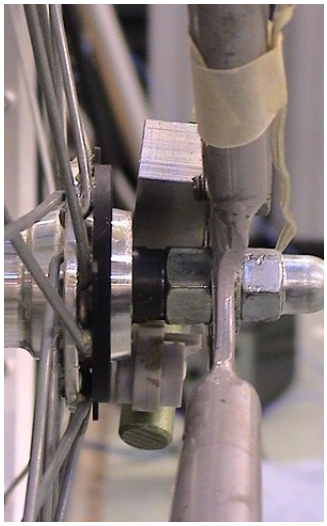

Figure 3.5: The Altimeter 50 magnetic ring glued to the test bike hub and the pickup

Figure 3.5 shows how the magnetic ring is glued to the test bike's rear wheel hub. Most Dutch bicycles have 28 in rims and thus the rear wheel of the test bike can either be placed on another bike, or the ring must be cut off and reglued to another bike.

The pickup was positioned very closely to the magnetic rim by an L shaped bracket that was connected to the rear frame by a bolt via the hole that is normally used to keep the mud guard in place. Figure 3.6 shows the pickup and bracket.

The measured signal had to be fed to the data acquisition system and to the speed computer. The speed computer was placed on an aluminium shaft that was connected to the same standard saddle clamp as the angular rate sensor bracket. With the speed computer in this position the speed values shown on its screen were clearly legible when running behind and alongside the bike. Unfortunately, this did not work out in practice. The refresh rate of the computer was to slow and the attention of the launcher had to go to launching the bicycle in a stable manner.

The signal fed to the computer was tapped off to the data acquisition unit at the bike mount. Two pieces of copper film were each connected to a wire at one end which in turn connected to the data acquisition unit and the other end of the copper film sat snugly between the computer and the bike mount as shown in figure 3.7.

Figure 3.6: The pickup and its bracket

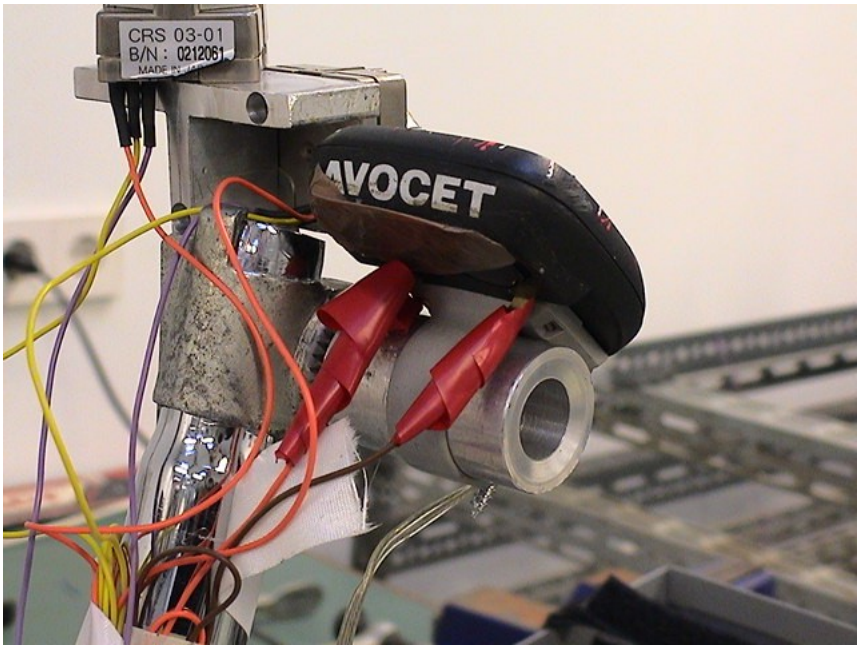

Figure 3.7: The Altimeter 50 computer connected to the seat saddle clamp and the connection of the data acquisition wires

Data Acquisition Unit and Battery

The location of the data acquisition unit and the battery were not crucial for the measurements, therefore the most convenient position to fix them to the rear frame were used. The data acquisition unit was bolted onto the rear carrier and the battery was cable tied to the frame. The Battery had a standard connector added to it to allow it to be easily recharged and disconnected from the sensors when the computer is not being used as shown in figure 3.8.

Figure 3.8: The battery pack and connector

3.1.2 Sidewheels

The initial idea behind the sidewheels was that they simply restricted the angle that the bicycle could fall over by. By reducing the angle from 90° to around 30° that the bike could tip over by, the tip over impact force would be greatly reduced. The initial side wheels were a set of training wheels that were kept 90cm apart by a steel rod and bolted to the bicycle stand bracket as shown in figure 3.9. During the first tests it was noted that the angle that the bicycle was able to tip over was sufficient, however the impact caused with the ground was still very violent. It was therefore decided that the sidewheels had to be connected by a type of suspension. This suspension had to have little damping. If the suspension had a large damping coefficient, it would rapidly reduce the rate that the bicycle was falling over at and thus basically induce a shock. This shock would be felt by the laptop and is obviously undesirable.

The second sidewheel prototype shown in figure 3.10 had a type of McPherson suspension. There was an A-arm made of thin steel strips and a strut to ensure that the arms only bent upwards and not backwards. The strut was made from a telescopic damper from the hatchback of a Suzuki Alto. The gas had been been removed from the damper to reduce the spring stiffness and damping. Smaller wheels which could also rotate were used in this version because

Figure 3.9: Stiffly added sidewheels

Figure 3.10: McPherson style side wheels

whilst testing the first version it was noted that the bike wanted to tip over the sidewheels because they restricted lateral motion.

The suspension mechanism worked by bending the A arms and in theory the strut would only be used as a bump stop for extreme cases. However initial calculations had suggested that this set up would probably not work as the steel strips were required to be 4mm thick, whilst we were only able to produce strips to a maximum thickness of 2mm in the workshop. This design subsequently failed with embarrassing ease as shown in figure 3.11.

Figure 3.11: After one static test the sidewheels were plastically deformed to a large extent

The third sidewheel prototype which is shown in figure 3.12 thus consisted of 2 layers of 4mm thick steel strips (2cm wide) placed one on top of the other. 1 strip would be sufficient to act as a spring but the rod would be plastically deformed each time that it was used. By placing the second rod on top of the first, the deformation remains elastic. The top rod is half the length of the lower rod to reduce weight.

During a static test (the bike was not moving forwards) recorded on film it was noted that this third set up allowed the bike to fall over by about 30°, before the sidewheels made contact with the ground. Upon making contact the rods bent (elastically) and the damper (strut) length decreased, but not all the way to the stop. At the same time the bike was able to dissipate most of its kinetic energy via a lateral sliding motion. This motion was rated as sufficient and no further improvements were made. Unfortunately the sidewheels could not prevent mishap.

At one point during the testing we tried to cause a large excitation of the steering angle by deflecting the handlebars by a large angle. This was done by simply pushing one side of the handlebars forward in an impulsive manner. This caused the bicycle to gain a large lean rate and bounce on the left trainer

Figure 3.12: McPherson style side wheels

wheel. This in turn caused the bicycle to flip over the top to the right, breaking the laptop screen as shown in figure 3.13.

Figure 3.13: Broken laptop screen after the bicycle flipped over

3.1.3 Bike Set Up

Before the tests started the bike was set up in the following manner and kept in the same configuration for all the tests.

Front Fork

To reduce the speed at which the bicycle becomes stable (according to the linearised model) the front fork was flipped (rotated by 180 degrees) to increase the trail. The advantage of decreasing the minimum stable speed was that the limited space in the launch hall could be used more effectively. It takes longer for the bike to reach the the other end of the sports hall at this lower speed and thus the measurements could be carried out over a longer period of time. Another advantage of flipping the front fork was that the minimum stable speed for the bicycle reduced by more than 1 m/s to 4 m/s. As the top speed that most people can run alongside a bike is around 6m/s by decreasing the minimum stable speed it became possible to make more measurements in the stable speed range.

Bearings

Before initiating the testing program the bike was taken apart and the bearings were all cleaned to minimise the friction at the joints.

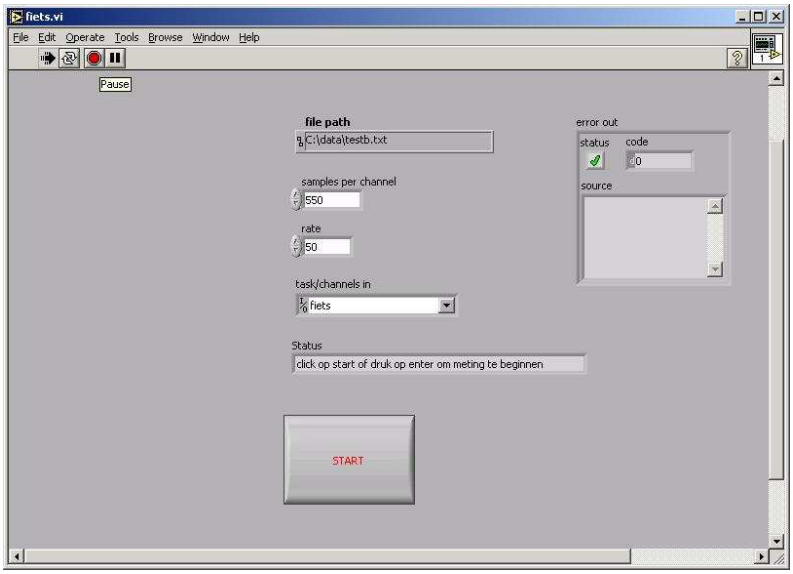

Figure 3.14: The interface used when carrying out the data acquisition

The head tube bearings were cleaned and when the front fork was reinstalled extra care was taken to ensure that there was no play and no excessive friction at the bearings.

The bearings at the wheel hubs were also cleaned and tightened to ensure that there was no lateral play on the wheels. The wheels were then placed vertically in the frame.

Tires

New tires were used for the tests because the tires on the bike were old, worn, dried out, ruptured, had flat spots and were oddly shaped from being parked for over a year. Standard Halford 28 x 1 3/8 outer tires and inner tubes were inflated to 3.5 bar overpressure. In retrospect it would have been better to mount slick tires with a low rolling resistance and at a high pressure (around 8 bar). This would reduce the rolling resistance even more. The rims were checked for trueness. No rim "wobble" was noted.

3.2 Data Acquisition Program LabView

The data acquisition was carried out in the National Instruments program LabView. This program has a graphical interface as shown in figure 3.14 called the Front Panel. The program is coded using building blocks that are connected to each other as shown in figure 3.15.

Next a description is given on how the program works. When the program is started in the Front Panel, it produces a new file (or writes over an existing file with the same name) in the directory mentioned, as shown in figure 3.14 under "file path". The file is given the name as mentioned in the "file path" caption. After the start button is pushed, the program fills the file with a row

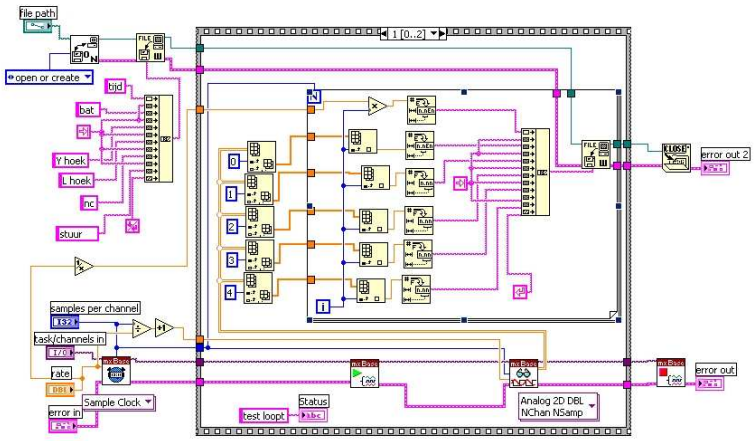

Figure 3.15: The building block representation of the program code

of titles for the time, battery voltage, yaw angle rate, lean angle rate, speed and steering angle. It then measures the signals that come in on the channels 0, 1, 2, 3, and 4 and places them in the following row of the file next to the time. The program continues to add a row of data for each measurement next to the time, till the pre-set number of measurements have been completed. The file is then complete, and is closed.

The number of samples per channel can be changed in the Front Panel along with the sample rate. The computer is capable of sampling these 5 channels at a maximum frequency of 960 Hz. The first tests were carried out at 100 Hz. Then after experimenting with the frequency range we decided to use 400 Hz. The choice for the higher frequency range was made because, firstly we wanted to increase the precision of the measured speed. Secondly we also wanted to test the bike at a higher speed and we wanted to ensure that there was no aliasing occurring in the speed signal. The value of 400 Hz was chosen after the measured signal for 100, 200, 300, 400 and 500 Hz had been examined. The higher the sampling frequency, The more erratic the recorded steering angle signal became. The signals' tendency to "drop off" at 500 Hz was considered unacceptable whilst at 400Hz it was still considered acceptable.

Before each run the name of the file in which the data will be stored must be adjusted. If not, the previous run will be written over.

3.3 Test Procedure

3.3.1 Constant Factors

The linearised dynamic model assumes that there is perfect rolling contact between the wheels and the road surface. This assumption will have most chance of being true under dry, flat conditions. Furthermore the model doesn't take air resistance into account and thus the less wind present during the tests the better. A third aspect that had to be taken into consideration is that all the

tests had to be carried out under identical conditions. By this we mean that the above mentioned factors are kept constant. Each test should be carried out on the same, completely dry surface, with no wind acting on the bike. Most preferable would be to carry out the tests at the same temperature and pressure, but due to the size of the required testing facility this would not be practical.

The most important factor for the tests is that the surface on which the tests were to take place had to be level. Most roads and car parks in the Delft area are made of tightly packed industrial bricks and are far from being flat! There are only a few locations with an asphalt surface, most of these are privately owned and all are used intensively.

The only possible and available option that fulfilled the three requirements was the university sports hall. The drawback to this location was that the relatively small space for testing a moving bike. The bike had to be restricted from rolling into a wall, therefore the person that propelled the bike had to follow the bike and stop it before it rode into a wall. The largest hall in the complex has a rectangular shape of 25 by 42 meters. This meant that the longest distance that the bike could move before hitting a wall was restricted to about 45m.

3.3.2 Testing Procedure

Each run consisted of three segments. In the first segment the bike was be brought up to speed, the following period the bike was allowed to coast freely and finally during the third part the bike was brought back to standstill (before it hit a wall!).

A major restriction on the spread of the measurements was the top speed of the person propelling the bike along. The person propelling the bike not only had to be able to accelerate the bike to its top speed in an as short a time as possible (the quicker the bike reached top speed the less distance it had covered and the more space that was left for the free coasting of the bike) but he had to also be able to keep up with the bike and then bring it back to standstill before it collided with a wall. World class sprinters cover the 100m in about 10 seconds. Therefore they have a top speed above $10ms^{-1}$ however at that speed they are not able to run with a bike. We are not world class sprinters and had to be content with a lower top speed. The top speed that was measured was around $6.5ms^{-1}$

The safest speeds for the electronics on the bike are the bikes' "stable range" speeds as at these speeds the bike would not fall over, possibly causing a malfunction.

The dynamic model predicted that, when the bike was coasting at a slower speed than the lowest stable speed, the bike would weave in an unstable manner and the slower the bike was going the more unstable the motion would be (The real part of the eigenvalue becomes larger with decreasing speed).

At speeds above the stable speed range it was predicted that the bike would only tip over (capsize) after a long time (the positive eigenvalue remains very small). According to the model this would only occur above $7.8ms^{-1}$ which

is a speed that would not be reached during the tests! The tests thus started by measuring at the lower end of the stable speed range and increased to the maximum attainable speed before tests at the lower speeds were carried out(in steps decreasing to $0ms^{-1}$).

We wanted to measure the dynamic response of the bike at the different speeds and calculate the corresponding motion eigenvalues. To achieve this the bike had to show some lateral dynamics. At speeds below the stable speed range no lateral excitation was required as the bike was never released perfectly vertically and moving in a perfectly straight line, allowing the bike to remain in equilibrium. Furthermore at the lower speeds and due to the small asymmetry of the bike, the bike automatically tended to lean to the right when released, thereby ending up rolling in a large circle rather than a straight line. This circular path allowed us to extend the length of the measurement as the bike could be set on a path that allowed it to practically return to the starting position (like a boomerang!). At the low speeds the bike always started to weave about its general heading and this motion was measured.

At speeds in the stable speed range however the bike set it self in an upright position and showed no dynamic behaviour unless it was given a lateral excitation. This excitation was achieved by applying a lateral impulse to the bike. Such an impulse was accomplished by simply hitting the bike's rear frame by hand in the lateral direction.

3.3.3 Data Storage

Each measurement started as soon as the "start" button is pressed on the computer. From then on, data from the sensors was recorded on the laptop. Essential for the processing of the run data were the videos made of each run. In order to be able to differentiate between the three parts of each run - the speeding up, coasting and slowing down, each run was filmed. The video also helped to identify nonstandard measurements and the quality of the launch etc. It was thus possible to compare the recorded data afterwards with the video images and extract the relevant data for the calculation of the eigenvalues from each file.

To ensure that each run had its data saved separately, each run was saved under a different name, starting with run 01 for the first run, 02 for the second and so on. Runs never receive the same name, even if they were made on different different days, and placed in different directories as they would undoubtedly get mixed up at some point.

To ensure that each filmed run was compared with the correct data, the run name was visible in the video. The run number was shown in the video by having a white board with the run number on it in the initial shot, before the run started. This way if the video was altered or renamed the run name was still visible and the video could still be compared to the actual data. The visible run number in the video also helped when the video was being edited and cut from one long video to the shorter individual run videos. The editor did not have to ensure that he kept track of where he was in the film during the editing to ensure that each run received the correct name.

Chapter 4

Bike Parameter Measurements

Before the physical rolling tests with the bicycle were carried out, all twenty five design parameters of the silverbike were measured. The bicycle was measured with all the measurement equipment including the laptop and sidewheels, installed as shown in figure 4.1. The results are presented in table 4.1 on page 50.

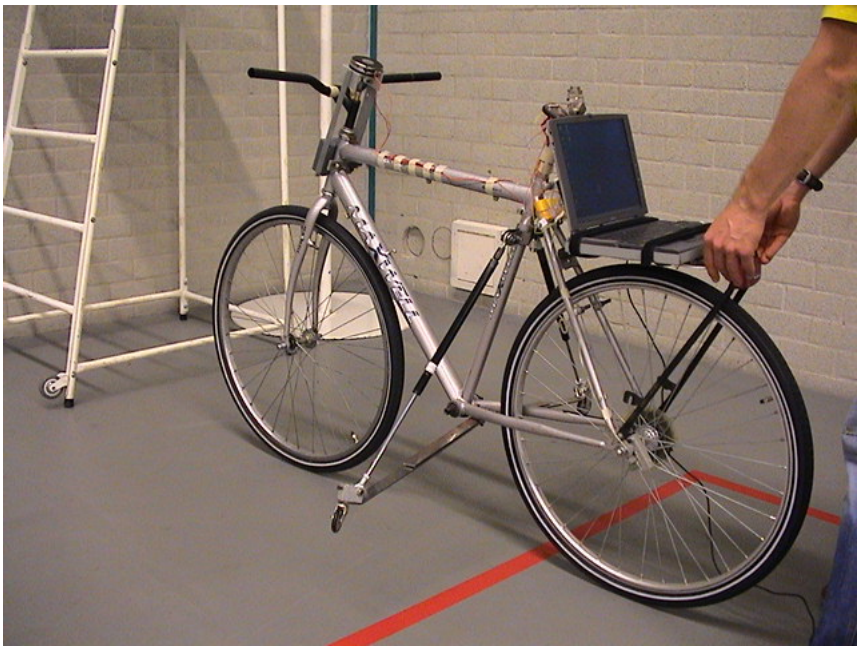

Figure 4.1: The "stripped" bike as it was measured: with all the measuring equipment and training wheels

The twenty five parameters can be divided into two groups, geometrical properties and mass properties.

4.1 Geometry

The following geometrical parameters of the bike are important for the validation of the model: The wheelbase, head angle, trail and wheel radius of the front and rear wheels. In figure 1.2 the head angle, wheelbase, and trail of a bike are shown schematically.

The wheelbase was measured on flat ground by measuring the distance from the centre of the front contact patch to the centre of the rear contact patch whilst clamping the bike in position and ensuring that the front fork was aligned with the rear frame.

The head angle was measured by placing the bike on level ground (measured with a spirit level), whilst keeping the bike perfectly vertical (also measured with a spirit level) and placing a protractor with integrated spirit level against the front of the head tube.

The measurement of the trail was more complicated. The bike was placed on flat ground in the vertical upright position with the front fork facing forwards. The bike was held in place by a clamp. The head tube was extended by means of a plate and rod such that the point of intersection with the level ground was located. The contact point of the wheel was located by visual inspection. The trail was measured by measuring the distance parallel to the x-axis of the bike between the contact point of the wheel and the point of intersection of the head tube with the ground.

There are two different criteria for the wheel radius. The unloaded radius, and the loaded radius, or rolling radius of the wheel. In the model the wheels are modelled as stiff and non-slipping. This project is about determining whether they can indeed be modelled as such. The unloaded radius is the radius of the wheel when it is not loaded, for example when the wheel is held in the air. The tyre in this case is round and is not deformed at the contact patch. The loaded radius is the radius of the wheel under its normal load.

The loaded radius is always smaller than the unloaded radius. As such the centre of the wheel is therefore higher above the ground in the unloaded radius position than for the loaded radius.The measured speed will also be larger if the unloaded radius value is used in its calculation. Because we defined the forward speed as:

$$V = -R_{rw}\dot{\theta}_r \tag{4.1}$$

Then R_{rw} is the effective loaded radius.

The loaded radius was calculated by measuring the distance covered by the bike, when the wheel that was being measured, had travelled 9 full rotations along a straight line on the sports hall floor. The tyres were inflated to 3.5 bar overpressure during the measurement just as there was during the tests. If there had been less pressure in the tyre during the measurement the tyre would have deformed more at the contact patch under the bikes own load than it did during the tests. This larger deformation would cause a decrease in the effective rolling radius and thus a smaller distance to be covered during the

nine measured rotations. Therefore it was important to ensure that both the measurement and the tests were carried out with the tyres at the same pressure. Repeated measurements resulted in the same measured travel distance within $\pm$ 1 mm. Nine rotations were used because this was the maximum amount that we could measure with a 30 m long measuring tape. The distance measured was then divided by 9 to get the distance travelled during one rotation and then divided by 2π to get the radius.

4.2 Mass & Mass Moments of Inertia

The model is composed in such a manner that it requires the mass and moment of inertia of the bike to be split into four different parts: the front wheel, rear wheel, front frame and rear frame. For each part the mass, the location of its centre of gravity and the mass moments of inertia at the centre of mass about the global xyz-axes (see figure 1.2) must be found. Note that this is with all measuring equipment including the laptop and with the sidewheels on the bike.

4.2.1 Mass Measurement

The mass of the rear frame and wheels was measured to an accuracy of $\pm$0.01 kg using a digital, hook-type set of scales. The mass of the front fork assembly was measured on digital kitchen scales that was calibrated using known weights. The Front frame was therefore measured to an accuracy of $\pm$0.001 kg The measured weight of each part is listed in table 4.1.

4.2.2 Mass Moments of Inertia Measurement Methods

Three methods for finding the mass moments of inertia were investigated. Firstly by a virtual model, then by a trifilar suspension and finally a torsional pendulum before the choice for the torsional pendulum was made. Experiments were then carried out and the values for the different parts were calculated.

Virtual Pro-Engineer Model

The DUT03, DUT04 Formula Student cars were completely designed in Pro-Engineer. From these models their mass and moment of inertia matrices were extracted and compared to values measured with the real cars. The results were very similar and thus the assumption to use the values from such a virtual model of the car could be considered validated. If such a complex vehicle could be accurately modelled in Pro-Engineer, the obvious assumption was to do the same for a very simple vehicle: the bicycle.

The main advantage with such a virtual model is that once the bike and its parts have been drawn, if the configuration of the bike is changed, for example because the front fork is rotated 180°, only a small adjustment in the digital model is required to quickly produce the new moment of inertia values. Another advantage is that the effect, of for example the position of the data acquisition system, on the moment of inertia could easily be examined.

The main problem with constructing an accurate Pro-Engineer model of a bike is that a bike is quite a large, but relatively light product. Therefore any inaccuracies in the model, especially at its outer ends, where tubes come

together, will have a large affect on the calculated moment of inertia. Pro-Engineer for example doesn't take into account that where two steel tubes are joined, a weld is required. The percentage of material that is present in a bike in the form of weld material, is relatively high, and thus if this is not modelled the resulting model would not be accurate.

Another problem when trying to construct an accurate model in Pro-Engineer is that without physically damaging the bike, the model will be very difficult to make precisely. For example: to model the frame's sloping tube, we need to know the tube wall thickness. to be certain that the wall thickness is modelled correctly a hole must be drilled into the pipe so that the thickness can be measured. This method assumes that the wall thickness is equal everywhere along the pipe and cross section even though the cross section of the tube varies along its length.

A third problem with making a precise Pro-Engineer model is that practically none of the tubes on the bike are made of constant cross section tubes. Only the saddle tube and the head tube are made from constant cross section tubes whilst all the other tubes have varying cross sections. Therefore to make a precise model of the tubes a vast amount of time and effort would be required.

A fourth, very important problem with constructing a Pro-Engineer model is that all the measurement equipment (the sidewheels, laptop, battery and all the other measuring equipment including the wires connecting them)have to be drawn and have their mass moments of inertia assigned to them. Practically non of these have a constant density and thus assigning them the correct mass moments of inertia would be virtually impossible without actually measuring them first.

After weighing the pros and cons, it was decided that the effort required to make a precise bicycle model in Pro-Engineer did not weigh up to its advantages. On top of this, the model would have to be validated with a physical test at some point to ensure that the values produced by the model were accurate.

Trifilar Suspension

A trifilar suspension (figure 4.2) can be used to determine the moments of inertia of an object. This type of apparatus is often used for objects with an irregular shape, which makes the calculation of the moment of inertia impractical. They are also used when CAD modelling packages (such as Pro-Engineer) are insufficient or impractical.

A trifilar suspension is a type of rotational pendulum. Three vertically held strings are connected at their lower end to a plate on which the device for which the moment of inertia is to be measured is placed. The plate is given a small angular displacement and the time of the resulting vibration is measured and is proportional to the moment of inertia of the plate and device.

The equation of motion for a trifilar suspension is:

$$\ddot{\Theta} + \left[\frac{Mgr^2}{I_G l}\right]\Theta = 0 \tag{4.2}$$

or

$$\ddot{\Theta} + \omega_n^2 \Theta = 0$$

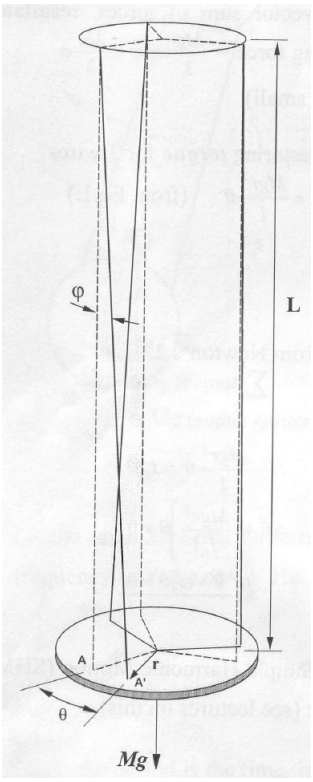

Figure 4.2: A trifilar suspension

with the period:

$$\text{period} = \frac{2\pi}{\omega_n} = 2\pi\sqrt{\frac{I_G l}{Mgr^2}} \text{ seconds} \tag{4.3}$$

Where:
I_G = Moment of inertia about the centre of the plate, for the plate plus object.
M = Mass of plate plus object.
l = Length of trifilar wires.
r = Radius from the centre of the plate to the attachment point of a wire.
g = Gravity = 9.81 m/s^2.

In order to measure the moment of inertia as precisely as possible the ratio of the moment of inertia and weight of the bike compared to that of the plate must be as large as possible. In other words, the weight and moment of inertia of the plate must be as small as possible.

The size of the plate is determined by the size of the bike rear frame as it must be positioned on the plate and kept in place. The easiest way of keeping the bike in place is by using a number of mechanical clamps that are placed on the plate. A problem however is that for every configuration of the rear frame the clamps will have to be repositioned. Not only the bike must be placed in such a manner that its centre of gravity is placed directly in line with the middle of the three wires, but also the clamps/plate centre of gravity must be directly in the middle of the apparatus. This last point makes this method difficult to carry out.

Magnetic Clamp. Instead of using mechanical clamps an idea was to use magnetic clamps for steel framed bikes. A magnet was used to clamp the bike between the magnet and the trifilar suspension plate. A test configuration was made of the following parts:
• 3 pieces of 1m long perforated L profile steel beams, connected to make a 4.0kg equilateral triangle.
• 2 industrial magnets (capable of carrying a 12 kg steel beam) weighing a total of 3.2 kg.

To calculate the time of the oscillation of the trifilar suspension apparatus alone, the moment of inertia of the triangle was assumed to be approximately mr^2 where, m = 7.2 kg and r = L/3. where L is the length of the perforated L profile. The length of the cables was chosen as long as physically possible (3 m) so that the time of one oscillation would take as long as possible. The radius, r of the centre of the trifilar suspension to the wires is equal to $\frac{1}{\sqrt{3}}$. These figures were placed in equation 4.3. The resulting time of one oscillation would be 1.737 seconds.

For the calculation of the time period for the bicycle rear fame and trifilar suspension together, the mass and moment of inertia of the rear frame had to be added to that of the trifilar suspension. Assuming that the bike weighs 8kg and can be modelled as (l) 1m long beam, then its moment of inertia about the centre is equal to $\frac{1}{12}ml^2 = \frac{2}{3}$. These values can then be added to those of the trifilar suspension and placed in equation 4.3 giving an oscillation time equal to 2.15 s.

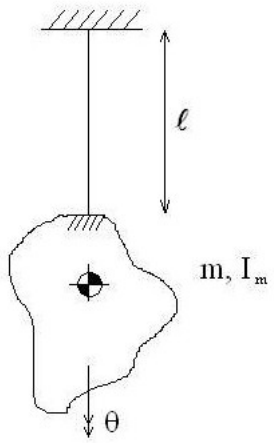

Figure 4.3: A schematic diagram of a torsion pendulum

The difference between only the trifilar suspension (1.7 s) and the trifilar suspension with the bicycle rear frame (2.15 s) can be measured.

The bicycle front frame can be modelled as a 2kg beam with an approximate moment of inertia of 0.1. When placed in equation 4.3 the resulting time for one oscillation is just 1.847 s. The difference between the the time for the trifilar suspension alone and that of the trifilar suspension with the front frame is only 0.11 s. This makes it very difficult to say to any degree of accuracy what the moment of inertia of the front fork will be in real life.

From the above it was concluded that the time of the oscillations had to be measured very precisely. Practically though this was very difficult because upon applying a torque to the test set up the apparatus would always start translating as well as rotating which makes the measurement of the time of the rotation extremely difficult to measure accurately.

An extra problem with the magnetic clamps that was noted with the test setup was that the magnets were not able to hold a bicycle in place. The tubes of both the bike and the perforated steel L profiles were to thin to produce sufficient magnetic force to clamp the bike to the triangular frame.

Torsion Pendulum

A third method for calculating the moment of inertia of the parts of a bicycle is by using a torsional pendulum. A schematic diagram of a torsion pendulum is shown in figure 4.3. The torsional pendulum is made of a long slender steel rod that is clamped vertically at its upper end. At the lower end the rod is connected via a stiff coupling to the bike part that is to be measured. The bike part is then set into an angular oscillation and the time period of the oscillation is measured and converted to the moment of inertia. The bike part is clamped underneath the rod with its center of gravity on the rotational axis of the rod to ensure that we measure about the centre of mass axis and that there is no bending moment in the rod that can disturb the angular oscillation of the system.

The torsional rigidity of a rod can be written as [18]:

$$\theta = \frac{TL}{GI_P} \tag{4.4}$$

Where:
θ = The angle rotated along the rod.
T = The applied torque to the rod.
L = The length of the rod.
G = Shear modulus of elasticity of the rod material ($75\times10^9\ N/m^2$ for steel [18]).
I_P = Polar moment of inertia of the rod, which for a cylindrical rod is equal to:

$$I_P = \frac{\pi d^4}{32} \tag{4.5}$$

Where, d is the diameter of the rod.

The equation of motion for the torsion pendulum can be written as:

$$I_M\ddot{\theta} + T = 0 \tag{4.6}$$

Where, I_M is the mass moment of Inertia of the bike and pendulum construction. Equation 4.6 is a second order linear differential equation with no damping which can be rewritten as follows:

$$I_M\ddot{\theta} + \left[\frac{GI_P}{L}\right]\theta = 0 \tag{4.7}$$

$$\ddot{\theta} + \left[\frac{GI_P}{LI_M}\right]\theta = 0 \tag{4.8}$$

$$\ddot{\theta} + \omega_n^2\theta = 0$$

In equation 4.7, the term $\left[\frac{GI_P}{L}\right]$ is called the "spring rate". The period of oscillation for the torsional pendulum is thus:

$$\text{period } t = \frac{2\pi}{\omega_n} = 2\pi\sqrt{\frac{LI_M}{GI_P}}\ \text{ seconds} \tag{4.9}$$

Assuming that the moment of inertia of the torsional pendulum is negligible compared to that of the different parts of the bike we can calculate the length of rod required for a 5mm thick steel rod.

By substituting 4.5 into equation 4.9 and solving for L we get:

$$L = \frac{Gt^2d^4}{128\pi I_M} \tag{4.10}$$

for an oscillation period, $t = 2$ seconds and assuming that the moment of inertia of the rear frame is $\frac{2}{3}$ kgm^2, then the required length of rod is just 0.70 m. For the front frame the time of an oscillation with a rod of length 0.70 m would be 0.77 seconds assuming that the front frame has a moment of inertia of 0.1kgm^2. If the diameter of the rod is reduced to 3 mm then the time of an oscillation for the front frame is increased to 2.2 seconds for a 0.70 m long rod.

The rod should only receive small distortions to ensure that the material is not plastically deformed and to ensure that the spring rate term in equation 4.7 remains a linear term. The maximum angle θ_{max} that the rod may be rotated by however, should always be kept such that the shear stress remains below the yield stress τ_{max}. The larger the angle through which the rod is distorted the larger the shear stress in the rod. The maximum allowable shear stress τ_{max} in the rod can be calculated using the torsion equation [18],

$$\tau_{max} = \frac{Tr}{I_P} \tag{4.11}$$

in which r is the radius of the rod. The corresponding maximum angle that the rod can be deflected by (θ_{max}) can be calculated by substituting equations 4.5 and 4.11 into equation 4.4 and noting that r is $\frac{d}{2}$. This gives:

$$\theta_{max} = \frac{2\tau_{max}L}{dG} \tag{4.12}$$

Structural steel is the most common type of steel available. τ_{max} for this steel is rated between 200 – 700 MPa [18]. When using a 0.7 m long, 5 mm wide diameter rod, θ_{max} is between 43° and 150°. However to remain in the linear elastic region it is wise to keep the deflections small, to about $\frac{1}{10}\theta_{max}$. For this 5 mm thick steel rod this would correspond to angles between 4 and 15 degrees.

Chosen Method

The method by which the mass moments of inertia of the parts of the bike could be measured with that had the best prospects was obviously the torsional pendulum. The torsional pendulum didn't have a serious construction problem (or, at least it had a simple, readily available solution to the construction problem) which the trifilar suspension did have, neither did it leave a large uncertainty which a Pro-Engineer virtual model had. Therefore the torsional pendulum was chosen.

There are three main parts in the construction of the torsional pendulum (figure 4.11):
- the upper clamp
- the torsion rod
- the bike clamp

The Upper Clamp. This clamp holds the upper end of the rod and has to be constructed in such a way that it does not allow the clamped part of the rod to undergo a rotation. The clamp also has to ensure that the rod is held perfectly vertically to ensure that the rod does not bend when it is loaded which could disturb the oscillation.

An A-frame construction was made from perforated L shaped profiles as can be seen in figure 4.4. The A-frame was bolted to a structural pilar of the building at the top and bottom and at the two sides to ensure that the construction couldn't move or rotate. The rod was clamped between two plates by four bolts as shown in figure 4.5. The small plate had a vertical groove milled

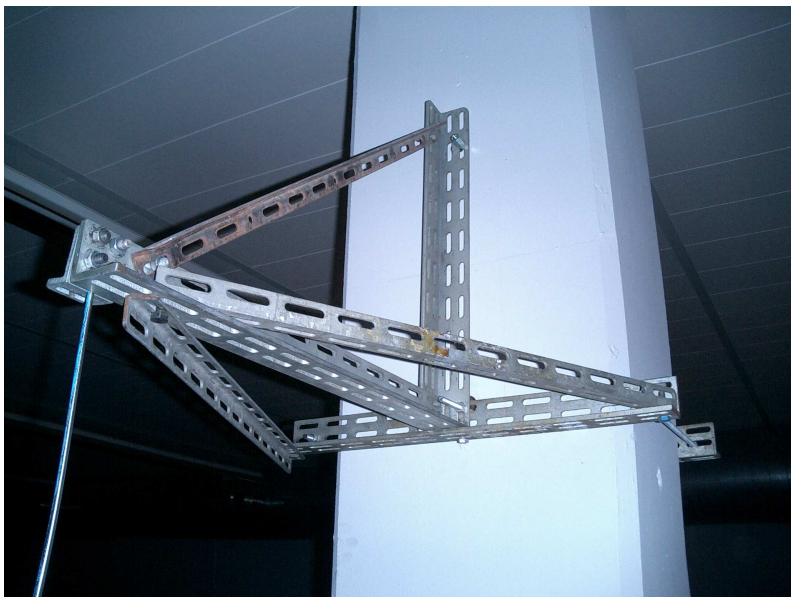

Figure 4.4: The stiff ground support for the torsional pendulum

in it to help with the alignment of the rod. The clamp was aligned using a spirit level.

The Torsion Rod. All the measurements were carried out with a standard 5 mm diameter, 1 m long steel rod. The torsion rod was clamped over 4 cm of its length at both ends leaving 92 cm free to rotate due to the applied torsional moment. This longer length was applied so that the maximum rotational angle allowed was larger than the 4 to 15 degrees, and a slightly longer period time was achieved. A 3 mm rod was acquired for the measurement of the front fork and wheels but in order to use the rod the bike clamp had to be redesigned and therefore it was not used.

The Bike Clamp. This clamp, shown in figure 4.6, was constructed in such a manner that the centre of the bike's tube is held in the clamp directly underneath the center of the torsion rod, ensuring that there is no bending moment in the rod. The clamp also had a hinge to ensure that the centre of mass of the part to be measured is in line with the torsion rod.

The clamp consists of two parts. the first, shown in figure 4.7, is made of two stiff aluminium blocks that were used to clamp the lower end of the torsional rod. The second part, shown in figure 4.8, is made of two steel plates that were bent such that they could clamp a bicycle tube between them. For the second part, three different sets of plates were used, each set having been bent such that a different diameter tube could be clamped between them. The two parts are connected to each other by an 8 mm nut and bolt. When the bolt is not tightened up it acts as the hinge. Upon tightening the bolt, the two parts form one single stiff unit clamping the bicycle to the rod.

Figure 4.5: A detailed view of the clamped rod in the ground support

Figure 4.6: The bicycle clamp assembly

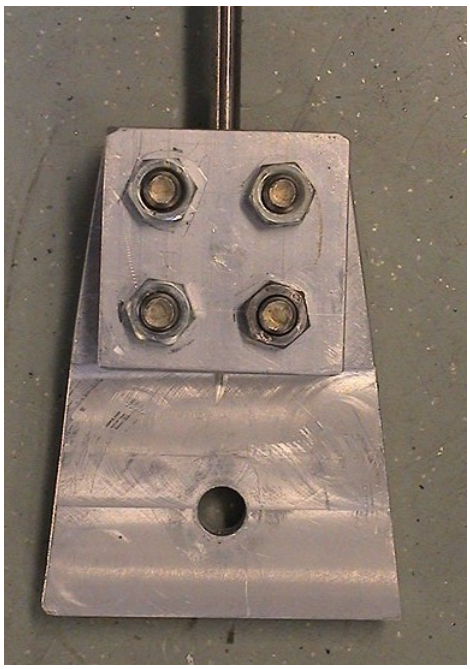

Figure 4.7: The clamp-to-rod connection part

Figure 4.8: The bicycle-to-clamp connection part

4.2.3 Data Collection and Processing of the Mass Moments of Inertia

The test procedure for the front and rear frame was essentially the same. The only difference between them was that the two metal plates that are used to clamp the bike part being measured had to be adjusted for each tube.

The frame was initially placed loosely in the lower part of the bike clamp, which had not been tightened against the upper part of the bike clamp to ensure that the rod did not receive a bending moment. The tube that would be clamped was then moved such that the it hung horizontally (measured using a spirit level). The lower clamp was then tightened around the tube. The lower part of the bike clamp was then tightened against the upper part of the bike clamp. The part then hung as shown in figures 4.10, 4.11 and 4.12. The bike part would then be given a small rotation and let go, causing it to oscillate. The time for 30 oscillations was measured for the rear frame, and the time for 50 oscillations of the front frame was measured. Each measurement was repeated three times. In retrospect we could have used the rate gyros instead and measured the frequency by curve-fitting the decaying oscillation.

The experiment was carried out on the three main frame tubes of the rear frame, the sloping lower tube, the top tube and the seat tube. For the front frame the experiment was carried out on the head tube about the pitch and roll axes and about the handlebars for the yaw axis.

The Pitch moment of inertia for the rear frame couldn't be measured directly with this experimental setup because the centre of gravity of the rear frame is not located in one of tubes of the frame about which it can be clamped. The centre of gravity is located slightly towards the rear of the seat tube. However the mass moment of inertia about the pitch axis does not show up in the linearised equations of motion and is therefore not important.

To calibrate the clamp and rod's moment of inertia, a standard steel 1.79 m long 5.18 kg weighing rod was placed in the bike clamp and allowed to oscillate. We then assumed the clamp to be infinitesimally stiff and the rod to have a stiffness according to [18]. The resulting calculated mass moment of inertia for the bike clamp was so small that it was decided that it would be assumed to be zero (see appendix D).

To reduce the uncertainty of the experiment, the term $\frac{GI_P}{L}$ in equation 4.9 for the torsion rod was calculated from the oscillation time of the test weight.

$$I_M \left[\frac{2\pi}{t}\right]^2 = \frac{GI_P}{L} = K, \quad \text{where } K\text{is a constant} \tag{4.13}$$

$$K = 5.0140\ kgm^2s^{-2}$$

This value was compared to 4.9751, the value that was generated by using the measured length of the rod (0.925 m), the calculated value for I_P (0.6136 m^4) and the standard value for the sheer modulus (75 GPa). The two were noted to be similar however by using K three uncertainties were removed:

•The exact value for the shear modulus (G) of the torsion rod did not have to be measured.

•The exact diameter of the rod, which probably was not exactly equal over the complete length of the rod, did nog have to be measured.

•The exact length of the rod that underwent torsion did not have to be found.

With this constant (K) the mass moments of inertia for the bike parts about there vertical axis perpendicular to their tubes was calculated as follows:

$$I_M = \left(\frac{t}{2\pi}\right)^2 K \tag{4.14}$$

To calculate the mass moments of inertia in the global axes about the centre of mass of the parts, we had to rotate the moment of inertia tensors. To do this we had to calculate the angle under which each measurement was made with respect to the global axes. Firstly though we located the centre of mass and found its position with respect to the global coordinates.

To find the position of the centre of mass, photographs taken horizontally at 90° to the frame, in the same position and the same distance from the bike for each of the three experiments. The photographs were then placed on top of one and other as shown in fig 4.9. The lines of the torsion rod were extended as shown. The point where the three (extended) torsion rods meet is the location of the centre of mass for the rear frame.

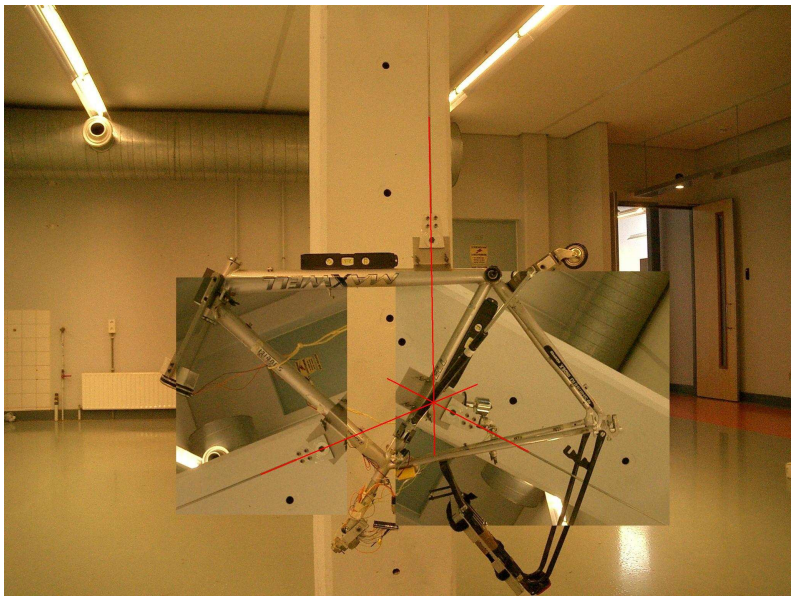

Figure 4.9: The location of the centre of gravity of the rear frame

To find the angle under which each tube was hung with respect to the global axes, the following information had to be taken into account: The top tube has a 5° slope relative to the global X-axis when the bike is on level ground. With this information and using fig 4.9 the angle of each tube relative to the global axes was calculated.

The location of the centre of mass of the bike was found in global coordinates by measuring the tube lengths in the picture and comparing them with the real lengths and calculating the scale factor. Then the distance from the rear axel

to the centre of mass could be measured in the figure and from these the global coordinates were calculated as shown in appendix D.

To calculate the global mass moments of inertia of the rear frame the inertia about the tubes had to be transformed to the inertia about the global X, Y and Z axes. This was done by noting that:

$$\begin{aligned}
\mathbf{M} &= \mathbf{I}\dot{\boldsymbol{\omega}} + \boldsymbol{\omega} \times (\mathbf{I}\boldsymbol{\omega}) \text{ , where} && (4.15)\\
\boldsymbol{\omega} &= \dot{\varphi}\mathbf{e}_i \\
\dot{\boldsymbol{\omega}} &= \ddot{\varphi}\mathbf{e}_i \text{ , and where} \\
\mathbf{e}_i &= \text{ is the unit vector rotation axis. Therefore :} \\
\mathbf{e}_i^T\mathbf{M} &= \mathbf{e}_i^T(\mathbf{I}\ddot{\varphi}\mathbf{e}_i + \dot{\varphi}\mathbf{e}_i \times (\mathbf{I}\dot{\varphi}\mathbf{e}_i)) && (4.16)\\
M_i &= \mathbf{e}_i^T\mathbf{I}\mathbf{e}_i\ddot{\varphi} \text{ , where} && (4.17)\\
\mathbf{e}_i^T\mathbf{I}\mathbf{e}_i &= \begin{bmatrix} e_{x_i} \\ 0 \\ e_{z_i} \end{bmatrix}^T \begin{bmatrix} I_{xx} & I_{xy} & I_{xz} \\ I_{xy} & I_{yy} & I_{yz} \\ I_{xz} & I_{yz} & I_{zz} \end{bmatrix} \begin{bmatrix} e_{x_i} \\ 0 \\ e_{z_i} \end{bmatrix} && (4.18)
\end{aligned}$$

Thus:

$$e_{x_i}I_{xx}e_{x_i} + 2e_{x_i}I_{xz}e_{z_i} + e_{z_i}I_{zz}e_{z_i} = I_i \text{ , for i} = 1, 2, 3$$

Where 1,2,3 are the three different axes about which the mass moment of inertia was measured. By solving the following matrix equation,

$$\begin{bmatrix} e_{x_1}^2 & 2e_{x_1}e_{z_1} & e_{z_1}^2 \\ e_{x_2}^2 & 2e_{x_2}e_{z_2} & e_{z_2}^2 \\ e_{x_3}^2 & 2e_{x_3}e_{z_3} & e_{z_3}^2 \end{bmatrix} \begin{bmatrix} I_{xx} \\ I_{xz} \\ I_{zz} \end{bmatrix} = \begin{bmatrix} I_1 \\ I_2 \\ I_3 \end{bmatrix} \tag{4.19}$$

the components of the mass moments of inertia with respect to the global reference from I_{xx}, I_{xz} and I_{zz} were found.

The mass moments of inertia about the Y-axis I_{yy} is not important because the pitch motion is not a parameter in the linearised equations of motion of the bicycle during small deviations from the straight ahead motion. The value for I_{yy} was therefore estimated from previous measurements such as those carried out by [6]. Since the xz-plane is a symmetry plane of the bicycle, the off diagonal terms I_{xy} and I_{yz} are both zero. Obviously a frame is not exactly symmetrical due to the small welded parts that are used to attach accessories, such as the dynamo, to the frame but these can be ignored as they have an insignificant contribution.

The calculation of the mass moment of inertia of the front fork was carried out in a similar manner as the rear frame except for the fact that five measurements were carried out on the front fork. One measurement was made, approximately about the y-axis through the centre of mass, to measure I_{yy} and four measurements were made in the xz-plane. The I_{xx}, I_{xz} and I_{zz} were then calculated as follows:

$$\begin{bmatrix} e_{x_1}^2 & 2e_{x_1}e_{z_1} & e_{z_1}^2 \\ e_{x_2}^2 & 2e_{x_2}e_{z_2} & e_{z_2}^2 \\ e_{x_3}^2 & 2e_{x_3}e_{z_3} & e_{z_3}^2 \\ e_{x_4}^2 & 2e_{x_4}e_{z_4} & e_{z_4}^2 \end{bmatrix} \begin{bmatrix} I_{xx} \\ I_{xz} \\ I_{zz} \end{bmatrix} = \begin{bmatrix} I_1 \\ I_2 \\ I_3 \\ I_4 \end{bmatrix} \tag{4.20}$$

Using the Matlab backslash operator a least square fit for the 4 measurements was then calculated to give the I_{xx}, I_{xz} and I_{zz} as shown in Table 4.1.

Figure 4.10: The rear frame clamped with its sloping tube in the horizontal position

Figure 4.11: The rear frame clamped with its saddle tube in the horizontal position

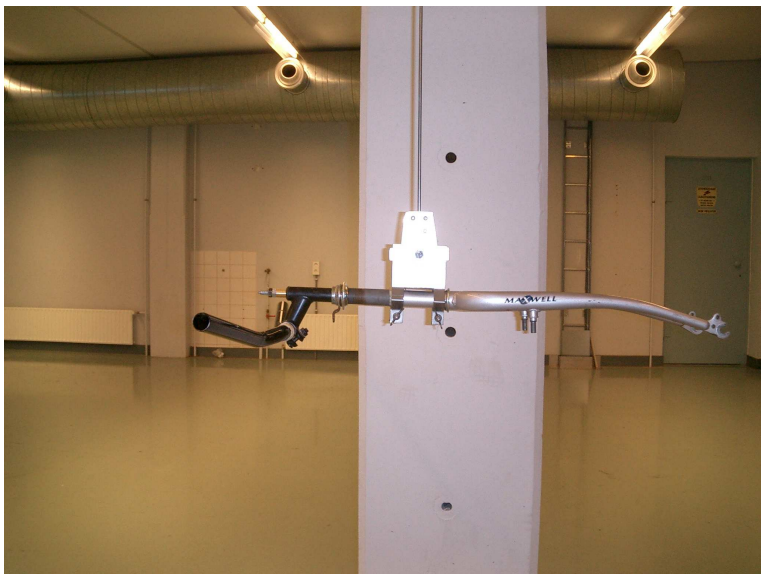

Figure 4.12: The front frame clamped such that the steering axis is horizontal

Some items had to be taken into consideration with the measurement of the mass moments of inertia measurement of the wheels as not all of the the mass of the wheels is modelled as being part of the wheel.

The linearised dynamic model assumes that the complete wheel rotates, whilst in real life some parts of the wheel don't. The weight of the front wheel for example consist of weight that rotates at the same speed as the tires do. Weight that doesn't rotate at all such as the bolts and axle that hold the wheel in place and finally there is also weight that rotates at some unknown speed such as the bearings. Ideally the axle and bolts would be weighed as part of the rear frame and the bearings could be weighed as part of the wheels. This would give the most accurate weight measurement for the wheels. However this was not done and instead the wheels were weighed as one complete unit.

The inaccuracy for the model was considered negligible because the weight is all located at the very centre of the wheel and thus has little contribution towards the moment of inertia about the axle. The axle also weighs relatively little compared to the mass of the rear frame (and sensors, computer and sidewheels) and thus its exclusion wouldn't make a large difference to the final results.

The measurement of the wheel inertia was done in two different tests. The first was carried out using the above described torsion pendulum (figure 4.13) to measure the inertia about the wheel's global X and Z axis (figure 1.2). The second test was a compound pendulum experiment, where the wheel was hung from a horizontally placed nail and given a small offset to bring the wheel into an oscillation (figure 4.14). The time for thirty oscillations was measured and averaged. Again, in hindsight this could also have been measured using the angular rate sensors.

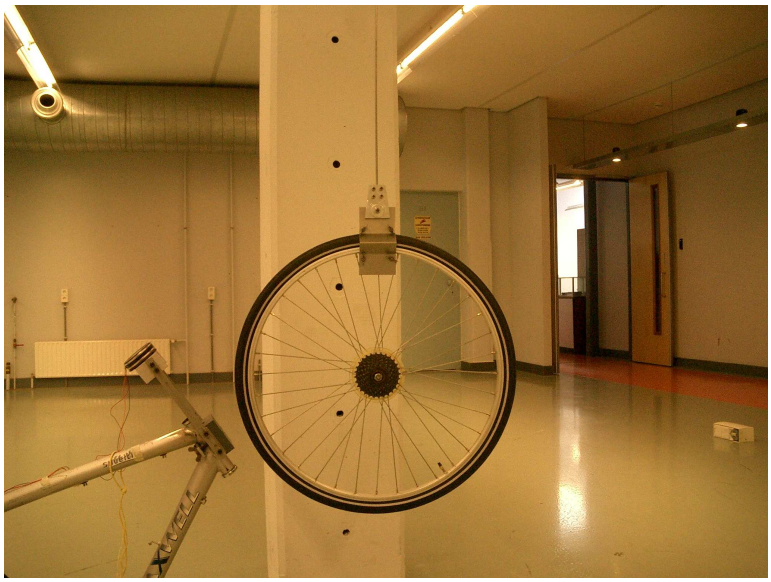

Figure 4.13: The rear wheel clamped in the torsion pendulum

Figure 4.14: The front wheel during the compound pendulum experiment

The equation for the motion of the compound pendulum is:

$$I_Y = \left[\frac{t}{2\pi}\right]^2 mgl - ml^2 \tag{4.21}$$

Where:
I_Y = The moment of inertia of the wheel about its axel
t = The time of one oscillation
m = The mass of the wheel
g = Gravity
l = The distance from the nail to the centre of mass of the wheel.

The calculation of the values are shown in the Matlab code in appendix D.

4.3 Parameter Measurement Results

The measured values for each of the twenty five parameters of the bicycle are listed below in Table 4.1. The eigenvalues for the test bicycle in the speed range 0 m/s to 10 m/s as calculated by the linearised dynamic model are shown in figure 4.15.

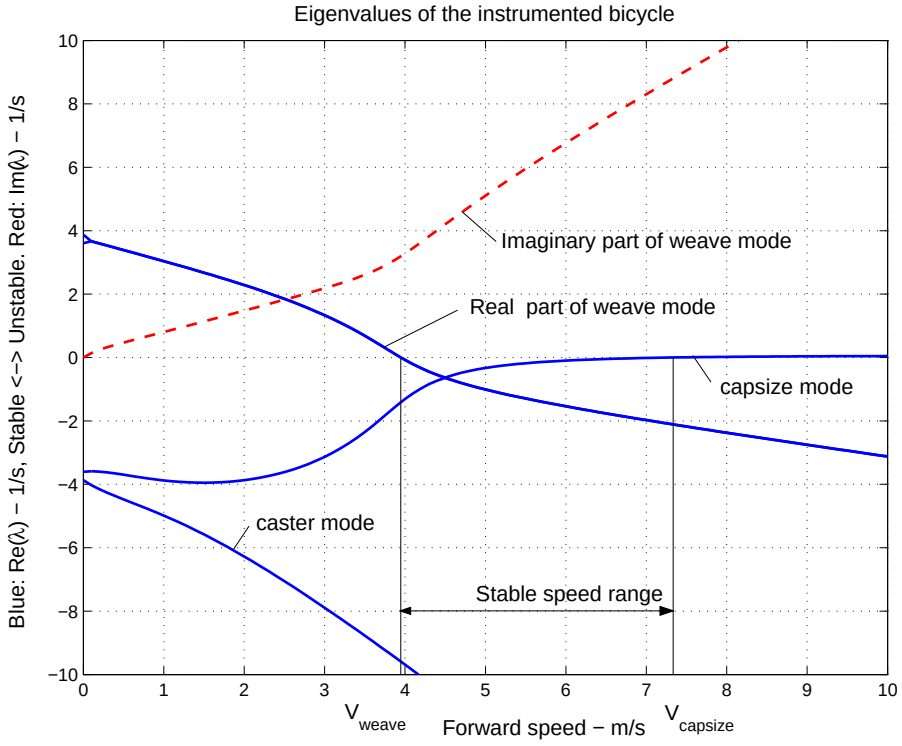

Figure 4.15: The eigenvalues for the instrumented bicycle as calculated by the linearised model.

Parameter	Symbol	Value
Wheel base	w	1.010 m
Trail	t	0.190 m
Head angle	α	69 °
Gravity	g	9.81 N/kg
Forward speed	v	*variable* m/s
Rear wheel		
Radius	R_{rw}	0.3500 m
Mass	m_{rw}	2.56 kg
Mass moment of inertia	$(\mathrm{A}_{xx}, \mathrm{A}_{yy}, \mathrm{A}_{zz})$	(0.078, 0.156, 0.078) kgm^2
Rear frame		
Position of centre of mass	$(\mathrm{x}_{rf}, \mathrm{y}_{rf}, \mathrm{z}_{rf})$	(0.320, 0, -0.627) m
Mass	m_{rf}	12.06 kg
Mass moment of inertia	$\begin{bmatrix} B_{xx} & 0 & B_{xz} \\ 0 & B_{yy} & 0 \\ B_{xz} & 0 & B_{zz} \end{bmatrix}$	$\begin{bmatrix} 0.8155 & 0 & 0.0327 \\ 0 & 1.2 & 0 \\ 0.0327 & 0 & 1.0825 \end{bmatrix}$ kgm^2
Front frame		
Position of centre of mass	$(\mathrm{x}_{ff}, \mathrm{y}_{ff}, \mathrm{z}_{ff})$	(0.909, 0, -0.793) m
Mass	m_{ff}	1.844 kg
Mass moment of inertia	$\begin{bmatrix} C_{xx} & 0 & C_{xz} \\ 0 & C_{yy} & 0 \\ C_{xz} & 0 & C_{zz} \end{bmatrix}$	$\begin{bmatrix} 0.0924 & 0 & -0.0232 \\ 0 & 0.0858 & 0 \\ -0.0232 & 0 & 0.0248 \end{bmatrix}$ kgm^2
Front wheel		
Radius	R_{fw}	0.3485 m
Mass	m_{fw}	2.05 kg
Mass moment of inertia	$(\mathrm{D}_{xx}, \mathrm{D}_{yy}, \mathrm{D}_{zz})$	(0.081, 0.162, 0.081) kgm^2

Table 4.1: The measured design parameters for the instrumented bicycle.

The stable speed range as shown in figure 4.15 for the instrumented bicycle is bounded by $V_{weave} = 3.95$ m/s and $V_{capsize} = 7.33$ m/s. In this speed range all real parts of the four eigenvalues are negative and thus the dynamics of the bicycle will damp out, returning the bicycle to the upright straight ahead position.

Chapter 5

Results and Validation of the Linearised Model

5.1 Collected Data and Challenges Encountered During Measuring

This section describes the tests that were carried out and the measured data. For a selection of the measurements, the collected data is discussed and the challenges encountered whilst carrying out the measurements and the solutions that were tried are explained.

5.1.1 Test Procedure

In total 76 runs were carried out. In each run the bicycle was propelled to approximately the desired speed and once steady it was released. During high speed runs the bicycle was then laterally perturbed. Figure 5.1 is a picture showing how the bicycle is propelled. Whilst a film of run 35 can be found on [17].

Two runs were carried out whilst stationary, eight runs were carried out at low speeds around 2 m/s. At a lower forward speed than this the bike was to unstable to be kept upright for long enough to be able to carry out any form of test. The majority of the tests were carried out in the transition region (4 – 5 m/s) and a number of tests were carried out at higher speeds up to about 6 m/s. Higher speeds than this were not attained because the operator of the bike was not able to run along side the bike, to ensure that it did not crash into one of the walls.

Each of the runs was captured on video which turned out to be extremely handy for the data analysis later on.

5.1.2 Data Collection

For each run the recorded data was stored in a text file. Shown below in Table 5.1.2 is the first part of the file for run 36.

Each data file was initially processed in Matlab and analysed by hand using a data plot as shown in figure 5.2 for run 36. In the figure the battery voltage

Figure 5.1: The bicycle being propelled during run 52

Time	Batery	Y-rate	L-rate	Speed	Steer
0.000000E+0	4.905845E+0	2.476254	2.467219	0.004715	2.896319
1.000000E-2	4.905845E+0	2.471144	2.469770	0.002166	2.896319
2.000000E-2	4.908396E+0	2.458369	2.459568	0.020014	2.891218
3.000000E-2	4.905845E+0	2.458369	2.449367	-0.000384	2.888668
4.000000E-2	4.913499E+0	2.463479	2.451917	0.002166	2.901420
5.000000E-2	4.910947E+0	2.453259	2.464669	0.009815	2.893769
6.000000E-2	4.910947E+0	2.468589	2.446816	-0.008034	2.901420
7.000000E-2	4.918601E+0	2.481365	2.449367	0.004715	2.909071
8.000000E-2	4.916050E+0	2.458369	2.449367	-0.002934	2.901420
9.000000E-2	4.913499E+0	2.471144	2.457018	-0.002934	2.903970
1.000000E-1	4.918601E+0	2.466034	2.449367	0.007265	2.903970

Table 5.1: The first part of the recorded data for run 36

can be seen (the blue line), the steering angle (magenta), the lean rate (red), the yaw rate (green) and the speed signal in cyan.

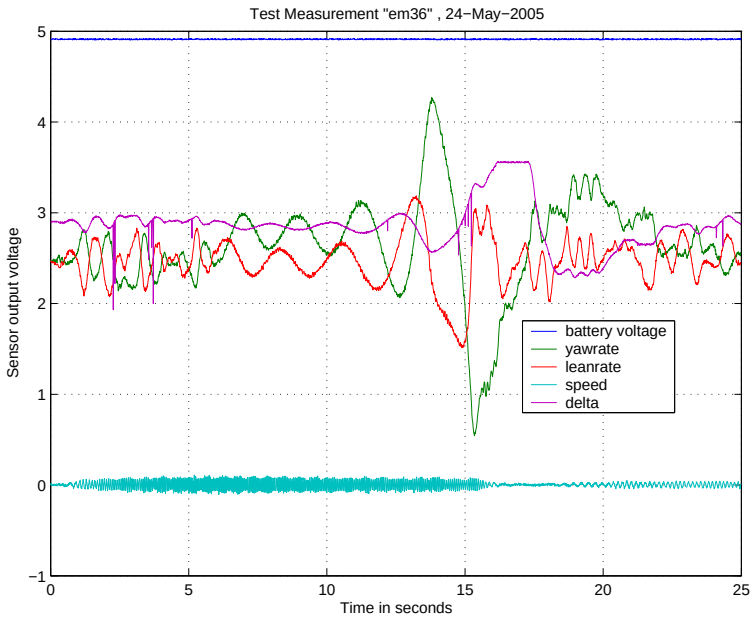

Figure 5.2: The raw data as measured by the computer for run 36

5.1.3 Challenges Encountered During Testing

The lack of lateral dynamics in the motion of the bicycle at higher speeds due to the stability of the bicycle presented a problem. The changes in sensor output for the freely coasting bicycle were very small, making it difficult to differentiate between noise and signal. This also made it difficult to locate the starting point and end point of the free coasting part of the measurement. Figure 5.3 showing run 17 is an example of such a run where the bicycle had practically no lateral dynamics. To overcome this problem we purposely initiated a dynamic response by applying an impulse in the lateral direction to the rear frame. Such an impulse can be seen in figure 5.4. The response was sufficiently large to be measured accurately, however the initial part of the response had to be neglected as it was to erratic.

In an attempt to carry out measurements at speeds above 6 m/s we tried to "pass" the bike from one person to another. The first person (the starter) accelerated the bicycle and just before he could nog longer keep up with the it he would give the bicycle an extra push, to excite the it laterally and to speed it up even further. The starter could then no longer keep up with the bicycle and it would coast freely for about 10 m to 15 m before the second person (the stopper), who would be running in the same direction as the bicycle, would be overtaken. The stopper would at this point (try to) grab onto the rear rack and bring the bicycle to a standstill before it reached the sports hall wall.

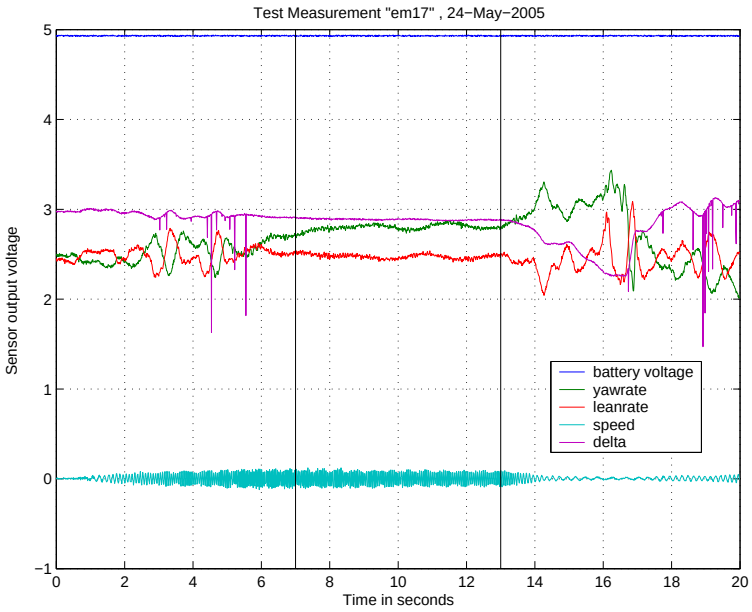

Figure 5.3: The changes measured during the free coasting period (7 to 13 seconds) are minute

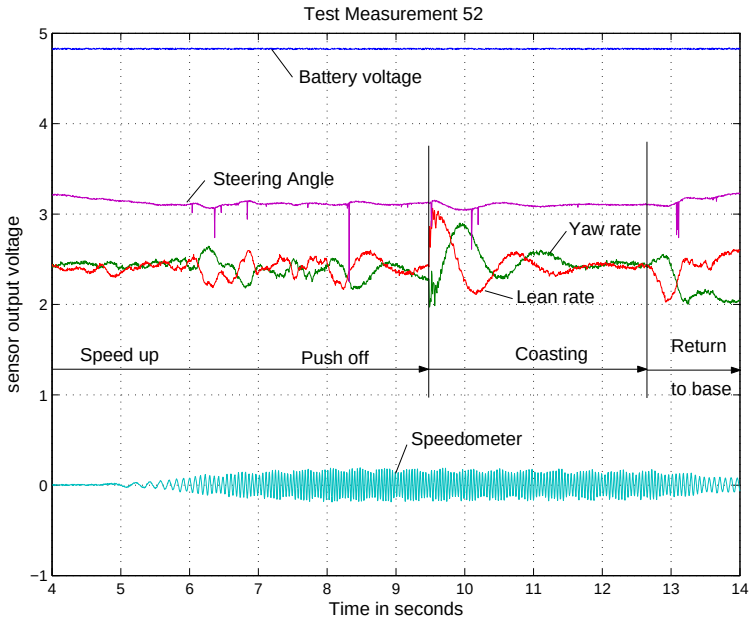

Figure 5.4: The impulse applied at t = 9.5 and the decaying response shown for run 52

During our first practice attempt in which the bicycle was propelled to a higher speed than that we could keep up with, the stopper was unable to grasp the bicycle properly. The bicycle therefore slipped out of his hands and rolled, at almost full speed, under only a slight angle from the straight ahead, into the sports hall wall. The bicycle bounced off the wall and the sidewheels rotated 45 degrees so that they no longer were held at 90 degrees to the rolling direction but instead at only 45, and came to a standstill. The computer and the sensors all seemed to function normally. However upon a further, closer inspection we noted that the steering angle coupling had been sheered from the potentiometer as shown in figure 5.5. At this point we decided that we would not attempt to carry out a measurement at high speed in the sports hall.

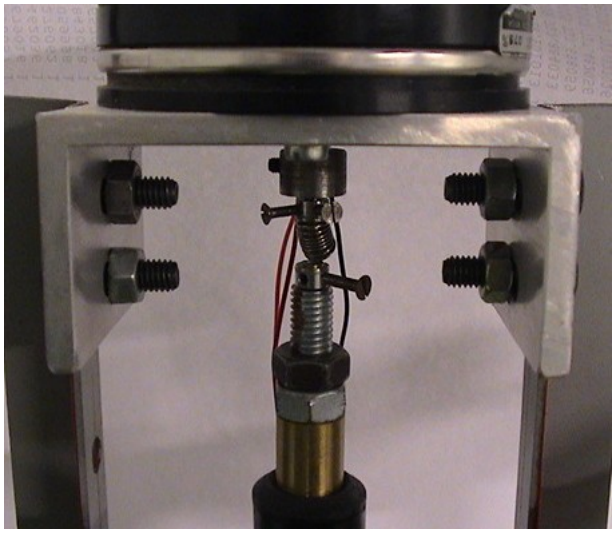

Figure 5.5: The broken steering angle coupling after crashing into a wall

The broken steering angle connector was not the only piece of apparatus that broke during the tests. In an attempt to bring some lateral dynamics into the motion, the handlebars were given an impulse. This is the standard test carried out on motorcycles. However the impulse was not a perfect impulse, but more like a step function, causing the bicycle to radically change direction and collide with the person who had just applied the impulse and causing it to flip over. The last moment before the laptop screen was destroyed can be seen in figure 5.6.

Luckily the person propelling the bicycle was not hurt in the incident and the sensors were not damaged and the computer still functioned properly after the crash. However from then on we had to connect a separate monitor to the laptop before every run to be able to adjust the file name and start the measurement. The most disappointing thing about the whole affair was that the battery voltage had dropped below 4V, thus the yaw and lean angle sensors had stopped operating, and measured nothing during the accident!

The recording of the battery voltage proved to be a vital for the analysis of the results. Not only as the absolute value of the angular lean and yaw rate

Figure 5.6: The bicycle crashing during run 107, causing the laptop screen to crack and malfunction

could be found, but it also allowed us to understand why the computer seemed to have stopped measuring these signals at a certain point! In figure 5.7, run 215 is shown. In the figure the battery voltage drops steadily from the start of the measurement till t = 15, at which point the voltage drops below 4 Volts causing the yaw and lean-rate sensors to stop functioning. From then on they give a constant signal that is approximately equal to that of the battery. As we carried out and analysed the runs in batches of 5, the following four recorded runs each had no angular lean- or yaw rate in them, which at the time did not seem logical. Upon seeing the data for run 215 it became clear that the battery pack was the cause.

5.2 Data Processing

Once the tests had been carried out, the collected data was analysed in detail. The first challenge was to make an accurate speed signal from the measured data. Then we looked at the steering angle data as this signal showed some erratic behaviour.

5.2.1 The Speed Signal

The minute speed signal that was measured as shown in figure 5.2 and 5.8 turned out to be a challenge. The signal was difficult to differentiate from background noise at low speeds as the amplitude of the noise and the signal were of a similar order. At higher speeds, and for constant speeds this was not a problem. The amplitude of the signal could not be used effectively to measure the speed however, as there was no linear relationship between the amplitude of the signal and the speed. Therefore to calculate the speed from the data we

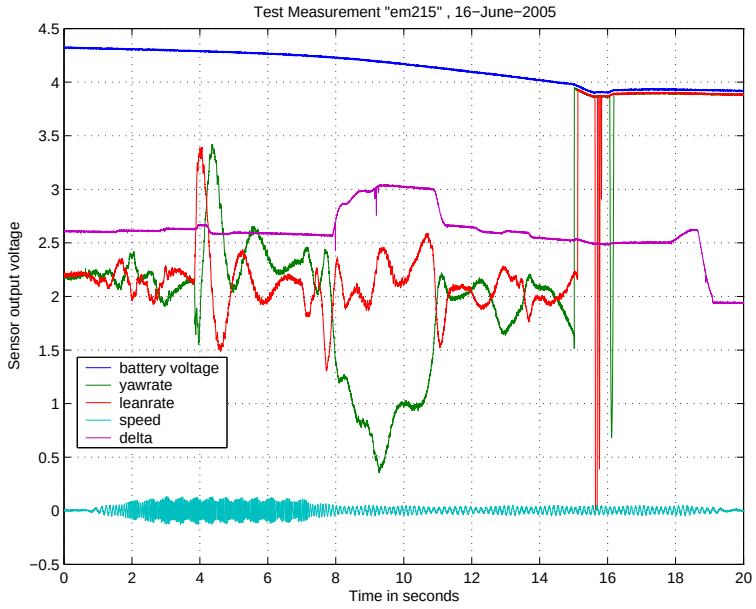

Figure 5.7: When the battery voltage dropped below 4V the rate sensors stopped working

measured the time between each zero crossing.

As the magnetic ring of the Avocet Altimeter 50, has ten (north) poles, the signal has to cross the zero axis 20 times during one rotation of the rear wheel. Therefore by measuring the time between each crossing, the speed V, can be found by:

$$V = R_{eff}\frac{2\pi}{20\Delta t} \tag{5.1}$$

Where, R_{eff} is the (rolling) radius of the rear wheel and Δt is the time between two zero crossings. We then assumed that the speed of the rear wheel remained constant between each crossing as the time between each crossing was relatively short, roughly 0.025 seconds. We thus got a signal as shown in figure 5.9 where the measured signal during free coasting is shown for run 17 (See figure 5.3 for the full measurement).

Because the speed during the free coasting did not remain constant,we calculated the line of best fit through the calculated speed in the form of:

$$V = u + at \tag{5.2}$$

where V = the speed and t = the time during the run (usually between 0 and 20 s), whilst a can be seen as a measure for the friction felt by the bike. Figure 5.9 shows the line of best fit (in red) for the free coasting portion of run 17.

At low speeds the resistance of a bike is influenced mostly by the rolling resistance C_r of the tyre, as a result of the hysteresis in the tyre due to the small

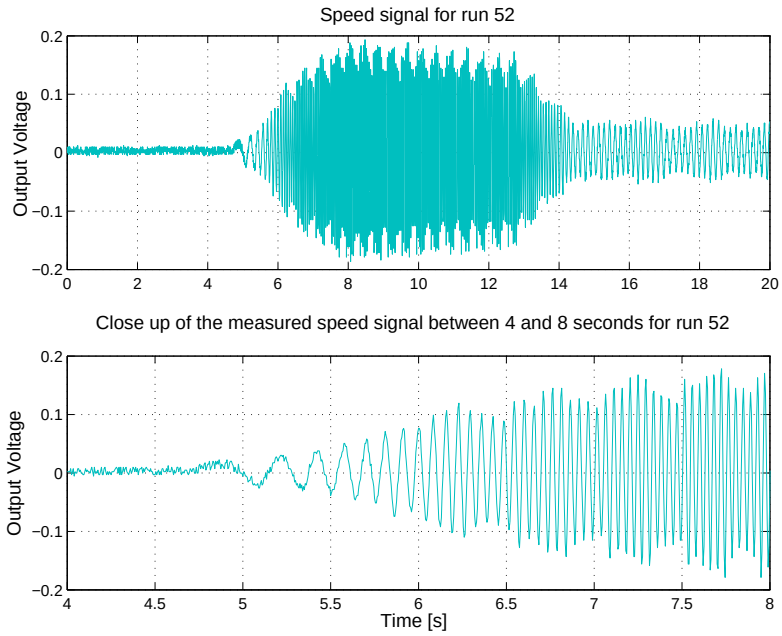

Figure 5.8: The measured speedometer signal

deformation in the contact patch, and the resistance in the bearings. At higher speeds air resistance starts to play a role as well. The measured values for a however ranged from -0.06 for lows speed measurements (2 m/s) to -0.20 for the higher speed measurements (6 m/s).

This pronounced difference between the values of a at the low and higher speeds is most likely due to the air resistance caused by the laptop screen. As it was placed almost vertically on the bicycle the screen will have almost doubled the frontal area of the bicycle. On top of this the screen's shape will not have helped matters either. Being a flat plate it has a very large drag coefficient C_d (about 1.98 whilst that of a circular cylinder (tubes of the frame) is 1.17 [19]). Thus upon increasing the speed the air resistance on the laptop screen will quickly have become the dominant resistive force for the bicycle.

If the total resistance felt by the bicycle at low speeds could however still be represented simply by the rolling resistance of the tyres (and thus ignoring the friction in the bearings and air resistance) then the rolling resistance, would be equal to:

$$C_r = \frac{-a}{g} \tag{5.3}$$

Where a is the same as in equation 5.2 and g is gravity. The rolling resistance would thus equal 0.006. Kyle and Edelman [19] measured the rolling resistance for a number of bicycle tyres and concluded that a similar tyre to the ones used in our experiment had a rolling resistance of 0.0066 making the measured speeds plausible.

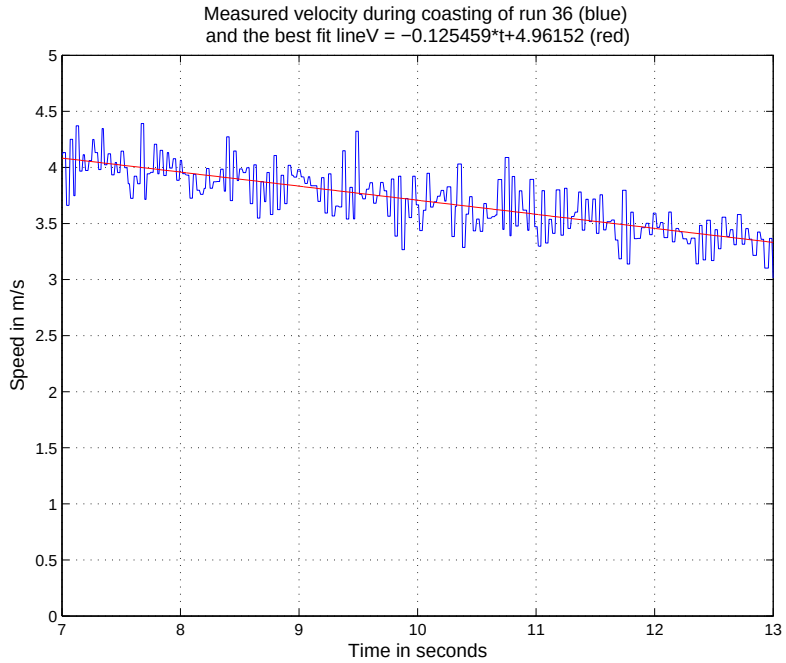

Figure 5.9: The measured speed during the free coasting period (7 to 13 seconds) showing a steady decline

Ideally we wanted to calculate the eigenvalues of the bike for each specific speed, however as the bike's speed did not remain constant, but reduced during the free coasting period, we could only calculate an eigenvalue to represent a speed range. We thus required the speed range of the bike during coasting. For this range we used equation 5.2 to calculate the initial and final speed that the bike had during the window.

5.2.2 The Steering Angle Signal

The data for the steering angle signal was rather erratic as can be seen in figure 5.10. The recorded data got worse when a higher sampling frequency was used. The signal could have been better if we had used shielded wires between the potentiometer and the USB-DAQ.

The steer-angle data almost represented a smooth line with just a couple of erratic points in the first couple of tests. Therefore we initially removed these erratic points by hand and replaced them with the value of the point measured just prior to the erratic behaviour, thereby smoothing the curve. However in later measurements, especially those measured at far higher sample rates, there were far more erratic points, and thus we automated the process.

The removal of the erratic points was done by realising that they were all caused by a "drop" in the measured voltage. By measuring the difference between each point and its previous and plotting the outcome in a graph it was noticed that there was a continuous line with a magnitude fluctuating about

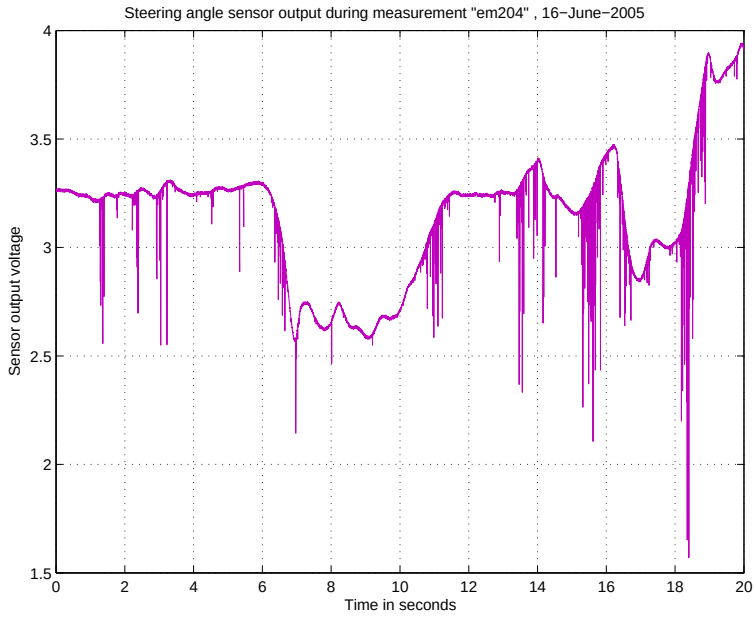

Figure 5.10: The raw measured steering angle data

the zero, with the odd large erratic spike. These spikes all acted in the same manner, they would firstly be largely negative followed by a large positive spike. Only the negative spike had to be removed as these indicated the drop in the voltage, the large positive spike indicated the return of the voltage to its original level. The spikes were then removed from the data by calculating the standard deviation of the difference line and recording the index of each point that was smaller than minus three times the standard deviation. Then with this index list we changed the measured data so that each negative spike point was changed to the same value as the previous data point. This is shown in figure 5.11. Some spikes were made of a voltage drop that lasted longer than 1 measuring point. Therefore the process was repeated until the data showed no large voltage drops anymore.

As we did not know the correct value of the "changed" data we changed the data points to "NAN" at a later stage. This meant that gaps in the steering angle graph appeared where the spikes had previously been. As a consequence of changing the data in this manner the non-linear fit function did not work if there was a "NAN" in the portion of the data that was being analysed. Therefore the "changed" data was "changed" again to the same value as the previous point in the data list.

5.3 Data Analysis

To validate the linearised model we compared the eigenvalues of the linearised model with those that could be extracted from the measured data. To extract eigenvalues from the measured data, non-linear fit optimisations were carried

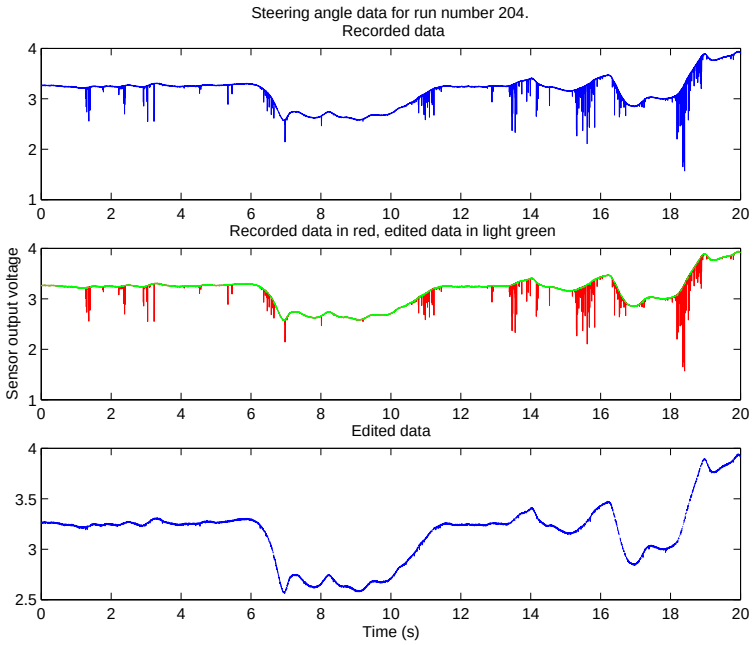

htbp

Figure 5.11: The measured and edited steering signal

out with predetermined functions on the data.

Both the weave and capsize modes were fit as well as only the weave mode on the measured data. At high speeds the calculated eigenvalues for the weave motion matched those of the model very well. It was thought that the short measurement window available during the low speed runs was the cause for the poor comparison to the model at low speed. The lean angle signal turned out to be the best signal for for the non-linear fit.

To get a better match at low speeds the weave frequency (imaginary part of the eigenvalue) was pre-described from the model thereby only the weave divergence rate (real part of the eigenvalue) had to be calculated. This did not lead to much better results.

Following a transient response analysis to small perturbations on the model at different speeds it was noticed that the capsize mode did have a direct influence on the motion at low speeds even though this eigenvalue was largely negative. It was also noted that the capsize mode had practically no influence on the dynamic behaviour at high speeds.

Another analysis of the low speed measurements was carried out where both the frequency of the weave mode and the capsize mode eigenvalue were preassigned. The resulting analysis was not better than that carried out previously.

Finally a transient response analysis was carried out for a stationary bicycle (zero speed). The analysis showed that the second largest eigenvalue can easily be extracted from the lean-rate data. This was confirmed by the analysis two separate measured runs.

5.3.1 Non-Linear Fit Function

Before we could fit a function on the collected data we had to choose the function.

Expected Signal Function

Chapter 1 describes the linearised model which this thesis is trying to validate. By fixing the speed, the equations of motion 1.2 becomes a coupled set of ordinary second order differential equations. During free coasting there is no acting force (T_ϕ and $T_\delta = 0$). Therefore equations can be rewritten as 5.4. By rewriting the equation to a set of four first order differential equations the eigenvalues of the model can be calculated. This is described below:

$$\mathbf{M\ddot{q} + C\dot{q} + Kq} = \mathbf{0} \quad \text{where,} \tag{5.4}$$

$$\mathbf{q} = \begin{pmatrix} \phi \\ \delta \end{pmatrix} \quad \text{then if,} \tag{5.5}$$

$$\mathbf{\dot{q}} = \mathbf{r} \quad \text{then,} \tag{5.6}$$

$$\mathbf{M\dot{r} + Cr + Kq} = \mathbf{0} \quad \text{which can be rewritten as :} \tag{5.7}$$

$$\mathbf{\dot{r}} = -\mathbf{M}^{-1}\mathbf{Cr} - \mathbf{M}^{-1}\mathbf{Kq} \quad \text{and thus :} \tag{5.8}$$

$$\begin{pmatrix} \mathbf{\dot{r}} \\ \mathbf{\dot{q}} \end{pmatrix} = \begin{pmatrix} -\mathbf{M}^{-1}\mathbf{C} & -\mathbf{M}^{-1}\mathbf{K} \\ \mathbf{I} & \mathbf{0} \end{pmatrix} \begin{pmatrix} \mathbf{r} \\ \mathbf{q} \end{pmatrix} \tag{5.9}$$

Equation 5.9 is of the form $\mathbf{\dot{x}} = \mathbf{Ax}$. Because $\mathbf{A}$ is non-singular it can in turn be written as:

$$\mathbf{\dot{x}} = \mathbf{TDT}^{-1}\mathbf{x} \tag{5.10}$$

where $\mathbf{T}$ is the eigenvector matrix and $\mathbf{D}$ the diagonal eigenvalue matrix. Multiplying both sides of equ 5.10 by $\mathbf{T}^{-1}$ gives:

$$\underbrace{\mathbf{T}^{-1}\mathbf{\dot{x}}} = \mathbf{D}\underbrace{\mathbf{T}^{-1}\mathbf{x}} \text{ or,} \tag{5.11}$$

$$\mathbf{\dot{y}} = \mathbf{D}\ \mathbf{y} \tag{5.12}$$

The solution to equation 5.12 is of the form:

$$\mathbf{y} = e^{\mathbf{D}t}\mathbf{B} \tag{5.13}$$

Where $\mathbf{B}$ is a vector of constants and $\mathbf{D}$ the diagonal eigenvalue matrix. This can be expanded as follows:

$$\mathbf{y} = e^{\begin{pmatrix} \lambda_1 t & & & \\ & \lambda_2 t & & \\ & & \lambda_3 t & \\ & & & \lambda_4 t \end{pmatrix}} \mathbf{B} \tag{5.14}$$

$$\mathbf{y} = \begin{pmatrix} e^{\lambda_1 t} & & & \\ & e^{\lambda_2 t} & & \\ & & e^{\lambda_3 t} & \\ & & & e^{\lambda_4 t} \end{pmatrix} \begin{pmatrix} b_1 \\ b_2 \\ b_3 \\ b_4 \end{pmatrix} \tag{5.15}$$

Thus by substituting $\mathbf{y} = \mathbf{T}^{-1}\mathbf{x}$ back into equation 5.13 we thus get

$$\mathbf{T}^{-1}\mathbf{x} = e^{\mathbf{D}t}\mathbf{B} \quad \text{or,} \tag{5.16}$$

$$\mathbf{x} = \mathbf{T}e^{\mathbf{D}t}\mathbf{B} \tag{5.17}$$

Therefore each of the four components of $\mathbf{x}$ ($\dot{\phi},\ \dot{\delta},\ \phi,\ \delta$) can be written as:

$$x_i(t) = \beta_{i,1}e^{\lambda_1 t} + \beta_{i,2}e^{\lambda_2 t} + \beta_{i,3}e^{\lambda_3 t} + \beta_{i,4}e^{\lambda_4 t} \tag{5.18}$$

Where $\beta_{i,j}$ is a constant.

According to the linearised model, Silverbike has a complex conjugant pair of roots at every speed above 0.067 m/s. Therefore the eigenvalues can be written as $\lambda_{1,2} = d \pm i\omega$ for the weave motion, $\lambda_3 = \lambda_{cap}$ for the capsize motion and $\lambda_4 = \lambda_{cas}$ for the stable castering mode. equation 5.18 can thus be rewritten as:

$$q_i(t) = e^{dt}(C_1\cos(\omega t) + C_2\sin(\omega t)) + C_3e^{\lambda_{cap}t} + C_4e^{\lambda_{cast}t} \tag{5.19}$$

To validate the linearised model we thus wanted to fit a similar function on the measured steering angle and lean-rate data. According to the linearised model, for a certain speed, the yaw-rate can simply be written as a linear combination of the steering angle and the steering rate ($\dot{\psi} = A\dot{\delta} + B\delta$ where A and B are constants). Thus the yaw-rate could also be fit using the same function.

If equation 5.19 describes the lean angle ϕ for example, then by differentiation we get the lean-rate:

$$\begin{aligned}
\dot{\phi}(t) &= de^{dt}(C_1\cos(\omega t) + C_2\sin(\omega t)) + \\
&\quad \omega e^{dt}(C_2\cos(\omega t) - C_1\sin(\omega t)) + \\
&\quad C_3\lambda_{cap}e^{\lambda_{cap}t} + C_4\lambda_{cas}e^{\lambda_{cas}t} \\
\text{or,} & \\
\dot{\phi}(t) &= e^{dt}((C_1d + \omega C_2)\cos(\omega t) + (dC_2 - C_1\omega)\sin(\omega t)) + \\
&\quad C_3\lambda_{cap}e^{\lambda_{cap}t} + C_4\lambda_{cas}e^{\lambda_{cas}t}
\end{aligned} \tag{5.20}$$

Equation 5.20 describes the lean-rate in a similar form as the lean angle. The magnitude of each mode of the lean-rate therefore depends on both the magnitude of the constant and of the eigenvalue of the mode (the size of its' λ). For example if λ_{cap} is very small, (almost zero) as is the case at around 6 m/s (according to the linearised model), then the $e^{\lambda t}$ component will be almost equal to 1 but the "constant" multiplying it, will still be small, thus the total value for the λ_{cap} component of the signal will be very small.

Fit Function Choice

In Figure 4.15 the calculated eigenvalues for the silverbike, according to the linearised model were shown. At every speed the caster eigenvalue (λ_{cas}) is largely negative. Therefore its' motion is damped out very rapidly, minimising the contribution to the total lean rate. We therefore did not try to reconstruct the caster mode from the gathered data.

A similar situation was expected in the low speed range (0 to 3.5 m/s) for the capsize eigenvalue (λ_{cap}). In this range the capsize eigenvalue is about -4 and thus expected to be damped out swiftly. At higher speeds the capsize eigenvalue becomes very small (initially slightly smaller than zero and from about 8 m/s onwards, slightly larger than zero) thus the capsize mode is not heavily damped. However due to the $C_3\lambda_{cap}$ coefficient multiplying the $e^{\lambda_{cap}t}$ in equation 5.20

the total size of the motion is tiny and thus have practically no contribution in the lean rate motion.

The weave mode's real eigenvalue (d), at low speeds, is largely positive. Its contribution to the lean rate was therefore expected be very measurable. At high speeds d is in the -1 to -2 range according to the model. This value is large enough to allow the mode to remain measurable and at the same time it is also still small enough to ensure that the mode does not damp out to rapidly. The frequency of the weave mode ω, can easily be measured from the oscillation period of the signal. The higher the speed, the higher the expected frequency of the weave mode and the easier it should be to measure this accurately as more oscillations will fit per measurement window.

In the transition speed range (3.5 to 5 m/s) the (real) eigenvalues of the weave and capsize mode are of a similar order and thus it was thought that it might be possible to measure capsize mode as well.

The Matlab command *fminsearch* was used to carry out the non-linear fit. We tried two different approaches simultaneously: Firstly we assumed that the measured steering angle, lean rate and yaw rate were only a function of the weave mode. For this "weave only" approach only the real and imaginary parts of the weave motion were assumed to be present in the measured signal. We used the following function in the non-linear fit:

$$y = C_1 + e^{dt}(C_2 cos(\omega t) + C_3 sin(\omega t)) \tag{5.21}$$

Where C_1, C_2 and C_3 are constants and d and ω are the real and imaginary parts of the weave motion.

The second approach also took the capsize mode into consideration in the non-linear fit. This "weave and capsize" approach used the following function to fit on the measured data:

$$y = C_1 + e^{dt}(C_2 cos(\omega t) + C_3 sin(\omega t)) + C_4 e^{\lambda_{cap} t} \tag{5.22}$$

Where C_1, C_2, C_3 and C_4 are all constants, d and ω are the real and imaginary parts of the weave eigenvalue respectively and λ_{cap} is the capsize eigenvalue.

5.3.2 Data Analysis by Eye

The start and end time for each runs' non-linear fit was chosen initially on the basis of the video of the run and by analysing the runs' data graph by eye. The resulting non-linear fit was then analysed, again by eye, and the chosen starting and/or finishing time of the fit was changed until we were satisfied with the resulting non-linear fit. To illustrate this procedure the steps carried out for run 36 are described below.

After analysing the video and figure 5.2 we chose a 3.5 second window starting at t = 8 on which to carry out the non-linear fit. First we found the speed range for the bicycle during the window period as shown in figure 5.12. Then we carried out a 2 and a 3-part eigenvalue non-linear fit on each of the three signals. The results for the 3-part eigenvalue fits are shown in figures 5.13 through

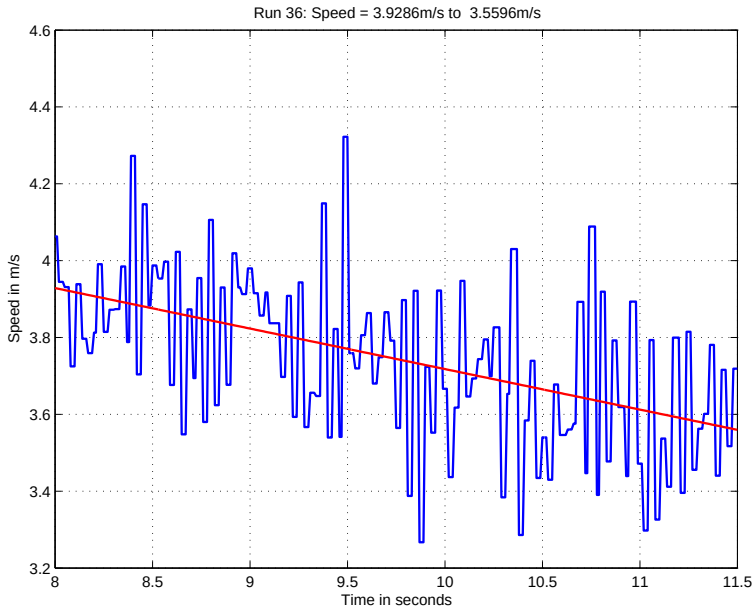

Figure 5.12: The calculated velocity for run 36 from t=8 till t= 11.5

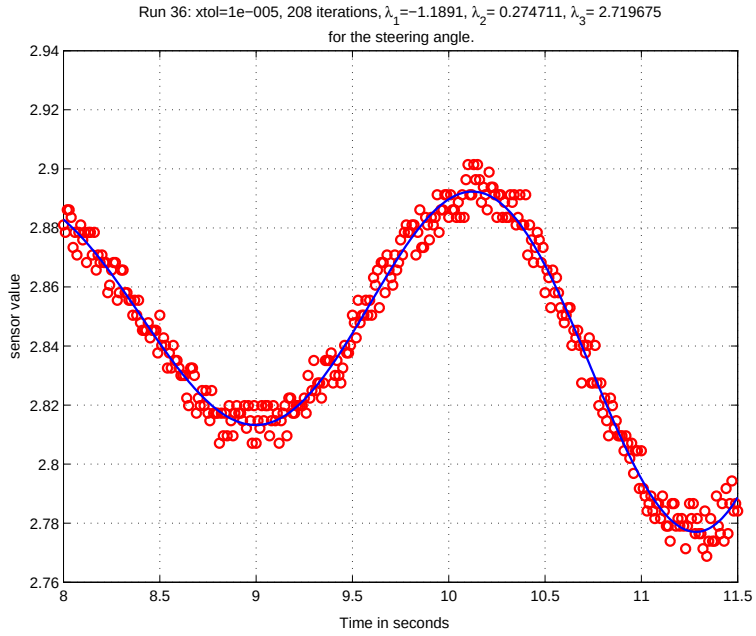

Figure 5.13: The non-linear fit of the steering angle data for run 36

5.15 for the steering angle, yaw rate and lean rate respectively. We then tried to optimise the fit. This was done by changing the time window and simply judging by eye how well the fit followed the data.

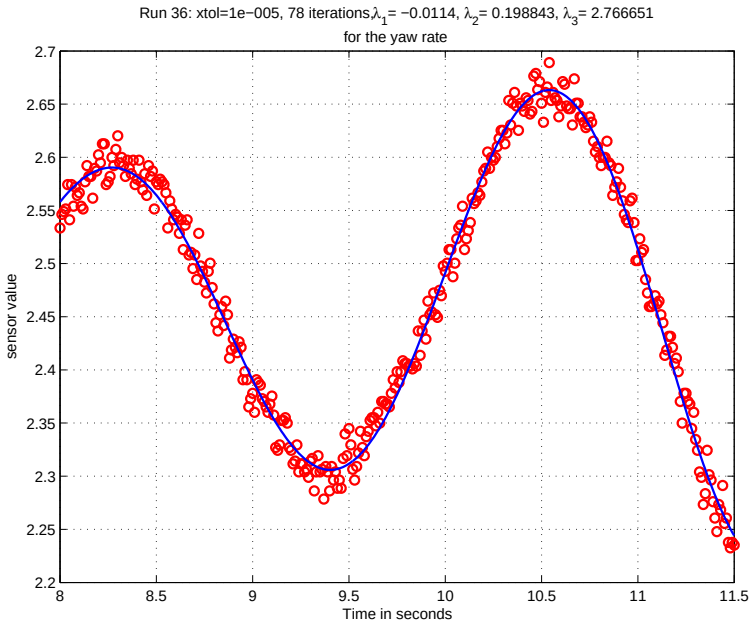

Figure 5.14: The non-linear fit of the yaw-rate data for run 36

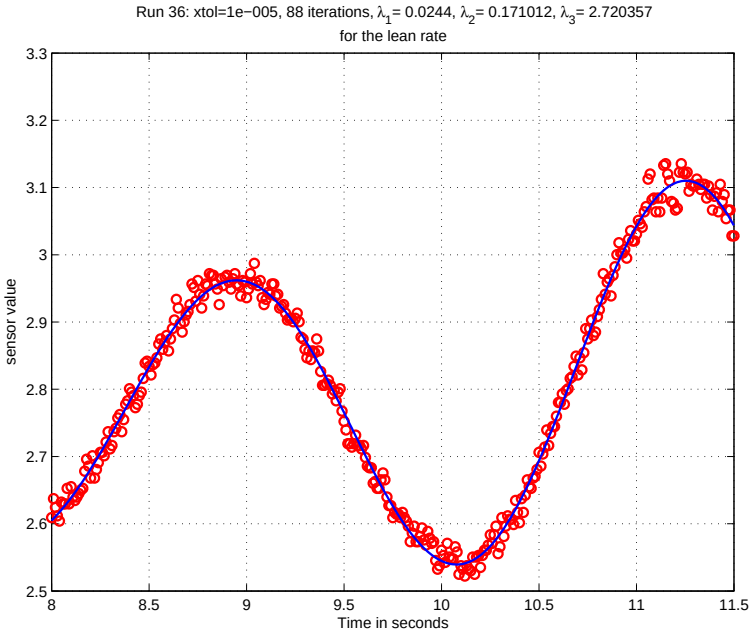

Figure 5.15: The non-linear fit of the lean-rate data for run 36

The, run number, window time, speed range during the window and the eigenvalues for each of the 2 and 3-eigenvalue fits were recorded in a text file. This file was then used to make a plot of the found eigenvalues to compare them with those of the model. This is shown in figure 5.16 for the 3-eigenvalue fit for run 36. As can be seen the non-linear fit eigenvalues were not always similar to those of the model. Once all the runs had been processed we were able to,

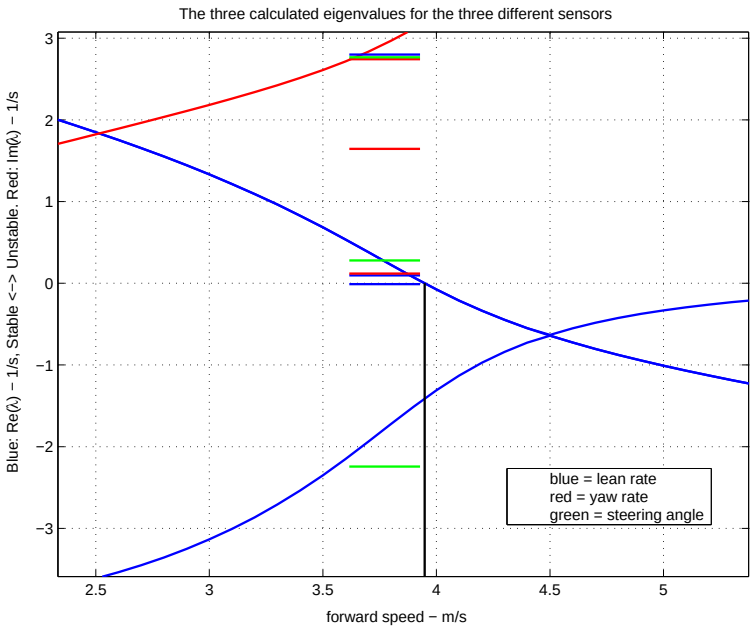

Figure 5.16: The 3 non-linear fit eigenvalues for each of the 3 sensors in relation to the eigenvalues calculated by the model

for the 2 and 3-eigenvalue fits separately, compare the calculated eigenvalues for each signal with the model's eigenvalues. Figures 5.17, 5.18, 5.19 are the graphs for the lean-rate, yaw-rate and steering angle for the "weave only" fits respectively. In the same order figures, 5.20, 5.21 and 5.22 show the fits for the "weave and capsize" function.

After analysing the graphs 5.17 through 5.22 and all the results gathered, we concluded the following:

1. The capsize mode eigenvalue could not be calculated accurately at any speed range. The value for the capsize mode varied tremendously between measurements and when the measurement window was adjusted slightly. It had a very random nature. This was true for each of the three measured signals.

2. The weave eigenvalues that were calculated from the data of each sensor and for both the "weave" and "weave and capsize" methods were very similar to those of the model for speeds above 3 m/s. However there were a couple of "odd" results. Upon inspecting the original data of these results, we found that each of these runs had practically no dynamics in them. i.e.

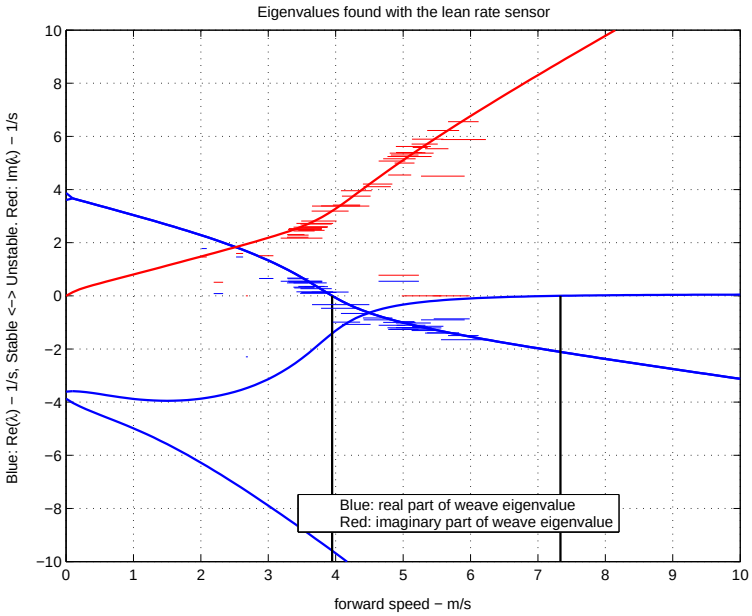

Figure 5.17: The calculated weave eigenvalues using the lean rate sensor with data chosen by eye

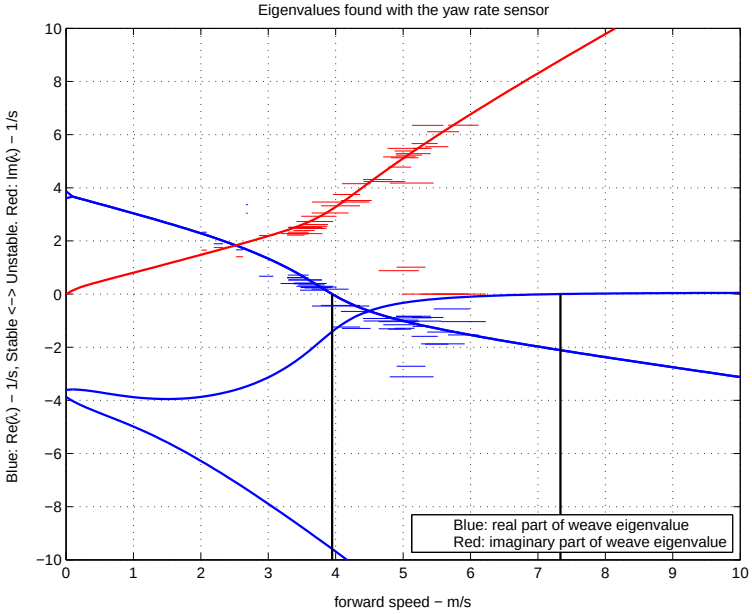

Figure 5.18: The calculated weave eigenvalues using the yaw rate sensor with data chosen by eye

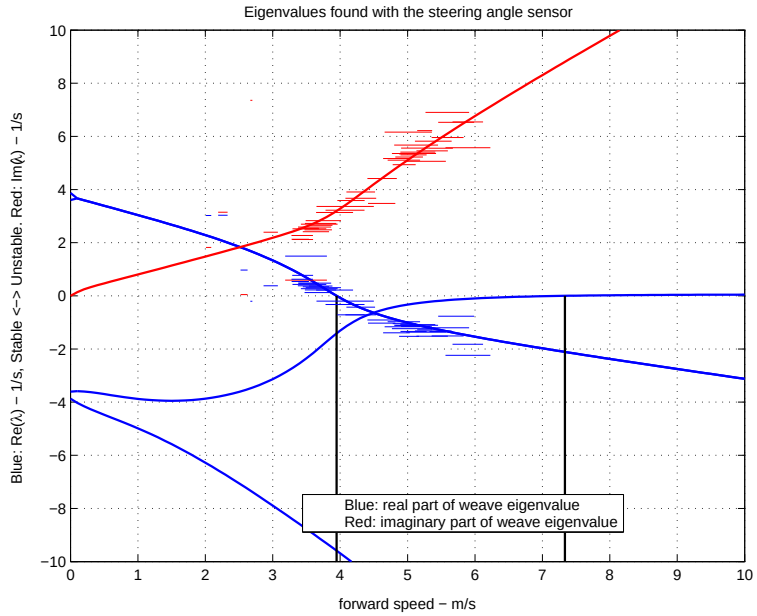

Figure 5.19: The calculated weave eigenvalues using the steering angle sensor with data chosen by eye

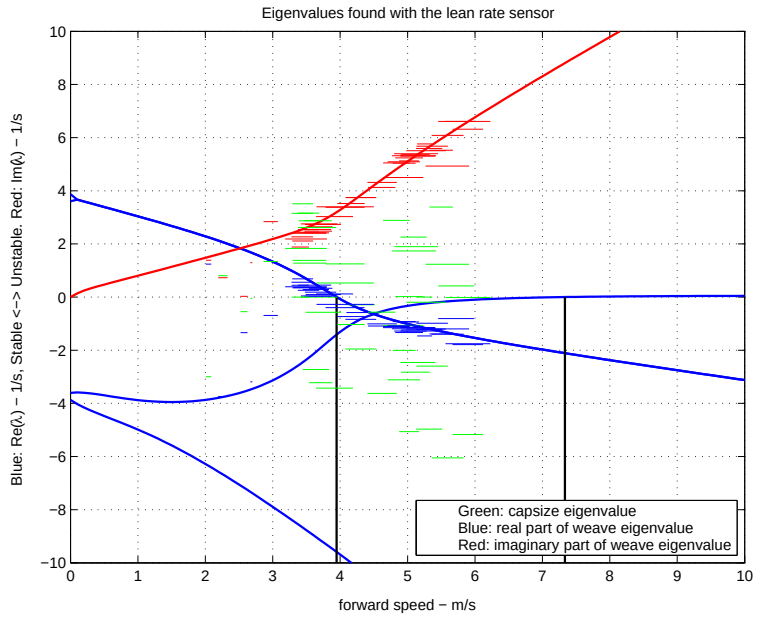

Figure 5.20: The calculated weave and capsize eigenvalues using the lean rate sensor with data chosen by eye

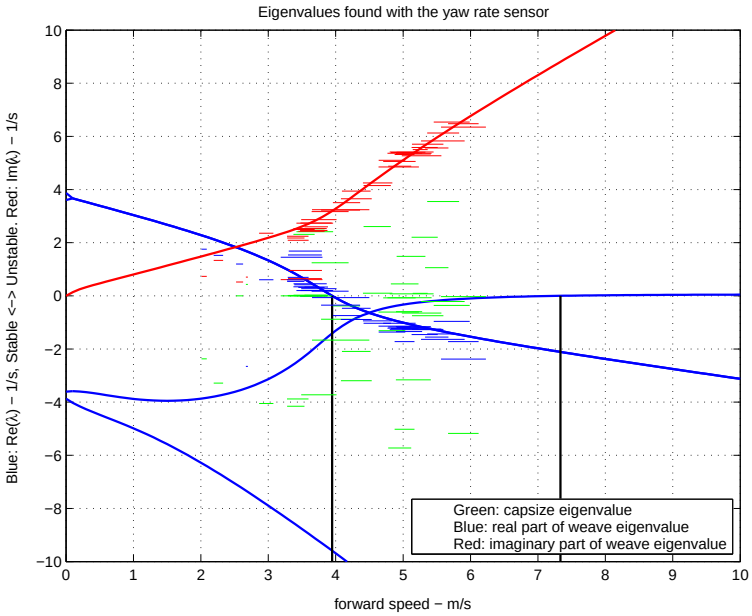

Figure 5.21: The calculated weave and capsize eigenvalues using the yaw rate sensor with data chosen by eye

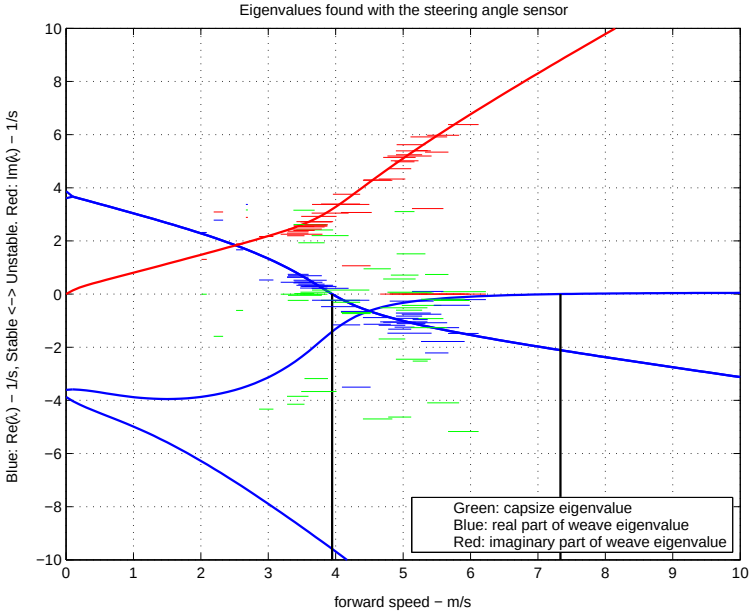

Figure 5.22: The calculated weave and capsize eigenvalues using the steering angle sensor with data chosen by eye

the bicycle moved in an almost perfectly straight line whilst almost perfectly vertical. This lack of dynamics turned out to be the problem. Upon changing the window slightly the results changed dramatically. Therefore these measurements were not used in further analysis.

3. Between 2 and 3 m/s it was not possible to extract the weave mode eigenvalues from any of the signals accurately. The window for these runs was very small and upon changing the time window slightly, very different results were calculated.

4. The size of the steering signal output was a problem. The maximum range that the handel bars turn during a test is only about 10 degrees. Figure 5.13 shows the steering angle for run 36 which had a very large dynamic signal compared to most of the other runs. As a result of this small steering signal and the large overall range of the sensor there is only a voltage change of around 0.15 V at the most during the measurement window. The precision of the sensor was thus clearly visible in the measurements. For this reason the steering data was not analysed further.

5. The yaw-rate fits looked similar to those of the lean-rate, but did not fit quite as many of the runs as the lean-rate did. The slight symmetry off-set in the bicycle caused it to lean to the right and go round in (large) circles during the tests. This caused a noticeable offset for the yaw-rate in the data. Therefore the yaw-rate data was not investigated further.

5.3.3 Speed Prediction Using Extracted Weave Eigenvalues

Even though the results were only based on judging the non-linear fit by eye at this point, they were good enough to detect a problem. Initially a mistake had been made in entering the silverbike parameters in the JBike6 program. The location of the centre of gravity of the front frame had been modelled too far forward. As a result the calculated eigenvalues for the weave mode were basically shifted to the right (in the graph) compared to what they should have been. This meant that the vast majority of the calculated non-linear fit weave eigenvalues seemed to be shifted to the left (ie, they had a slower speed for the same eigenvalue) by about 0.3m/s with respect to the eigenvalues of the model. Figure 5.23 shows the misalignment.

If the linearised model was correct, then there had to be a mistake in our execution of the experiments. Initially it was thought that there was an error in the program that calculated the speed from the measured data, however after an extensive search no error had been found. Our next assumption was that the design parameters of the model then had to be incorrect, and upon inspection this turned out to be the case. The location of the centre of gravity of the front frame was to far forward due to a misunderstanding of how the u v-coordinates in the program had to be interpreted. When this was changed the measurements fitted the model very nicely.

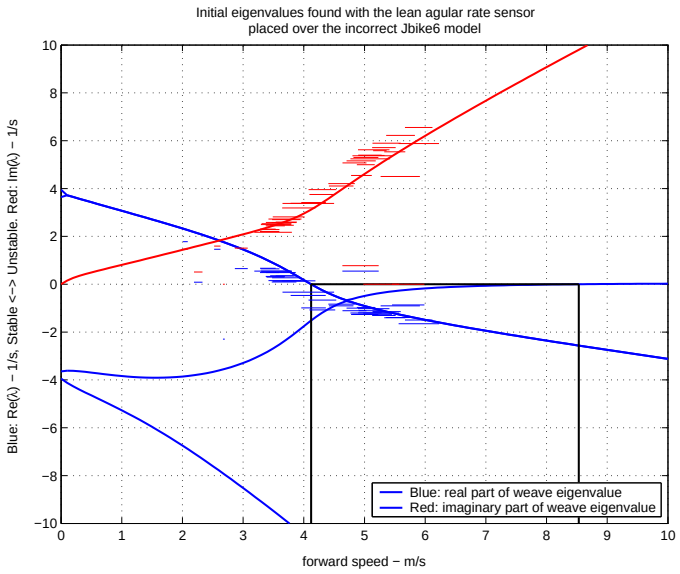

(a) The incorrect JBike6 model.

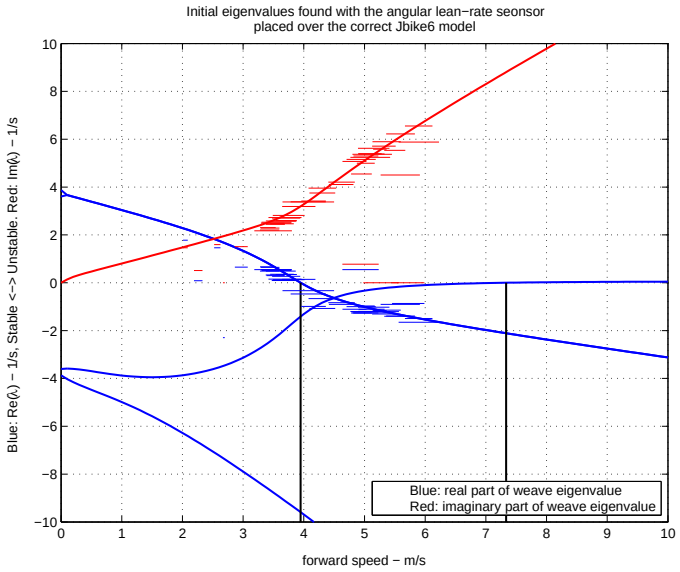

(b) The correct JBike6 model.

Figure 5.23: The two different models shown with the measured lean-rate data

5.3.4 Data Analysis Using Standard Deviation

To try to give a more "scientific" description for the accuracy of a fit, we reexamined and optimised the all lean-rate measurements that showed good dynamic behaviour and used the standard deviation of each fit as a measure for its accuracy. The standard deviation for each fit was found by:

$$\sigma = \sqrt{\frac{1}{N}\sum_{i=1}^{N}(x_i - \overline{x})^2} \tag{5.23}$$

where x_i is the measurement, $\overline{x}$ is the non-linear fit and N the number of data points in the window.

It is however not possible to simply optimise the standard deviation for each run by varying the length of the window and its starting time. This is because the speed of the bicycle during the measurements was not constant. Each non-linear fit is therefore simply no more than a fit with a set of eigenvalues that "on average" have the best fit on the data and thus give the smallest standard deviation. Therefore optimising a window purely on its standard deviation can result in a poor optimisation of the eigenvalues as both very short windows and windows in which there are relatively more extreme data points can give a false optimum. The shorter the window, the more constant the speed will remain and thus the better a fit should be. However if the window becomes very short, the dynamic behaviour of the motion is lost and the optimised function does not have to resemble the rest of the data. A window with a smaller σ therefore does not always have to be a better fit for the data.

Another point that had to be taken into consideration when using the standard deviation as a measure for the preciseness of the fit was the size of the signal's amplitude. When two data windows each had approximately the same σ, but very different amplitudes for the motion, then the window with the larger motion (signal amplitude) had to have been fit far more precisely relative to the motion. For example, when two data windows were examined from a single run where the bike was in the unstable weave motion speed range. The first window was made just after the release of the bicycle, whilst it was still in an almost perfectly vertical and stable position, and the other, several seconds later, where the lateral motion was far larger. If the standard deviation for both signals were the same then the second fit would have to be far better. The first fit could simply be a straight line not following the motion, whilst the second would have to actually follow the motion of the signal to be able to have the same standard deviation.

The process that was followed during the optimisation of the window was as follows:

1. Initially we found the point where the bicycle had the largest lean rate during the freely coasting region. For the high speed runs we located the point that the bicycle received an impulse. For low speed runs we located the point that one of the sidewheels made contact with the ground for the first time. Then we found the point where we were certain that the bicycle was still coasting freely and there was still enough dynamics in the motion to be sure that the fit could not draw a straight line through the

points. Thus for the high speed runs we chose a point at a later point in time, whilst for the low speed runs we chose a point earlier in time.

2. Next we carried out a non linear fit for the complete window and calculated its' standard deviation. The results were recorded in a file.

3. We then repeated the non linear fit and calculated its standard deviation, but this time on a window that was 0.1 seconds shorter. The last (or first) 0.1 seconds where the largest dynamics were taking place were removed from the window.This process was repeated until the window was only about 0.8 seconds long.

4. Using the file with the list of eigenvalues and standard deviations the windows with the smallest standard deviations were compared to one and other using the previously explained guidelines and an eigenvalue set was chosen for that run.

Table 5.2 shows the optimisation for run 16. The table shows the starting and finishing time of each window, the speed (linearised) range during this time, the real (d) and imaginary (ω) parts of the weave eigenvalue, the three constants as described in equation 5.21 and the standard deviation σ. After analysing the table we opted for the window 7.6 to 11 seconds. The standard deviation is relatively small in comparison with the longer windows, and the initial motion that it is fit on is larger than for those windows lower down in the list.

5.3.5 Low Speed Analysis

Even with this more "scientific" approach we could not produce a reliable result for the low speed runs. The real and imaginary parts of the weave eigenvalue seemed to fluctuate randomly from one window to the next.

The low speed runs all deal with the same problem: During the complete run, less than a quarter of a weave oscillation takes place before the bicycle has fallen over and touched the ground. This means that weave frequency is very difficult to measure.

In an attempt to try to reduce the options for the non-linear fit we fixed the imaginary part of the weave eigenvalue so that only the real part had to be calculated in Matlab. The imaginary part of the weave eigenvalue was calculated by interpolating it from the model using the mean speed of the chosen window. This calculated weave eigenfrequency was then used as ω in the non-linear fit so that only d had to be calculated.

This method did not improve the outcome. we therefore had to reassess the problem.

5.3.6 Transient Response Analysis

To come to a better understanding of the contribution of each eigenmode, a transient response analysis was carried out. The aim was to find the contribution of each mode in the measurable lean-rate signal. With this information our previous assumption that the caster and capsize modes were probably not measurable could either be verified or dismissed.

Start time	Finish time	Start speed	Finish Speed	d	ω	C1	C2	C3	σ
6.50	11.00	4.540	3.897	-0.6260	3.7914	2.4768	16.7939	16.3186	0.001291279
6.60	11.00	4.519	3.900	-0.5767	3.7786	2.4761	10.2104	12.0462	0.001272904
6.80	11.00	4.498	3.897	-0.4416	3.6671	2.4728	-1.1604	5.0490	0.001045082
6.90	11.00	4.486	3.896	-0.4271	3.6026	2.4709	-3.2486	3.2458	0.000938654
7.00	11.00	4.459	3.902	-0.4402	3.5545	2.4692	-4.8293	1.8338	0.000866379
7.10	11.00	4.435	3.907	-0.4554	3.5383	2.4685	-5.7720	1.2896	0.000857432
7.20	11.00	4.408	3.914	-0.4619	3.5358	2.4683	-6.1458	1.2262	0.000870011
7.30	11.00	4.414	3.904	-0.4529	3.5359	2.4685	-5.6641	1.1378	0.000881075
7.50	11.00	4.389	3.903	-0.4091	3.5096	2.4697	-3.8783	0.1634	0.000869449
7.60	**11.00**	**4.367**	**3.907**	**-0.3754**	**3.4603**	**2.4710**	**-2.5016**	**1.3642**	**0.000825521**
7.70	11.00	4.355	3.906	-0.3685	3.4251	2.4716	-1.8101	1.9729	0.000815526
7.80	11.00	4.349	3.902	-0.3762	3.3878	2.4722	-1.0995	2.6716	0.000801355
7.90	11.00	4.349	3.895	-0.3909	3.3683	2.4726	-0.6777	3.2630	0.000804829
8.00	11.00	4.328	3.898	-0.4121	3.3569	2.4730	-0.3919	4.0721	0.000808398
8.10	11.00	4.309	3.900	-0.4260	3.3542	2.4732	-0.3239	4.6696	0.000828679
8.20	11.00	4.293	3.901	-0.4178	3.3520	2.4730	-0.2074	4.3156	0.000842385
8.30	11.00	4.296	3.893	-0.4132	3.3480	2.4730	-0.0407	4.1279	0.000855179
8.40	11.00	4.298	3.884	-0.3992	3.3306	2.4726	0.5701	3.5491	0.000876617
8.50	11.00	4.278	3.886	-0.3890	3.3041	2.4721	1.3185	2.9683	0.000895429

Table 5.2: Table for the optimisation of run 16. The bold row indicates the chosen window

Using equation 5.17 and and a set of initial conditions the constants $\beta_{i,j}$ in equation 5.18 were calculated for each speed. Then with the constants $\beta_{i,j}$, the (normalised) initial contribution of each mode was calculated for each speed. Following this the transient response of each of the components and total, the measurable signal, at a number of fixed speeds was calculated. The following is an example of how one of the initial conditions was investigated.

The initial condition is as follows: The bicycle is moving along in an upright position and is given a lateral impulse, or the bicycle is released (and allowed to coast freely) just as it returns to an upright position, with no steering angle or steering rate, but with a measurable lean-rate. The initial conditions can then be written as follows: $\dot{\phi} = 1,\ \dot{\delta} = 0,\ \phi = 0,\ \delta = 0$ and $t = 0$. substitution into equation 5.17 gives:

$$\underline{x}(0) = Te^{D0}B \tag{5.24}$$

$$\begin{pmatrix} 1 \\ 0 \\ 0 \\ 0 \end{pmatrix} = Te^{0}B \tag{5.25}$$

$$T^{-1}\begin{pmatrix} 1 \\ 0 \\ 0 \\ 0 \end{pmatrix} = \begin{pmatrix} b_1 \\ b_2 \\ b_3 \\ b_4 \end{pmatrix} \tag{5.26}$$

Thus the constants $b_1,\ b_2,\ b_3$, and b_4 can be calculated for each speed using the eigenvector matrix (T) for that speed.

Figure 5.24 is a graph showing the normalised amplitude of each eigenmode component for the above mentioned initial conditions. The graph shows the contribution of each of the three different eigenmode components (the weave in blue, capsize in green and caster in red). Below 3.5 m/s the weave mode and capsize mode have about an equal contribution where as the caster mode can be "discarded". Above 3.5 m/s the initial contribution of the capsize mode drops dramatically whilst the contribution of the weave increases equally dramatically. above 4.5 m/s almost 95 % of the total measurable initial angular rate is caused by the weave mode. Therefore at high speeds, upon applying an impulse to the bicycle, only the weave mode will initially be measurable, whilst at low speeds the capsize mode will initially also have a significant share.

Next the contribution, in the time, of the separate modes to the total motion for a certain speed was investigated. This was required to be able to conclude wether, a mode is damped out rapidly or not. If a mode damps out rapidly, even though it initially has a large influence on the total motion, after a short time (0.5 seconds for example) it will have practically no contribution to the total motion, and thus it will not be measurable anymore.

Using equation 5.17 and the values calculated for B for a specific speed with equation 5.26 the contribution to the lean-rate of each of the modes was calculated as follows:

$$x_{weave}(t) = b_1 T_{1,1} e^{D_{1,1}t} + b_2 T_{1,2} e^{D_{2,2}t} \tag{5.27}$$

$$x_{capsize}(t) = b_3 T_{1,3} e^{D_{3,3}t} \tag{5.28}$$

$$x_{caster}(t) = b_4 T_{1,4} e^{D_{4,4}t} \tag{5.29}$$

$$x_{total}(t) = x_{weave}(t) + x_{capsize}(t) + x_{caster}(t) \tag{5.30}$$

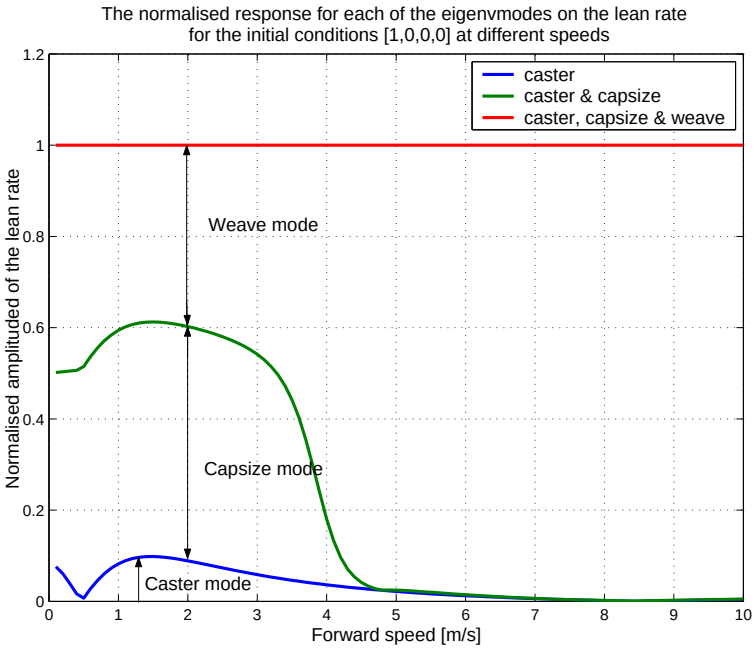

Figure 5.24: The normalised initial angular rate response to a $\dot{\phi}$ perturbation for different speeds

Figures 5.25, 5.26, 5.27, 5.28 and 5.29 show the transient response to the initial conditions described above for speeds of 2, 3, 4, 5 and 6 m/s. Figure 5.25 clearly illustrates that if the bicycle is not released perfectly still ($\dot{\phi} \neq 0$) whilst moving at a very low speed of 2 m/s the capsize mode greatly influences the measurable motion. At this speed the bicycle generally has fallen over completely within 1 second, therefore each measurement will have to take the capsize mode into consideration.

At 3 m/s the influence of the capsize mode is all ready far less profound. beyond 0.5 s the mode is practically no longer measurable. At 4 m/s the effect of the capsize mode is visible for the first second, however the motion caused by the weave mode is far greater than that of the capsize mode. This will make it very difficult to extract the capsize mode from the data. At even higher speeds the capsize mode is no longer measurable for any period of time.

The graphs of the analysis of the effect of an initial lean angle, steer angle, and steering rate on the lean-rate are shown in Appendix E.

After analysing graphs 5.25 through 5.29 and those in Appendix E we concluded that:

Low Speed: For speeds up to about 3 m/s, it should be possible to calculate the weave and capsize modes. As the bicycle was never released perfectly vertically whilst moving in a straight line, there will always have been either a small lean angle, lean-rate, steering angle, steering rate or combination of these in the initial conditions. The capsize mode will thus have been present in the signal.

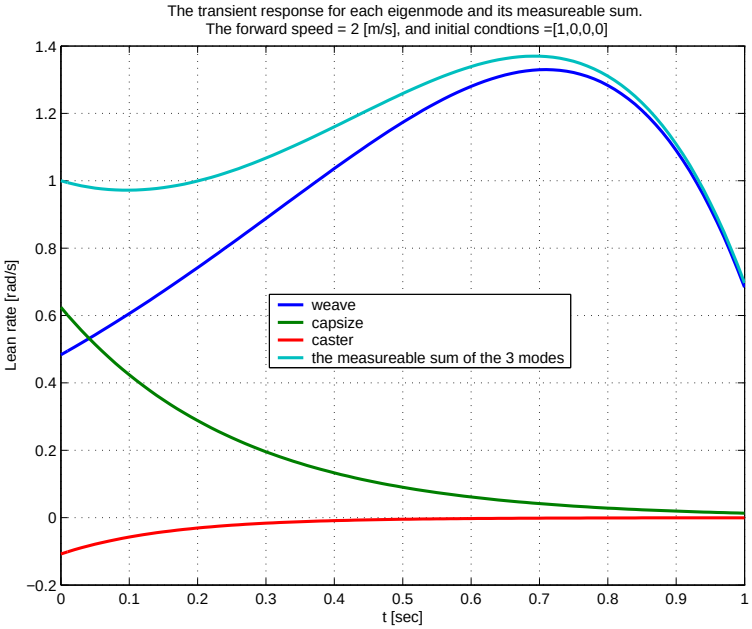

Figure 5.25: The transient response of the lean-rate to an impulse when the bicycle is moving at 2m/s

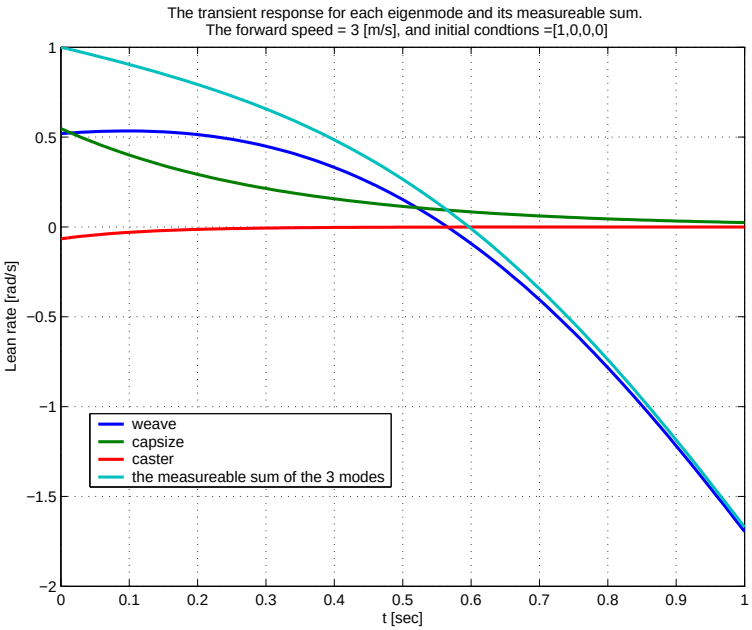

Figure 5.26: The transient response of the lean-rate to an impulse when the bicycle is moving at 3m/s

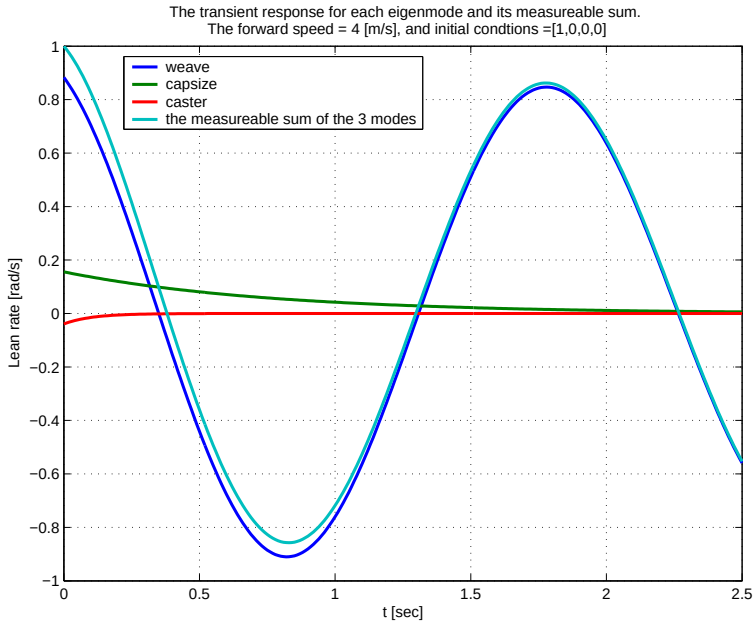

Figure 5.27: The transient response of the lean-rate to an impulse when the bicycle is moving at 4m/s

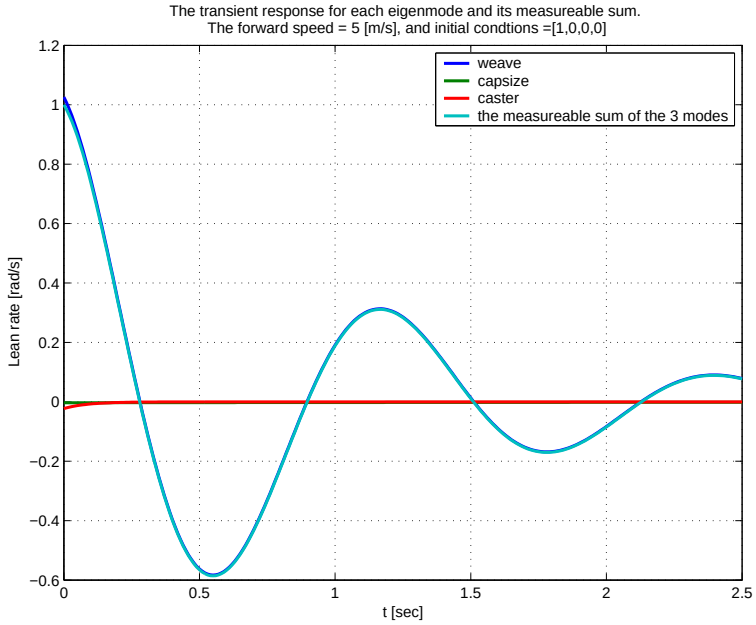

Figure 5.28: The transient response of the lean-rate to an impulse when the bicycle is moving at 5m/s

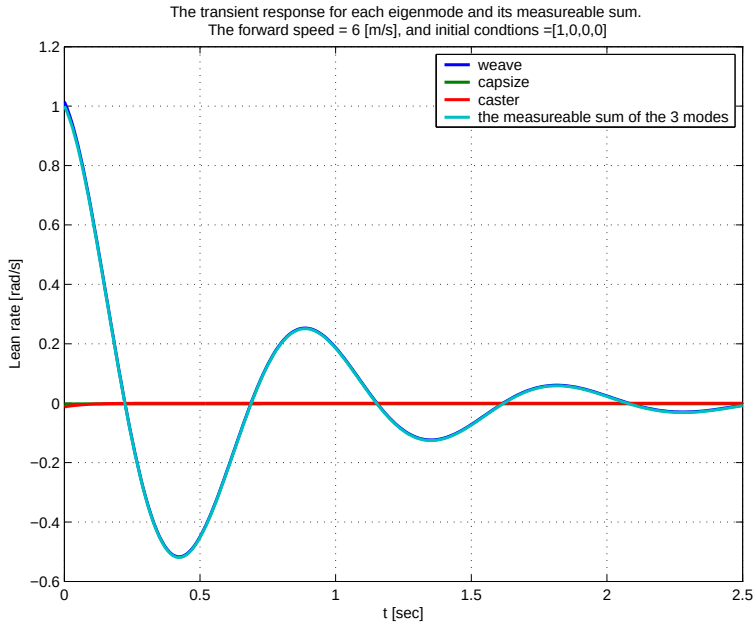

Figure 5.29: The transient response of the lean-rate to an impulse when the bicycle is moving at 6m/s

However the effect of the capsize mode is damped out rapidly. At a speed of just 2 m/s the influence of the capsize mode can be seen for approximately 0.8 seconds, which is also about as long as the test measurements last at this speed. At 3 m/s the influence of the capsize mode can only be seen for the first 0.5 seconds. The most important aspect for calculating the capsize mode will thus be locating the exact moment that the bicycle was released. If the window of the measurement starts 0.2 seconds later, the portion of the lean-rate that is caused by the capsize mode is halved, making the calculation of the capsize mode very difficult.

Transition Range: At around 4 m/s the lean-rate transient response almost looks like a a vertically shifted weave mode response for the first second to second and a half after release. From then on there is basically no difference between the lean-rate and the weave mode. extracting the capsize will not be possible.

High Speed: The lean-rate measured at speeds above 5 m/s are dominated by the weave mode. The capsize mode however can,in some cases cause a vertical "offset" in the lean-rate. However this offset is so small compared to the weave mode that it is not possible to extract the capsize mode from the data.

Caster Mode: The caster mode only showed a large enough contribution to the lean-rate for it to be calculated in the first 0.2 seconds after release whilst moving at 2 m/s and having a steering-rate initial condition. Besides the fact

that this it is unlikely that these initial conditions occurred, the short time span that this mode is effective make the mode undetectable.

5.3.7 Low Speed Capsize Mode Analysis

Initially, as explained in section 5.3.2, we tried to calculate the weave eigenvalues alone and the weave eigenvalues together with the capsize eigenvalues, by non-linear fit. At the time non of the eigenvalues were fixed. The capsize mode could not be calculated properly, and at low speeds non of the eigenvalues could be calculated. In section 5.3.5 another attempt was made at calculating the weave eigenfrequency at low speeds. The frequency of the weave mode was fixed and only the real part of the weave eigenvalue was extracted from the measured data. This method also did not work. Next it was shown in section 5.3.6 that the capsize mode had to be taken into account to be able to accurately describe the total lean-rate motion.

We thus once again fixed the weave frequency in the same manner as described in section 5.3.5 but this time we also took the capsize eigenvalue into account and fixed the capsize eigenvalue in the non-linear fit. We therefore only extracted the real part of the weave eigenvalue. The capsize eigenvalue was interpolated from the model using the mean speed of the window.

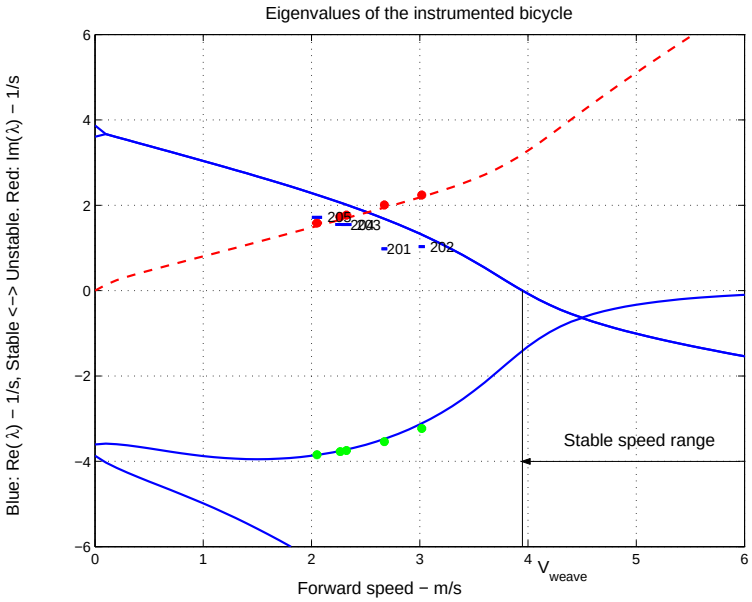

Figure 5.30: The calculated real part of the weave eigenvalue for the low speed measurements using predetermined weave eigenvalue imaginary parts and the capsize eigenvalues.

In section 5.3.6 it was discovered that the capsize mode has the largest influence on the lean-rate immediately after releasing the bicycle. Thus each low speed runs' video was analysed once again, this time, frame by frame, to locate the exact moment that the bicycle was released and the moment one of the side wheels touched the ground. The time between the release and first contact

was recorded. Next we analysed the data file once again. The moment that the bicycle was released was back-casted from the clearly visible initial moment that the side wheels made contact with the ground. Non-linear fits were then carried out on the data between the moment of release and the moment the side wheels made contact with the ground. We tried a number of different window lengths and for different (slightly later) starting times.

The method was again unsuccessful at calculating the real part of the weave eigenvalue. Figure 5.30 shows the calculated real part of the weave eigenvalues (in blue) for the low speed measurements when the capsize eigenvalue and the imaginary part of the weave eigenvalue have been fixed. As can be seen the extracted eigenvalues do not compare well to those of the model. Furthermore within each run the extracted real part of the weave eigenvalue varies dramatically upon slight changes in the chosen measurement window. Figure 5.31 shows how the real part of the calculated weave eigenvalue changes upon slight changes in the window length for run 201.

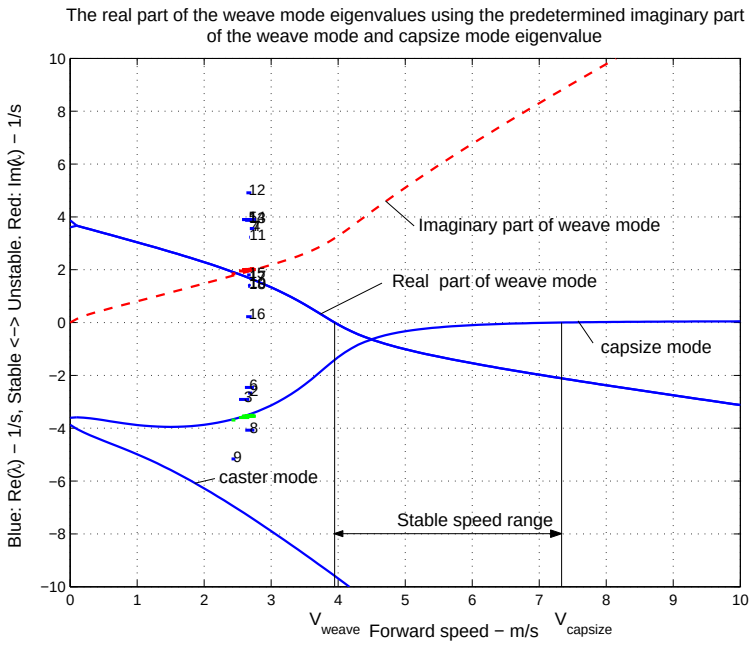

Figure 5.31: The calculated real parts of the weave eigenvalue for the different window lengths during run 201

We thus have to conclude that in the unstable speed range, at speeds below approximately 3.0 m/s we cannot calculate the eigenvalues for the bicycle.

5.3.8 Stationary Analysis

Two tests were carried out with the bicycle in a stationary position (zero speed). According to the linearised model the bicycle has four real eigenvalues when it is stationary. These eigenvalues come in pairs, $\lambda_3 = -\lambda_1$, $\lambda_4 = -\lambda_2$. In figure 5.32 the time response for a stationary bicycle is shown as predicted according to

the linearised model. The bicycle has been given a small lean angle offset as its' initial condition.

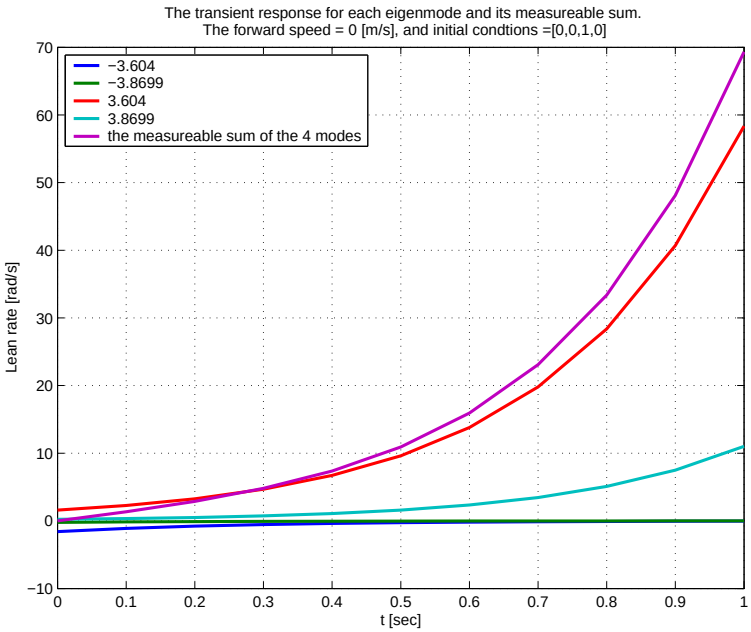

Figure 5.32: The time response for a stationary bicycle

From figure 5.32 it can be seen that the main part of the measurable lean-rate signal is caused by the second largest eigenvalue, and not the largest eigenvalue!

Start time	End time	λ	σ
3.0	4.0	3.698447	0.00097203266
3.0	3.9	3.734908	0.00104801336
3.1	**4.0**	**3.712059**	**0.00097152503**
3.1	3.9	3.769149	0.00104787197
3.1	3.8	3.804621	0.00114322861
3.1	3.7	4.028425	0.00121591335
3.2	4.0	3.700655	0.00106739926
3.2	4.0	3.700655	0.00106739926
3.2	3.9	3.762086	0.00116972264
3.2	3.7	4.084030	0.00141309115
3.2	3.6	4.547710	0.00158824367
3.3	3.9	3.672776	0.00121272676
3.3	4.0	3.649267	0.00108469110
3.3	3.8	3.578695	0.00135723875
3.3	3.7	3.648223	0.00150996525
3.3	3.6	3.533750	0.00176770983

Table 5.3: The different windows tried for run 41

The large difference in size of the motion caused by each of the two eigen-

values is due the difference in the constant multiplying the exponential (see equation 5.18). Whilst the largest eigenvalue is multiplied by 0.23, the second largest eigenvalue is multiplied by 1.59 making its' motion almost 7 times as large. As a result it is not possible to extract both eigenvalues from the measured signal.

Table 5.3, shows the calculated eigenvalue for the second largest eigenvalue for run 41 along with the standard deviation for the window and the window time. As can be seen, the calculated values for this eigenvalue compare well with that of the model (model value is 3.60). The window shown in bold is the window that was chosen using the same reasoning as in section 5.3.4.

5.3.9 Concluding Remarks

Figure 5.33 shows all the extracted eigenvalues in relation to those of the linearised model and table 5.4 lists the eigenvalues for the the measurements along with the standard deviation for the measurement, the window, the speed during the window and the run number.

For all speeds above 3.5 m/s the measured data and the manner in which it can be interpreted fairs well with that of the proposed model.

Between 3 and 3.5 m/s (runs: 29, 31, 32 and 33) two types of non-linear fit were used to attempt to describe the eigenvalues. However the weave and capsize mode non-linear fit did not improve on the results previously found by only fitting the weave-mode. For the weave-only fit the real part for the weave eigenvalue fit well with that of the model, but the imaginary part do not fit as well. The imaginary part of each of the weave eigenvalues are all slightly smaller than that of the model. In this speed range the bicycle doesn't quite manage one complete weave oscillation before it makes contact with the ground. This is a problem for the non-linear fit function.

At speeds below 3 m/s (runs: 201, 202, 203, 204 and 205) the non-linear fit cannot extract eigenvalues accurately. Nether the weave nor the capsize mode can be extracted from the data at these speeds because the available window for the non-linear fit is to short.

When stationary (runs: 40 and 41) the extracted eigenvalue clearly matches that of the linearised model.

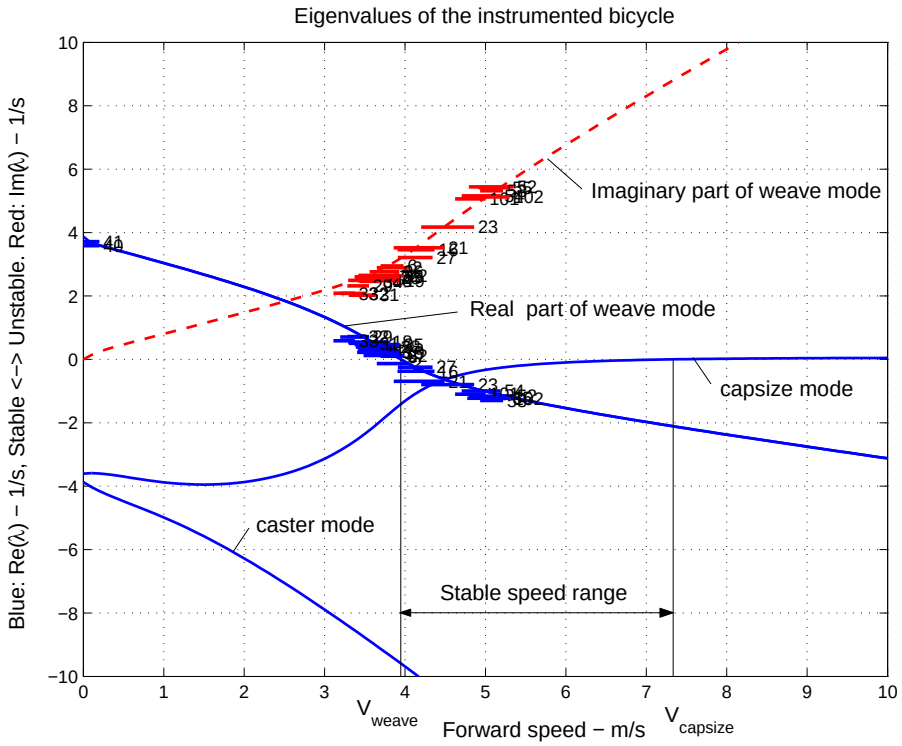

Figure 5.33: The final results shown graphically including the inaccurate low-speed measurements

Run	Start time	End time	Start speed	End Speed	$\lambda 1$	$\lambda 2$	σ
2	8.00	11.50	4.05	3.65	-0.133	2.893	0.000889721
3	8.00	11.30	3.90	3.42	0.247	2.650	0.000943865
6	8.30	10.70	3.98	3.70	0.097	2.948	0.000823893
7	10.30	13.80	3.88	3.41	0.283	2.613	0.000806409
8	7.10	10.00	3.79	3.44	0.280	2.502	0.000813856
16	7.60	11.00	4.37	3.91	-0.375	3.460	0.000825521
18	12.00	16.00	3.80	3.29	0.551	2.495	0.000888972
19	11.00	15.00	3.95	3.40	0.221	2.483	0.000616655
21	6.30	10.50	4.49	3.86	-0.690	3.521	0.000737732
22	7.00	11.00	3.98	3.49	0.123	2.629	0.000796677
23	6.50	10.50	4.86	4.20	-0.795	4.173	0.000785002
27	7.00	10.00	4.34	3.91	-0.246	3.211	0.000815505
28	8.00	12.00	3.90	3.39	0.387	2.572	0.000706528
34	6.50	9.50	3.68	3.43	0.310	2.459	0.000843746
35	7.50	12.00	3.93	3.37	0.470	2.603	0.000632793
36	8.00	11.50	3.93	3.56	0.200	2.765	0.000736421
52	9.90	12.50	5.34	4.79	-1.159	5.443	0.000664655
53	9.00	10.50	5.22	4.93	-1.294	5.318	0.000738492
54	8.75	11.20	5.19	4.70	-0.999	5.157	0.000504782
55	7.00	8.75	5.28	4.91	-1.221	5.419	0.000446864
101	6.10	8.20	5.00	4.62	-1.099	5.063	0.000675617
102	6.50	9.00	5.30	4.77	-1.224	5.124	0.000715869
40	0.05	1.05	0.00	0.00	3.586	NA	0.001008523
41	3.10	4.00	0.00	0.00	3.712	NA	0.000971525
29	6.50	9.00	3.55	3.28	0.718	2.320	0.000811882
31	6.00	9.00	3.63	3.30	0.505	2.023	0.000778822
32	6.50	9.00	3.50	3.19	0.704	2.082	0.000849162
33	7.50	10.00	3.38	3.11	0.585	2.089	0.000845189

Table 5.4: The results

Chapter 6

Conclusions and Recommendations

For speeds above 3.5 m/s the measured data and the manner in which it can be interpreted fairs well with that of the proposed model.

At speeds between 3 and 3.5 m/s the real part of the measured weave eigenvalues fit well with that of the model but the imaginary parts did not fit as well. The imaginary part of the weave eigenvalues were all smaller than that of the model. This can be explained by the fact that in this speed range the bicycle doesn't quite manage one complete weave oscillation before it makes contact with the ground, making it difficult to fit a harmonic function accurately.

At speeds below 3 m/s the non-linear fit could not extract eigenvalues accurately simply because the available window for the non-linear fit was to short. However when stationary the extracted eigenvalue clearly matched those of the linearised model.

It is therefore possible to conclude that overall, the experimental results show a very good agreement with the data obtained from the linearised dynamic model of an uncontrolled bicycle. Thus proving that the tire slip and frame and fork compliance are not important for the lateral dynamics of the bicycle in the speed range up to 6 m/s.

The following discussion is about possible refinements that can be made to improve future measurements and also to be able to say more about the limits of the linearised dynamic model.

The oscillation time of the front frame in the torsion pendulum was very short, making it difficult to measure the period accurately. By using a thinner torsional rod for the three parts with small mass moments of inertia, the front wheel, front frame and rear wheel, the oscillation time for them will increase, enabling a better measurement of the oscillation time. A reduction to a 3 mm diameter steel rod is sufficient.

A further refinement to the mass moments of inertia measuring system would be to fix the horizontal position of the lower end of the torsion rod. The horizontal fixation of the position of the lower end of the torsion rod would ensure that the rod does not start to oscillate in any other mode other than that of

the rotational mode. At present a lateral pendulum type mode is very present during the measurements and makes the measurement of the oscillation time very difficult. The horizontal fixation could be achieved by using a 5 mm cup-bearing through which the rod is placed. The bearing could be held in place by a stiff steel shaft. The torsion rod could then still rotate freely about its axis of rotation, but could no longer move horizontally in the plane perpendicular to the rotational axis.

Finally instead of measuring the oscillation time of the parts clamped in the torsion pendulum using a stop-clock the period could be measured more accurately using an angular rate sensor, similar to those used to measure the lean and yaw rate.

The use of slick, racing style tyres that are highly pressurised (to 8 bar) would significantly reduce the rolling resistance. This would radically reduce the reduction in speed during the free coasting. To reduce the speed reduction even further during the free coasting a motor(and battery pack) could be added to ensure that the bicycle moves at an (almost) constant speed. It will then be possible to pinpoint the exact speed for each eigenfrequency instead of a speed range as at present. Further more, by adding such a motor (and battery pack) it becomes possible to test at higher speeds, enabling us to prove that there is indeed an unstable capsize motion as described by the linearised model. Thus an increase of the maximum speed to about 10 m/s is desired. To achieve this not only another form of propulsion is required but also a larger test area is required.

The measurement of the speed of the rear wheel can, if the rear wheel is driven directly by an electric motor, also be carried out by using a tacho that is connected directly to end of the motor. This would ensure that a large (amplitude difference) speed signal could be measured, improving the measurement of the speed, especially at low speeds. A tacho provides an analogue signal and thus could easily be incorporated into the presently used system.

The sensor that worked least satisfactorily was the steering angle potentiometer. By replacing the potentiometer with one that has a much smaller overall range a much larger change in signal magnitude can be measured, allowing a better non-linear fit to be carried out on the signal, whilst keeping an analogue signal. Another method would be to add a gear ratio to increase the range that is used of the current potentiometer. This method would however increase the friction between the front and rear frame and thus have a negative effect on the motion of the bicycle.

After the destruction of the laptop screen, between each of the following runs we had to connect an external monitor to the laptop. By connecting a wireless network PCMCIA card to the laptop, the laptop can be controlled from another computer and thus; once booted up, not have to be controlled manually on the bicycle anymore. This has three distinct advantages. Firstly, as the screen is no longer required the operational time of the laptop, the time between requiring to be recharged, is increased dramatically. Secondly the laptop can be located in a more favourable position and placed in a more 'padded' environment on the bicycle as manual operation of the computer is no longer required. Thirdly as the screen is no longer required it can be removed, drastically reducing the

wind resistance on the bicycle during the experiments.

Now that the motion of 'a' bicycle has been verified to follow that of the linearised model, the next step is to examine to what extent this model holds under different conditions. We only carried out tests with one type of tyre, at one tyre pressure and only on one type of surface and with "no person" on the bicycle. Each of these factors are very important aspects as each can have a very large influence on the coefficient of friction between the tyre and the road and the tyre characteristics in general. Furthermore the type of tyre and its pressure might also cause extra dynamical aspects that were not modelled. Therefore tests on other road surfaces, with other tyres, at several different pressures and with several different extra mass'added to the bicycle could be carried out to examine to what extent this simple linearised model can be used to describe the motion under all conditions.

Appendix A

Measuring Equipment Options

A.1 PC104

This is a small, compact and light weight computer that can weigh less than a kilogram and has no moving parts. The PC104 type computers are designed for rugged environments and as thus have a minimal power consumption and size. If required they can operate using a 12V battery pack. The computer comprises of no more than the bare essential components. For example they do not have a normal hard drive, instead they uses a small, 32Mb solid state memory. Another example is that due to the minimal amount of components and small operating system the processor does not require a cooling fan.

The computer parts are placed in a sturdy aluminium casing with a frontal area that is no larger than approximately 15x15cm. The computer is built up of a number of boards. The more functionality that is required from the computer the more boards that are required. The Boards are placed on top of each other and thereby the depth of the computer can vary from about 5cm to 25cm.

To program a PC104 computer you program the code on a normal desktop PC, for example in Matlab-Simulink and then with a program such as XPC-Target you upload C-code directly onto the PC104 computer. This way only a tiny amount of data is required for the operating system and the program to run the measurements on the PC104 computer and thus it can use the small solid state memory. With such a tiny operating system, a relatively slow processor, 400Mhz, can be used because the actual speed of the measurements is still very high. An added advantage that this relatively slow processor has is that it requires less power, and thus less cooling, than a similar but faster version.

For Data acquisition purposes where large amounts of data are collected the solid state memory will not be sufficient and extra memory will be required. For our measurements, we would collect data for around 10 to 15 seconds and have a data collection rate of around 100Hz, and thus we would not require an extra hard drive.

The following parts are delivered in a standard development kit by Diamond Systems: A 486, 100MHz processor board, an I/O panel, a VGA board,a 32Mb flashdisk memory module that acts as the hard drive, a flashdisk programmable

expansion board, set of cables and a 3" housing. In order to use a number of optical encoders we would require an extra encoder board. The development kit is not supplied with a DC/DC converter board however as would be running the computer using a battery we would require one.

A DC/DC converter board ensures that the computer and the sensors that are connected to the computer are fed at a constant voltage. Without such a DC/DC converter board the voltage supply to the computer and sensors would drop as the battery juice runs out. This change in voltage can affect, amongst others, a sensor's output voltage as this is often directly related to its input voltage.

A.2 USB-DAQ

This system data acquisition system (offered by amongst others, National Instruments and Measurement Computing) is connected to a laptop or PC via its USB 2.0 port. It is operated using the program LabView (also by National Instruments) and has eight analogue inputs, two analogue outputs, twelve digital I/O ports and one 32 bit counter. There were two versions, one 12 bit system with a maximum sampling frequency of 10K S/s (with one signal) and a control speed of 150Hz. The second version is a 14 bit system, which is also capable of sampling at a higher speed; 48K S/s. The weight of the USB-DAQ is negligible (85grams). The minimum operating system requirement for the USB-DAQ is Windows 2000.

A.3 Digital Sensors

A.3.1 Optical and Incremental Encoders

Optical and incremental encoders operate by giving off an electric pulse when rotated a certain fraction of a rotation (or even degree). The more pulses that are provided per rotation the higher the resolution and the more accurately the angle can be measured.Tipical values are between 500 and 25000 pulses per rotation. There is no stop on the encoder so any size angle can be measured. The angles greater than 360 degrees and relative angles can be measured by a second pulse that is given off when the encoder goes through the zero.

A.3.2 Reed Relet and Magnet

Most ordinary bicycle computers work by the reed relet and magnet principle. A magnet is placed on a spoke of either the front or rear wheel and when the wheel rotates the magnet moves past the reed relet. When it does this the relet closes and there is a voltage change (pulse). This pulse is registered in the the computer along with the time, (or the number of pulses that are recorded in a period of time are registered). One pulse is equal to one complete rotation of the wheel, and thus the distance travelled and speed can be calculated once the wheel radius has been registered in the computer.

To increase the preciseness of the computer the number of magnets spread equally around the wheel can be increased - for example 2 magnets can be placed 180° apart from each other.

A.4 Analogue senors

A.4.1 Potentiometers

A potentiometer is basically an angular variable resistor.The larger the angle, the larger the resistance and the lower the output voltage. A potentiometer gives off an analogue signal that is easy to measure. The winding of the potentiometer is proportional to its accuracy and linearity. If the windings have a constant diameter and they are equally spaced then the potentiometer will be highly linear. Most potentiometers cannot measure more than one complete revolution but they often are not fitted with a mechanical stop. This means that there is a voltage change from the maximum to the minimum (or vice versa) when crossing the end of the windings.

A.4.2 Piezoelectric Vibrating Gyroscope

Piezoelectric vibrating gyroscopes are lightweight (1 gram), cheap, mass produced gyroscopes that are used in consumer electronics such as video cameras for steady shot technology. An example is the Murata ENC series that [9] used in their experiments. These gyroscopes only measure the rotational velocity in one direction and they are mainly used for measuring large angular speeds up to around 300 degrees per second. The sensor's output is a small analogue signal that needs to be amplified. A Murata ENC type gyroscope costs around €50.

A.4.3 Solid State Coriolis Force Detecting Gyroscope

Solid state Coriolis force detecting gyroscopes are mass produced gyroscopes for the auto and aero industry. The rotational speeds that they can measure are generally lower than those that the piezoelectric vibrating gyroscopes can measure but the accuracy is greater. The maximum angular rate that they can measure lies between 75 and 575 degrees per second depending on the type. An example is the Silicon Sensing Systems CRS-03 which has a maximum rotational speed of 100° per second. The sensor requires a $5V$ DC power supply and the output is an analogue signal that can range between 0 and 5 volts and thus does not need to be amplified. These gyroscopes cost around €130.

A.4.4 Tachometer

A tachometer is a type of direct current motor with very precise windings. The induced voltage is linearly dependant with the angular speed of the armature. A tacho supplies an analogue output signal that can be measured directly by the USB-DAQ data acquisition system's analogue input.

Appendix B

Acquired Measurement Equipment Specifications

Speed sensor
Make: Avocet
Model: Altimeter 50
Website: www.avocet.com
Comments: a magnetic ring with 10 north/south poles is used to measure the wheel angle.

Angular rate sensor
Make: Silicon Sensing
Model: CRS03
Website: www.siliconsensing.com
Comments: 5 volt input power supply required. Rate range ± 100 degs/s. Two sensors were used, rotated 90 degrees to each other. One sensor was used to measure the lean angle rate, the other the yaw angle rate.

Steering angle sensor
Make: Duncan Electronics Inc.
Model: 1801
Website: www.beiduncan.com
Comments: Single turn, 358 degree potentiometer. Resistance: 20K ± 3% Ohm. Linearity: ± 0.75%

Battery pack
Make: BMI
Model: 4.8V 2100mAh
Website: www.quartel.nl
Comments: Rechargeable NI-CD 4.8V 2100mAh battery pack.

Laptop
Make: ACER
Model: 340
Website: www.acer.com

Comments: Sitecom USB 2.0 PCMCIA card was installed.

Data acquisition unit
Make: National Instruments
Model: NI-USB-6009
Website: www.NI.com
Comments: Eight 14-bit analogue input channels, 12 digital I/O lines, 2 analogue outputs, 1 counter. Only the analogue inputs were used.

Data acquisition software
Make: National Instruments
Model: LabVIEW Express version 7.0
Website: www.NI.com/labVIEW

Appendix C

Dynamo Output Test Results

The measured output voltage for the standard dynamo at different speeds. The graph shows the linear relationship between the output and the RPM.

RPM	Voltage	RPM	Voltage	RPM	Voltage	RPM	Voltage
270	1,34	300	1,61	350	1,98	400	2,35
450	2,71	500	3,07	540	2,9	550	3,38
600	3,4	600	3,57	650	3,93	700	4,1
700	4,3	750	4,58	800	5	800	4,92
900	5,7	900	5,65	1000	6,3	1100	7,2
1100	7,14	1200	7,7	1300	8,5	1400	9,3
1500	10	1600	10,6	1800	12	2000	13,3
2200	14,4	2400	16	2600	17,2	3000	19,9

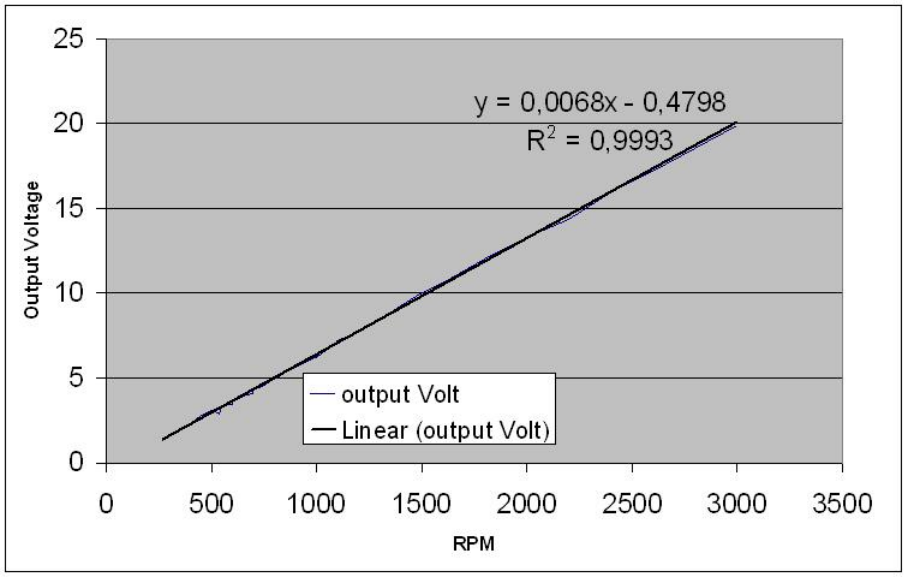

Appendix D

Matlab Code

D.1 Centre of Mass Location

```
%*************************************************************************
%-------------------------- rear frame -----------------------------------
%*************************************************************************
%Lengths in picture
cgxr=0.049;
cgzr=0.0355;
lachterbrug=0.064;
lzadelbuis= 0.08;

%Measured lengths
achterbrug=0.45;
zadelbuis = 0.56;

%Ratio
Ratio1=achterbrug/lachterbrug
%    Ratio1 = 7.0313
Ratio2=zadelbuis/lzadelbuis
%    Ratio2 = 7.0000
%Thus the ratio is = 7.0
ratior = 7.0;

%Toptube slopes 5 degrees (upwards towards the front).
%Thus x en y values must be corrected by 5 degrees.
xrf= ratior*(cgxr*cos(5/180*pi)-cgzr*sin(5/180*pi))
%    xrf = 0.3200
zrfl=ratior*(cgxr*sin(5/180*pi)+cgzr*cos(5/180*pi)); rrw=0.70/2;
zrf=-rrw-zrfl
%    zrf = -0.6274

%*************************************************************************
%-------------------------- front frame ----------------------------------
```

```
%*************************************************************************

%V
alpha=69/180*pi;    %  Head angle
Rfw=0.697/2;        %m Radius front wheel
trail=0.19;         %m trail
x1=Rfw/tan(alpha)   %m
v1= Rfw/sin(alpha)  %m V wheel centre
v2= (trail-x1)*cos(alpha)  %m V stukje tussen wheel centre en measurement
v3= 0.451           %m V measurement
V= v1+v2+v3         %m V totaal cofg =0.8444

%U
Dheadtube=0.0254;   %m Diameter head tube
U=Dheadtube/2       %m U cofg = 0.0127

%X,Z
wheelbase=1.01      %m Wheelbase
x=wheelbase+trail+U*sin(alpha)-V*cos(alpha); %m Front frame X-CofG
%x =  0.9092
z=-U*cos(alpha)-V*sin(alpha);               %m Front frame Z CofG
%z = -0.7929
```

D.2 Mass Moments Of Inertia Calculation

```
%*************************************************************************
%------------------------- Rod + Clamp ------------------------------------
%*************************************************************************
%Calculation the MOI of the clamp+rod from the oscillation time
%time = 2*pi*sqrt((L*Im)/(G*Ip)) of the system with a test weight
%with known MOI.

%MOI of Clamp+rod calculation:
mklem = 0.69;                       %kg     Mass bike clamp + torsion rod
l= 0.925;                           %m      Length torsion rod
d = 0.005;                          %m      Diameter torsion rod
G = 75e9;                           %Pa     Shear modulus  of torsion rod
Ip = (d^4)*pi/32                    %m^4    Polar MOI of the torsion rod
%    Ip = 6.1359e-011

mstaaf=5.18;                        %kg     Mass test weight rod
lstaaf=1.79;                        %m      Length test weight rod
Istaaf= 1/12*mstaaf*(lstaaf^2);     %kgm^2  MOI of test weight rod
%    Istaaf = 1.3831

ts = ((55+55+55)/100*60)/10/3;      %s      Oscillation time for the rod
Im = ((ts/(2*pi))^2)*G*Ip/l;        %m^4    MOI of (clamp + torsion rod
                                    %               + test weight rod)
Iklem=Im-Istaaf                     %kgm^2  MOI of clamp+torsion rod
```

```
%    Iklem = -0.0107

%MOI of clamp+torsion rod are so small that they can be neglected.
%To reduce errors G*Ip/L is made a constant:
w0=2*pi/ts;
K = Istaaf*w0^2                     %kgm^2/s^2  K
%    K = 5.0140
G*Ip/l                              %kgm^2/s^2  G*Ip/L
%    G*Ip/l = 4.9751
%************************************************************************
%-------------------- rear frame ------------------------------------------
%************************************************************************
%average time for 30 oscillations about the 3 main tubes. (using a
%stopclock that has 100 steps per 60 seconds!)
tr1 =((128+127+127)/100*60)/30/3;   %s      Average time about seat tube
tr2 =((142+143+143)/100*60)/30/3;   %s      Average about top tube
tr3 =((138+138+137)/100*60)/30/3;   %s      Average time about sloping tube

Ir1 = ((tr1/(2*pi))^2)*K;           %kgm^2  MOI about seat tube
Ir2 = ((tr2/(2*pi))^2)*K;           %kgm^2  MOI 27degrees about top tube
Ir3 = ((tr3/(2*pi))^2)*K;           %kgm^2  MOI about sloping tube

% change MOI to global MOI
% unit vectors wrt xz fixed to top tube, x-axis 5degrees below the top tube
phi1 = 161*pi/180; phi2 = 289*pi/180; phi3 = 41*pi/180;

e1 = [cos(phi1); sin(phi1)];        %       unit vector wrt xz
e2 = [cos(phi2); sin(phi2)];        %       unit vector wrt xz
e3 = [cos(phi3); sin(phi3)];        %       unit vector wrt xz

IIr = [ e1(1)^2 2*e1(1)*e1(2) e1(2)^2
       e2(1)^2 2*e2(1)*e2(2) e2(2)^2
       e3(1)^2 2*e3(1)*e3(2) e3(2)^2]
%    IIr =    0.8940   -0.6157    0.1060
%             0.1060   -0.6157    0.8940
%             0.5696    0.9903    0.4304

rhsr = [Ir1; Ir2; Ir3]; Icmr = IIr\rhsr;

%Paper coordinate system MOI:
B =[Icmr(1) 0 Icmr(2);
         0 1.2      0;
    Icmr(2) 0 Icmr(3)]
%B =    [0.8155         0    0.0327
%             0    1.2            0
%        0.0327         0    1.0825]
%************************************************************************
%-------------------- JBike 12 Rear ---------------------------------------
%MOI in J-Bike12 coordinate system:
P=[1 0 0;
```

```
   0 0 1;
   0 -1 0];
Bjbiker= P.'*B*P;

%principle axis calculation for J-Bike12 program
Jcm = [Icmr(1) Icmr(2);
       Icmr(2) Icmr(3)];

[VeigJcm,DeigJcm] = eig(Jcm);
thetar=atan(VeigJcm(2,1)/VeigJcm(1,1)); thetad=thetar*180/pi;

%*************************************************************************
%---------------------- Front Wheel ------------------------------------
%*************************************************************************
%x en z axis
tvoor= ((66+66+66)/100*60)/50/3;    %s      Oscillation time front wheel
Ixf = ((tvoor/(2*pi))^2)*K          %kgm^2  Front wheel MOI about x + z axis
%    Ixf = 0.0797

%y axis
tyvoor=((75+75+76)/100*60)/30/3;    %s      Oscillation time front wheel
g=9.80665;                          %N      Gravity
mfw=2.05;                           %kg     Mass front wheel
Rfw=0.3485;                         %m      Radius front wheel
pivlf=0.048;                        %m      Length between tire edge & pivot
Iyf= ((tyvoor/(2*pi))^2)*mfw*g*(Rfw-pivlf)-mfw*(Rfw-pivlf)^2
%    Iyf = 0.1623

D = [ Ixf   0   0;
        0 Iyf   0;
        0   0 Ixf]
%D =    [0.0797         0         0
%             0    0.1623         0
%             0         0    0.0797]

%*************************************************************************
%--------------------Rear Wheel ----------------------------------------
%*************************************************************************
%x and z axis
tachter=((64+65+65)/100*60)/50/3;   %s      Oscillation time rear wheel
Ixr = ((tachter/(2*pi))^2)*K        %kgm^2  Rear wheel MOI about x + z axis
%    Ixr = 0.0765

%y axis
tyachter=((71+71)/30+74/31)/100*60/3;   %s  Oscillation time rear wheel
mrw=2.56;                           %kg     Mass rear wheel
Rrw=0.350;                          %m      Radius rear wheel
pivlr=0.0475;                       %m      Length between tire edge & pivot
Iyr= (tyachter/(2*pi))^2*mrw*g*(Rrw-pivlr)-mrw*(Rrw-pivlr)^2
%    Iyr = 0.1559
```

```
A = [Ixr    0   0;
     0    Iyr   0;
     0      0 Ixr]
%A =    [0.0765         0         0
%             0    0.1559         0
%             0         0    0.0765]
%**************************************************************************
%--------------------- New Experiment -----------------------------------


%-------------------------- Rod + Clamp ---------------------------------
%**************************************************************************
%MOI of Clamp+rod calculation:
mstaaf=2.870;                          %kg     Mass test weight rod
lstaaf=1.156;                          %m      Length test weight rod
hstaaf=0.02;                           %m   de diameter van de staaf
Istaaf= 1/12*mstaaf*(lstaaf^2+hstaaf^2);     %kgm^2  MOI of test weight rod
%   Istaaf = 0.3197

ts = (44.2/27+40.2/25+48.8/30+48.7/30+49/30)/5; %s Oscillation time for the rod
%   ts = 1.6257 s

w0=2*pi/ts;
K = Istaaf*w0^2;  %kgm^2/s^2  K
%    K = 4.7757
%**************************************************************************
%--------------------- front frame ---------------------------------------
%**************************************************************************
%Average time for 50 oscillations about the 3 main axes through the main tube.
tf1 =((36.0/40+36.1/40+45.0/50+44.9/50+45.0/50+44.9/50))/6; %s In x axis
tf2 =(42.4+41.8+42.0+42.4+41.8+42.3)/50/6;  %s In y axis
tf3 =(27.1+26.5+26.4+27.0+27.5+27.7)/70/6;  %s About steering axis
tf4 =(31+31+30.9+31.3+31.1+30.9)/50/6;      %s Under angle with handle bars up
tf5 =(40.5+40.0+40.2+40.3+40.1+39.8)/50/6;  %s Under angle with handle bars down

If1 = ((tf1/(2*pi))^2)*K;       %kgm^2  MOI about the roll axis (x)
If2 = ((tf2/(2*pi))^2)*K;       %kgm^2  MOI about the pitch axis (y)
If3 = ((tf3/(2*pi))^2)*K;       %kgm^2  MOI about the steering axis
If4 = ((tf4/(2*pi))^2)*K;       %kgm^2  MOI about angle with handlbars up
If5 = ((tf5/(2*pi))^2)*K;       %kgm^2  MOI about angle with handlbars up

alpha=(69)/180*pi;              %rad    head angle
beta=alpha+(12.6)/180*pi;       %rad    off set from steering axis
kappa=alpha+(39)/180*pi;        %rad    angle with handlebars up
gammma=alpha-(54.5)/180*pi;     %rad    angle with handlebars down

E1= [sin(alpha);-cos(alpha)];   %direction of measurement 1 in global coordinates
E3= [-cos(beta);-sin(beta)];    %direction of measurement 3 in global coordinates
```

```
E4=[-cos(kappa);-sin(kappa)];   %direction of measurement 4 in global coordinates
E5=[-cos(gammma);-sin(gammma)]; %direction of measurement 5 in global coordinates

rhs = [If1; If3; If4; If5];

IIf =  [ E1(1)^2 2*E1(1)*E1(2) E1(2)^2
         E3(1)^2 2*E3(1)*E3(2) E3(2)^2
         E4(1)^2 2*E4(1)*E4(2) E4(2)^2
         E5(1)^2 2*E5(1)*E5(2) E5(2)^2];

Icmf = IIf\rhs;

C = [Icmf(1) 0 Icmf(2)
         0      If2   0
     Icmf(2) 0 Icmf(3)]         % C MOI matrix
 %C = [ 0.0924    0   -0.0232
 %      0    0.0858         0
 %     -0.0232    0    0.0248]

%*************************************************************************
%-------------------- JBike 12 Front ---------------------------------------
%MOI in J-Bike coordinate system:
Jcmfq = [Icmf(1) Icmf(2);
         Icmf(2) Icmf(3)];                      %Required parameters

%principle axis value and angle calculation
[VeigJcmfq,DeigJcmfq] = eig(Jcmfq);             %Eigenvector, eigenvalues
%DeigJcmfq =[0.0996         0
%                 0    0.0176]

thetarfq=atan(VeigJcmfq(2,1)/VeigJcmfq(1,1));   %Angle of Eigenvector
thetadfq=thetarfq*180/pi;                       %Angle in degrees
%thetadfq = 17.2474
%I11=0.0996                                     %Jbike I11
%I22=0.0176                                     %Jbike I22
%Izz=0.0858                                     %Jbike Izz
```

Appendix E

Transient Response Analysis

E.1 Response to an Initial Lean Angle Offset

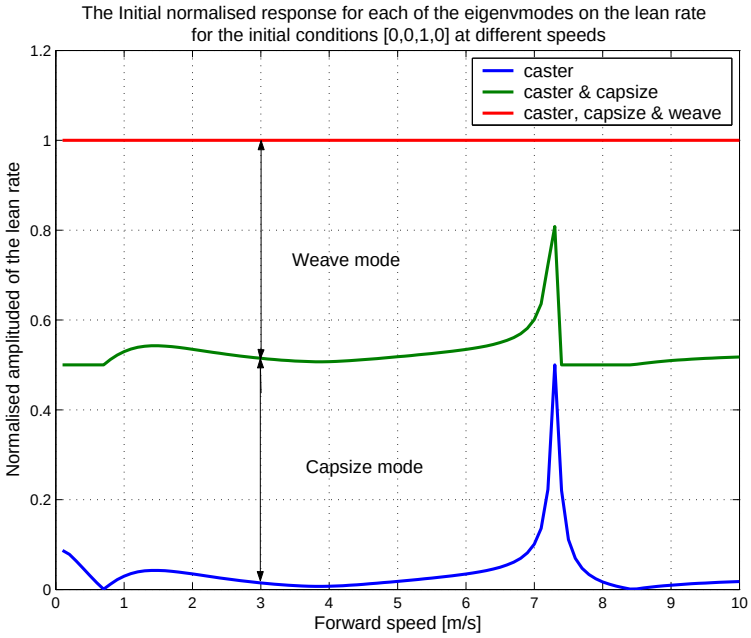

Figure E.1: The normalised initial angular rate response per mode to a ϕ perturbation for different speeds

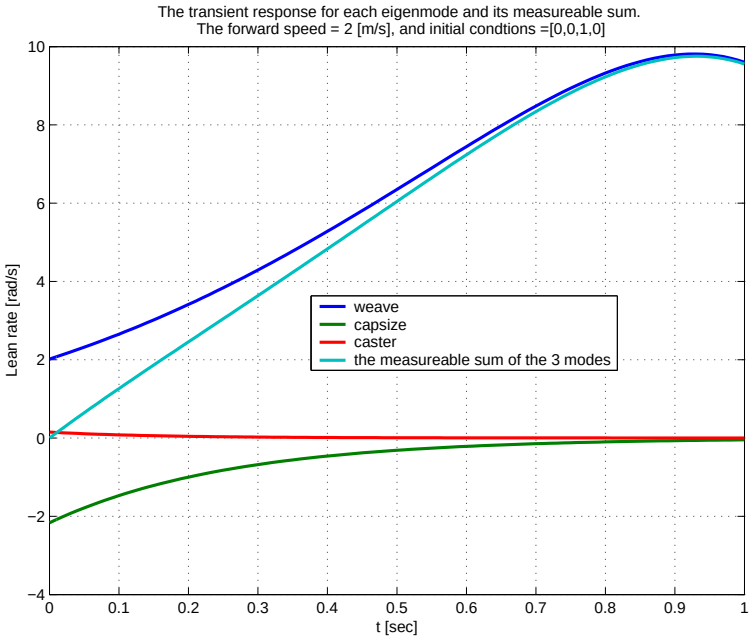

Figure E.2: The transient response of the lean-rate to an initial angle ϕ when the bicycle is moving at 2m/s

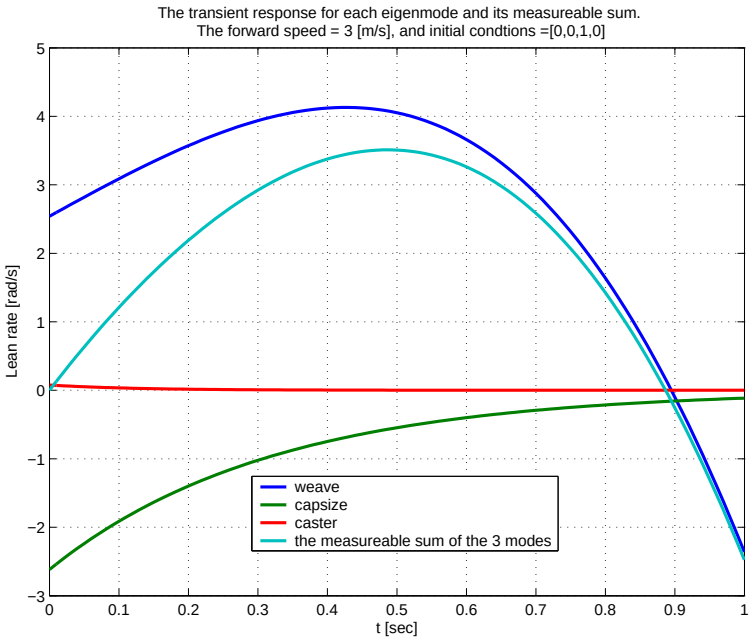

Figure E.3: The transient response of the lean-rate to an initial angle ϕ when the bicycle is moving at 3m/s

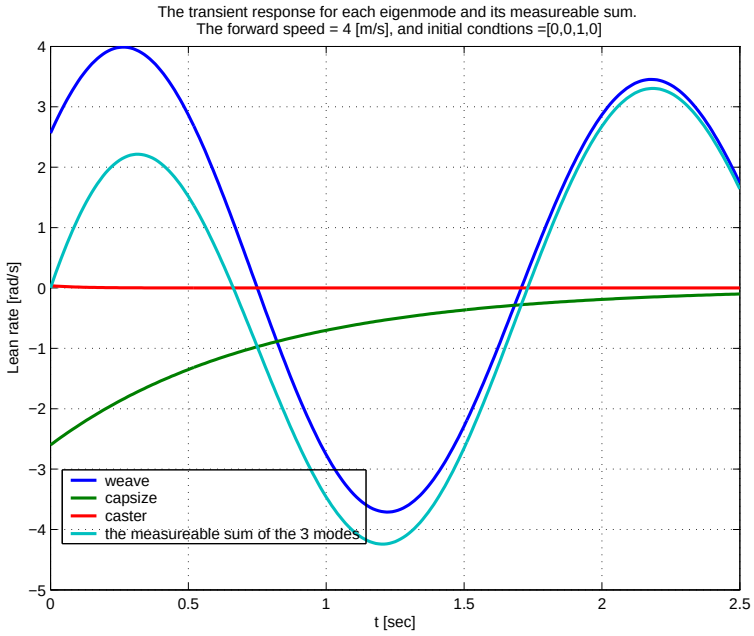

Figure E.4: The transient response of the lean-rate to an initial angle ϕ when the bicycle is moving at 4m/s

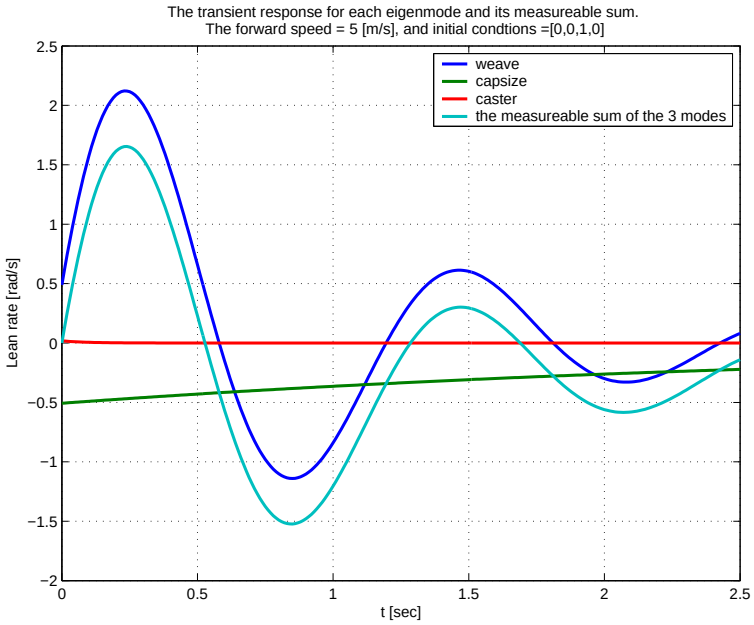

Figure E.5: The transient response of the lean-rate to an initial angle ϕ when the bicycle is moving at 5m/s

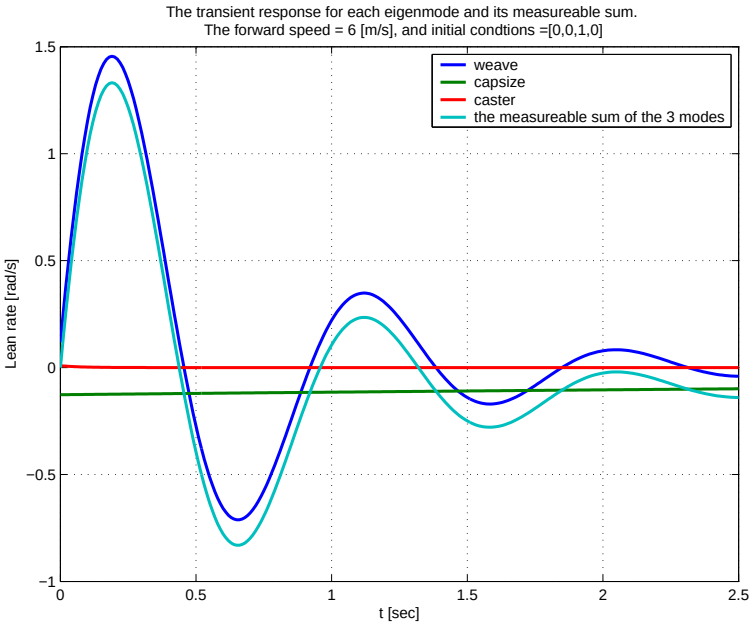

Figure E.6: The transient response of the lean-rate to an initial angle ϕ when the bicycle is moving at 6m/s

E.2 Response to an Initial Steering Angular-Rate

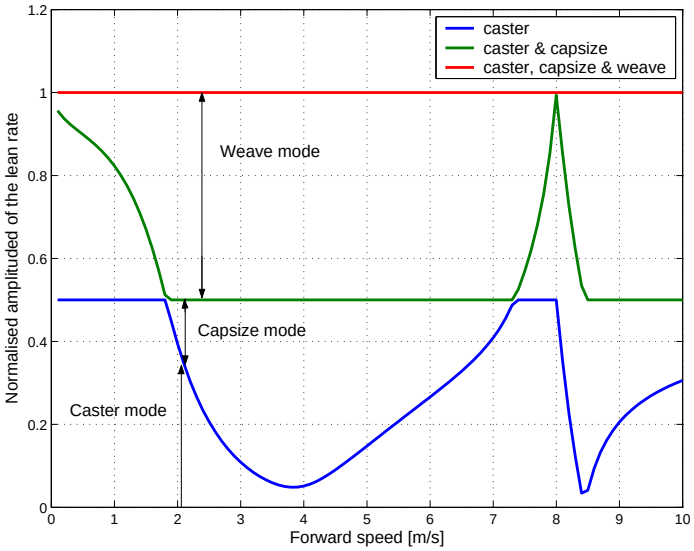

Figure E.7: The normalised initial angular rate response per mode to a $\dot{\delta}$ perturbation for different speeds

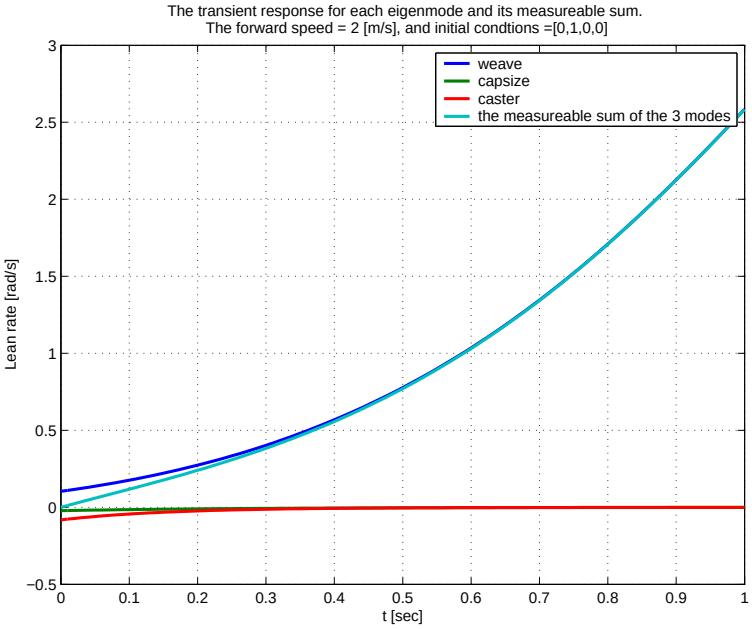

Figure E.8: The transient response of the lean-rate to an initial steering angle rate $\dot{\delta}$ when the bicycle is moving at 2m/s

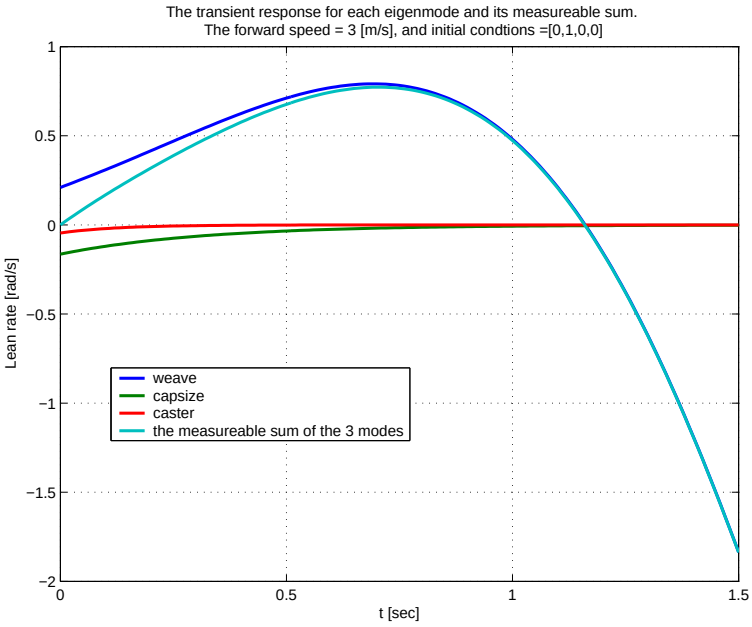

Figure E.9: The transient response of the lean-rate to an initial steering angle rate $\dot{\delta}$ when the bicycle is moving at 3m/s

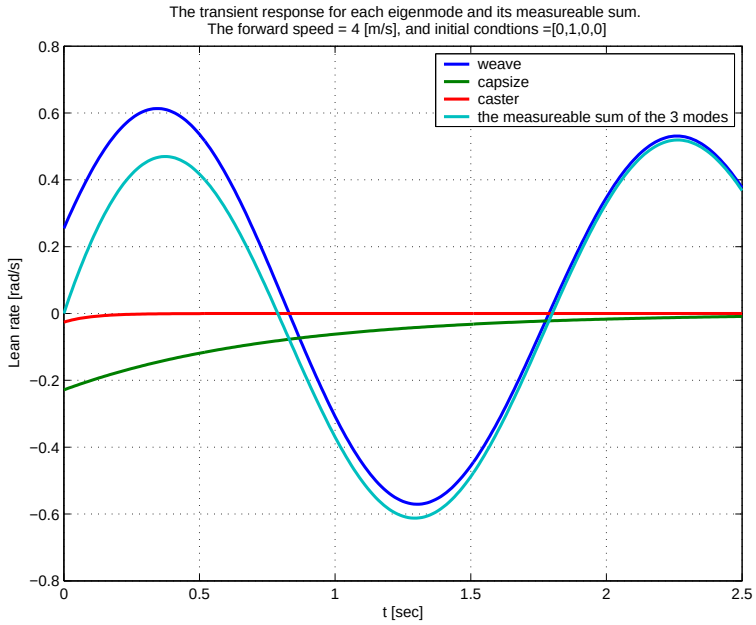

Figure E.10: The transient response of the lean-rate to an initial steering angle rate $\dot{\delta}$ when the bicycle is moving at 4m/s

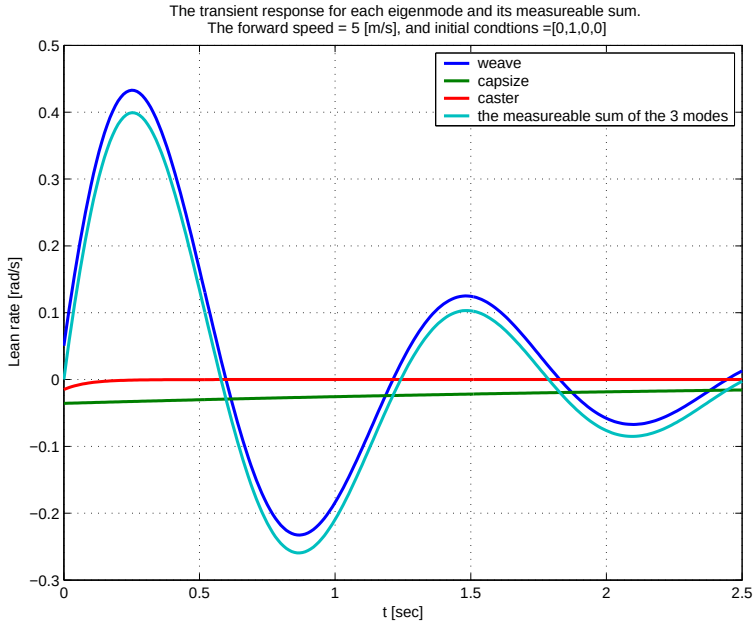

Figure E.11: The transient response of the lean-rate to an initial steering angle rate $\dot{\delta}$ when the bicycle is moving at 5m/s

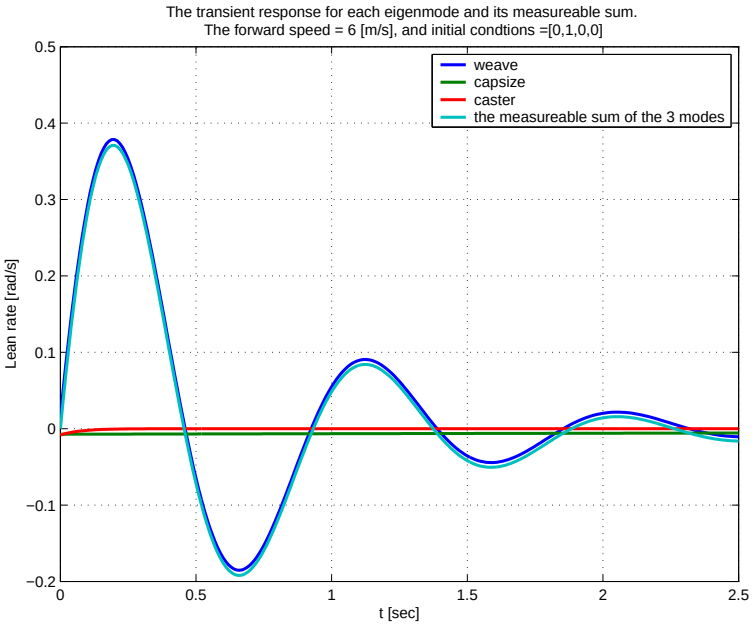

Figure E.12: The transient response of the lean-rate to an initial steering angle rate $\dot{\delta}$ when the bicycle is moving at 6m/s

E.3 Response to an Initial Steering Angle Offset

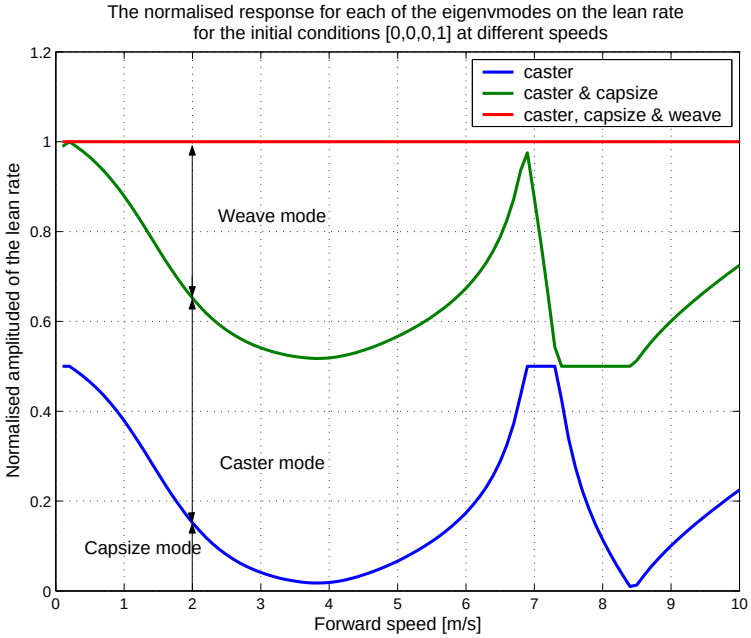

Figure E.13: The normalised initial angular rate response per mode to a δ perturbation for different speeds

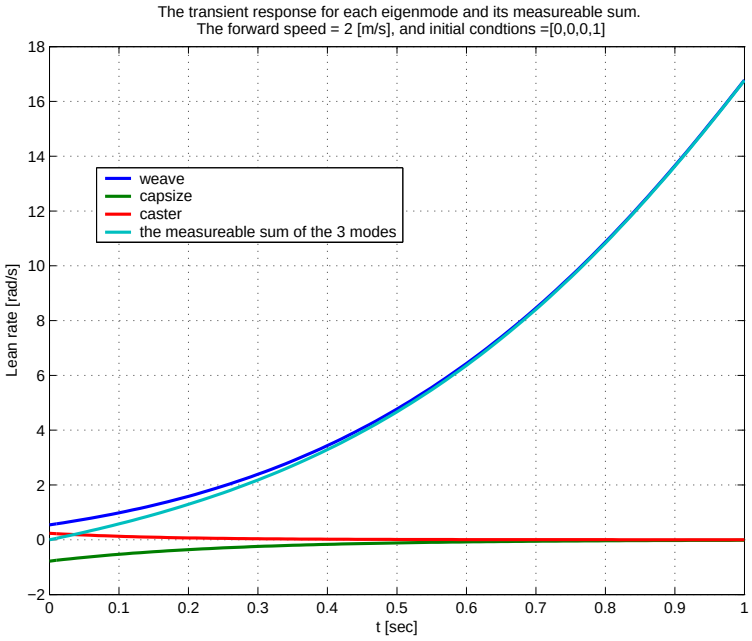

Figure E.14: The transient response of the lean-rate to an initial steering angle δ when the bicycle is moving at 2m/s

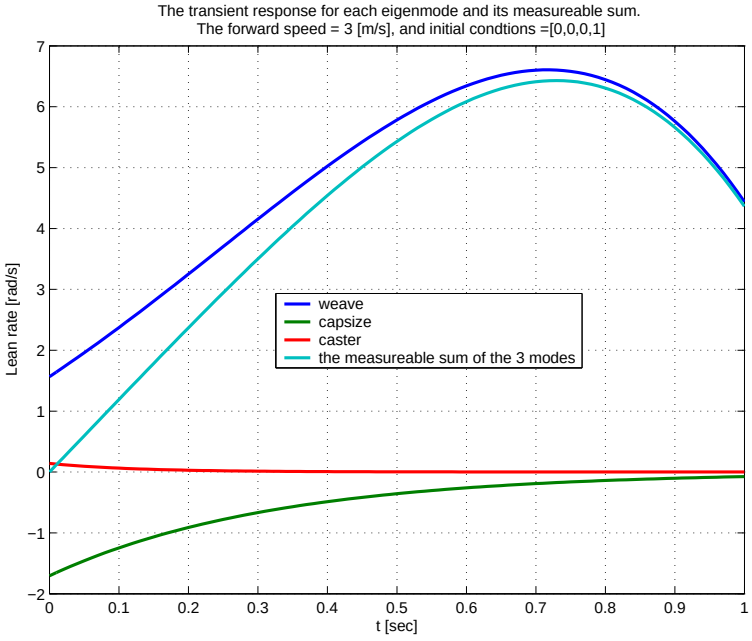

Figure E.15: The transient response of the lean-rate to an initial steering angle δ when the bicycle is moving at 3m/s

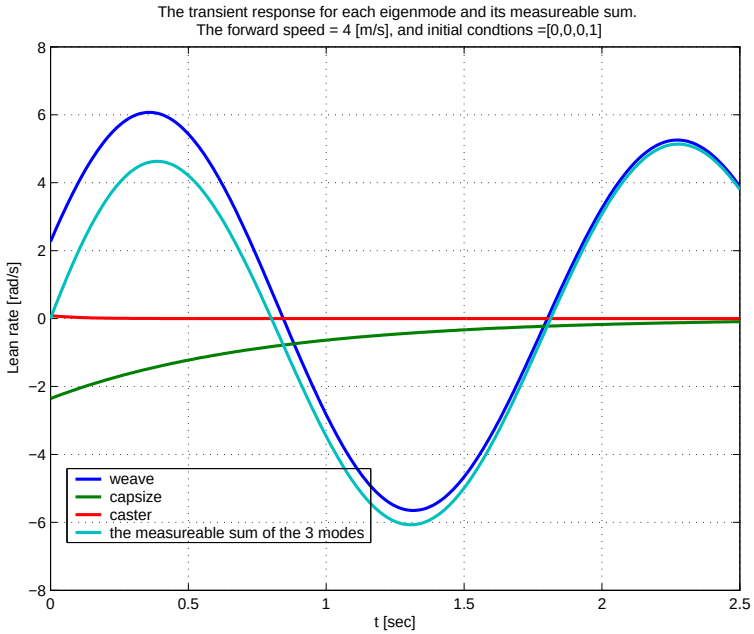

Figure E.16: The transient response of the lean-rate to an initial steering angle δ when the bicycle is moving at 4m/s

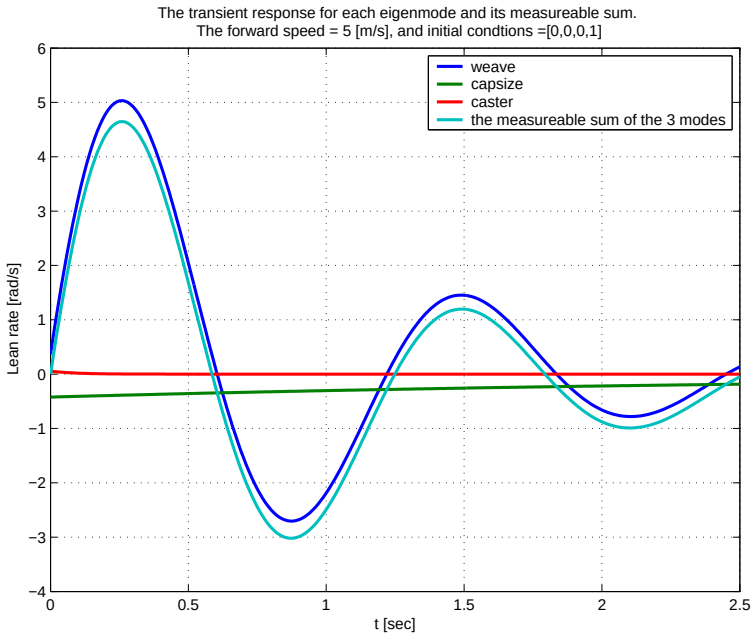

Figure E.17: The transient response of the lean-rate to an initial steering angle δ when the bicycle is moving at 5m/s

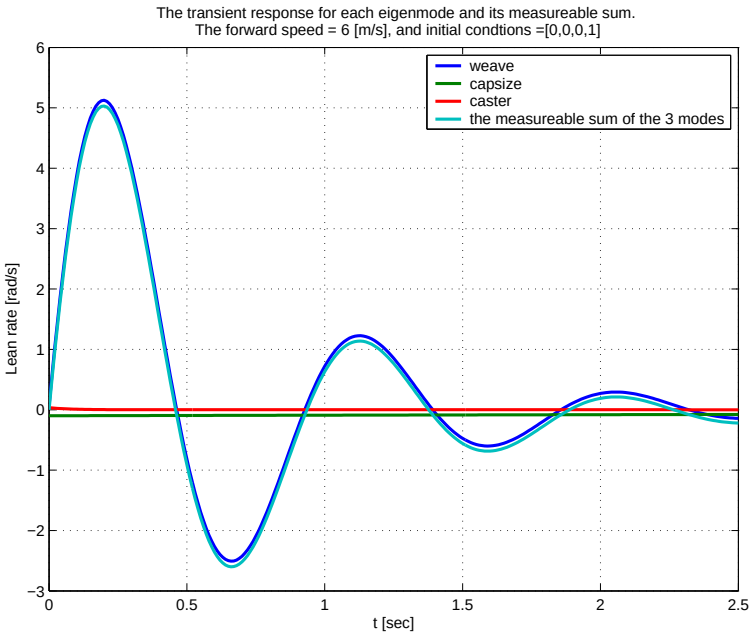

Figure E.18: The transient response of the lean-rate to an initial steering angle δ when the bicycle is moving at 6m/s

Bibliography

[1] A. L. Schwab, J. P. Meijaard, and J. M. Papadopoulos, A Multibody Dynamics Benchmark on the Equations of Motion of an Uncontrolled Bicycle. In *Proceedings of the Fifth EUROMECH Nonlinear Dynamics Conference, ENOC-2005, August 7–12, 2005, Eindhoven University of Technology, The Netherlands*, 511–521, 2005.

[2] E. Döhring, Über die Stabilität und die Lenkkräfte von Einspurfahrzeugen. Ph.D. thesis, Technical University Braunschweig, Germany, 1953.

[3] E. Döhring, Die Stabilität von Einspurfahrzeugen. *Automobil Technische Zeitschrift*, **56**(3), 68–72, 1954.

[4] R. S. Rice and R. D. Roland, An evaluation of the performance and handling qualities of bicycles. Cornell Aero. Lab. Report no. VJ-2888-K, 1970.

[5] R. D. Roland and J. P. Lynch, Bicycle dynamics tire characteristics and rider modeling. Cornell Aero. Lab. Report no. YA-3063-K-2, 1972.

[6] R. D. Roland and D. E. Massing, A digital computer simulation of bicycle dynamics. Cornell Aero. Lab. Report no. YA-3063-K-1, 1971.

[7] M. Wächter, Eine experimentelle Überprüfung des dynamischen Fahrradmodells. M.Sc. thesis, University of Oldenburg, Germany, 1991.

[8] W. Suhr, Entwicklung und Erprobung eines nichtlinearen dynamischen Fahrradmodells, excerpts from a Ph.D. thesis, University of Oldenburg, Germany, 1992.

[9] A. W. Jackson and M. Dragovan, An experimental investigation of bicycle dynamics. *American Journal of Physics*, (submitted) 1998.

[10] D. J. Eaton, Man-machine dynamics in the stabilization of single-track vehicles. Ph.D. thesis, University of Michigan, 1973.

[11] R. S. Rice, Accident avoidance capabilities of motorcycles. In *Proceedings International Motorcycle Safety Conference, Dec 16 & 17 , 1975*, USDOT, National Highway Traffic Safety Administration, Washington, DC, 121–134, 1975.

[12] D. H. Weir and J. W. Zellner, Lateral-directional motorcycle dynamics and

rider control. Technical report no. 780304, Society of Automotive Engineers, Warrendale, PA, 1978.

[13] P. A. J. Ruijs and H. B. Pacejka, Recent research research in lateral dynamics of motorcycles. In *Proceedings of the 9th IAVSD Symposium held at Linköping University, Linköping, Sweden, June 24–28, 1985*, 467–480, 1986.

[14] S. Miyagishi, I. Kageyama, K. Takama, M. Baba and H. Uchiyama, Study on construction of a rider robot for two-wheeled vehicle, *JSAE Review*, **24**(3), 321–326, 2003

[15] Blue Team, http://www.roboticinfantry.com/

[16] Cossalter, V., *et al.*, http://www.dinamoto.it/

[17] http://tam.cornell.edu/∼als93/bicycledyn.htm#May24

[18] J.M. Gere and S.P. Timoshenko, *Mechanics Of Materials*, Third SI Edition, Chapman & Hall. 1996.

[19] D. G. Wilson, *Bicycling Science*, with contributions by Jim Papadopoulos. 3rd edition. Cambridge, MA: MIT Press. 2004.